ARCHIVES OF ACOUSTICS
20, 3, 215–235 (1995)

DETECTION AND LOUDNESS OF AM SIGNALS FOR NORMAL AND HEARING-IMPAIRED SUBJECTS

W. GEERS* and E. OZIMEK**

*D-44137 Dortmund, Westenhellweg 68, Germany
** Institute of Acoustics
Adam Mickiewicz University
(60-769 Poznań, Matejki 48/49)

The study comprises two experiments pertaining to the perception of sounds with parameters changing in time, by normal-hearing subjects and by hearing-impaired subjects, who had a sloping high-frequency hearing loss originating from a cochlear impairment. The first experiment deals with the determination of the AM detection thresholds, for 3 normal-hearing and 3 cochlear-impaired subjects. In the second experiment, the loudness of AM signals of different parameters, relative to the loudness of a sinusoidal tone was determined by the same group of subjects. Measurements were made for carrier frequencies (f_c) equal to: 250, 500, 1000, 2000 Hz, and for modulation frequencies (f_m) equal to: 4, 8, 64, 128, 256 Hz. It was stated that for low f_m the determined detection thresholds for the normal-hearing subjects were roughly similar to those for the cochlear-impaired subjects. However, for higher f_m, the thresholds decrease for the normal-hearing subjects, whereas they tend to increase for the hearing-impaired subjects. Thus, one can assume that for higher f_m, temporal resolution of the auditory system is significantly affected by cochlear hearing loss. As regards the loudness of AM signals, the data showed that for f_m greater than the critical band, the loudness of AM signals increased with f_m for the normal-hearing subjects, whereas it remained independent of f_m for the hearing-impaired subjects.

1. Introduction

The ability to resolve amplitude changes of a signal in time is of crucial importance for the auditory processing of complex sounds such as speech or music. One way to determine auditory amplitude resolution for different rates of its changes is to measure the smallest amount for amplitude modulation, just-noticeable by a subject. The plot of the AM detection threshold againts modulation frequency is called the temporal modulation transfer function (TMTF) and is considered as a general description of the auditory temporal resolution. ZWICKER [40], using a 1-kHz carrier at 60 dB SPL compared modulation thresholds for sinusoidal AM and FM. Zwicker has shown that for the AM detection threshold there was a slight (2 dB) decrease in threshold around 4 Hz, followed by a 3 dB/oct increase in threshold up to

modulation frequency equal to approximately 60 Hz. Above 60 Hz, the AM detection threshold decreases again. Other data from Zwicker indicate that the shape of the threshold over the lower modulation frequency region is independent of the level and carrier frequency. The fact that for higher modulation frequencies the subjects resolve the spectral components of AM sinusoids (i.e. use the spectral cues to determine the threshold), limits in a sense the application of sinusoidal carriers for determining TMTFs. To diminish possible spectral cues, wideband noise as a carrier was used in different studies (ZWICKER and FELDTKELLER [43]; RODENBURG [28]; VIEMEISTER [38, 39]; BACON and GLEITMAN [2]; MOORE *et al.* [25]). For such a carrier, the long-time power spectrum of sinusoidal AM noise is uniform and invariant with changes in modulation frequency. The mentioned papers suggest that for low modulation frequency (above about 5 Hz), the TMTF shows a lowpass characteristic with a relatively high cutoff frequency and a low attenuation rate. The papers are not fully consistent as the parameters of the characteristic are concerned, and to whether or not there is a highpass segment at a low modulation frequency. BACON and VIEMEISTER [1], using sinusoidal AM noise stated, that TMTFs are similar, in the limit of error, for normal and hearing-impaired subjects at low modulation frequencies and worse for impaired subjects at high modulation frequencies.

The modulation threshold procedure using a broadband noise as a carrier has some limitations. The TMTF cannot be obtained for large modulation indexes and for precisely localized spectral regions. Besides, keeping a constant SL through a bandwidth of a broadband carrier often creates problems. Only a sinusoidal carrier or a narrowband carrier allow to control accurately the SL for a given frequency range. But on the other hand, this carrier can introduce some spectral cues for a subject and in this way can affect his performance.

Another approach aimed to determine the TMTFs involves measuring the threshold for a bandpass-filtered click at various temporal locations in sinusoidal AM noise (VIEMEISTER [38]; RODENBURG [28]). In this case the attenuation characteristic exhibited a lowpass from but had a greater attenuation rate than TMTF based upon the modulation threshold. Unfortunately, this procedure cannot be used to get TMTFs obtained at high modulation frequencies. The effect of the cochlear impairment on temporal resolution is not quite clear (MOORE *et al.* [25]), unlike frequency resolution where hearing loss affects it unequivocally (TYLER [37]; PICKLES [26]). Some papers indicate that, for example, the detection thresholds of gaps in noise stimuli are larger for subjects with sensorineural hearing loss than for subjects with normal hearing (FITZGIBBONS and WIGHTMAN [6]; FLORENTINE and BUUS [10]; GLASBERG *et al.* [14]). But when sinusoidal signals are used in the gap detection experiment, thresholds for hearing-impaired subjects are as good as, or even in some cases better than, those for normal-hearing subjects (MOORE and GLASBERG [23]; MOORE *et al.* [24]). It seems that an important parameter in this case, influencing the results, is the amplitude fluctuation which stimuli contain. The poor gap detection for stimuli with such fluctuations might result from the loudness recruitment.

Temporal resolution measures can also be affected by the sound level used. Some experimental data pertaining to temporal resolution indicate thatperformance by normal-hearing subjects worsens at low sensation levels (FLORENTINE and BUUS [9]; FITZGIBBONS [7]; VIEMEISTER [39]).

The second problem related to the hearing impairment is how loudness summates for complex sounds when impairment of the inner ear produces a high threshold and loudness recruitment. The quantitative psychophysiological approach towards the loudness summation problem was presented by ZWISLOCKI [44]. It was stated that the temporal summation of loudness is a result of neural summation at a high level of the auditory system. The basic problem in the loudness study of sounds, particularly when these are complex or transient-like sounds, is that loudness is a subjective quantity, and cannot be measured directly. One common method of loudness measurement is matching. Subjects are usually presented two sounds, one is the standard-tested stimulus, with fixed level, the other sound, as the comparison (often a 1000 Hz tone), is adjusted in level until the two stimuli are equal in laudness. In other methods subjects are asked to rate loudness of a tested stimulus on a numerical scale (direct magnitude estimation). The fundamental relation which governs the growth of loudness against the intensity is Stevens' power law. The power law asserts that loudness against the intensity is raised to the 0.3 power (or as pressure is raised to the 0.6 power). The power law suggests that a 10 dB increase in sound intensity produces a doubling in loudness. Practically, for individual subjects, this law only roughly holds true. The increase needed to double loudness changes from about 8 to 12 dB, depending upon the level of the stimulus.

An issue related to loudness estimation by subjects with hearing loss is loudness recruitment observed in cochlear-impaired subjects, whose physiological mechanism is still a subject of debate. The phenomenon exhibits an abnormality of intensity coding whereby the growth of loudness of a sound with increase in intensity is steeper than that for normal-hearing subjects. The first theory of recruitment assumed that in a set of fibers with widely differing thresholds the most sensitive receptors had been damaged. The eight nerve data rejected this theory. EVANS [5] pointed out that peripheral receptor damage often causes an elevation in the threshold and, in addition, a broadening of the frequency tuning curve. The broadening of tuning curves in individual fibers gives rise to the stimulation of more fibers for a given increase in intensity and hence a greater growth of loudness for the impaired ear. Loudness, like recruitment in general, is not fully consistent with the new information on peripheral encoding.

SCHARF and HELLMAN [32], investigated loudness of complex sounds composed of sinusoidal components as a function of the frequency spacing (ΔF) between the lowest and highest components and sensation levels. The loudness was measured for normal ears and for ears with a conductive and cochlear impairment. It was stated that subjects with normal and conductive hearing-impairment, when tested at the same sensation levels, estimate loudness in the same way. For higher sensation levels, loudness was constant within ΔF not exceeding the critical band. But for ΔF larger than the critical band loudness increased more and more with ΔF. This implies that as regards the loudness summation, a conductive impairment only changes the sen-

sitivity of the hearing mechanism, in the sense of a reduction of the sound energy that reaches the inner ear. However, for subjects with cochlear impairment, the loudness was approximately independent of the frequency spacing of the components.

LÜSCHER and ZWISLOCKI [22] reported that intensity jnd's (just noticeable differences) obtained with modulation technique, appear to be decreased by cochlear hearing loss when the comparison is made at equal SLs. A similar conclusion is reached by examining the results of SISI tests (SWISHER [35]). But, when the comparison is replotted in terms of equal SPLs, the two groups of subjects appear to perform more alike. Likewise, TURNER *et al.* [36] investigated intensity discrimination determined with two paradigms in normal and hearing-impaired subjects. It was stated that the jnd's obtained with the continuous-pedestal method were smaller than those obtained with the gated-pedestal method for both groups of subjects. When jnd's of the two groups were compared on the basis of equal SLs, the group with hearing loss showed smaller jnd values than the group with normal hearing for both paradigms. When the comparisons were made for equal (moderate and high) SPLs, both groups showed similar jnd values. Similar study, related to intensity jnd's at equal-loudness levels in normal and pathological ears was made by STILLMAN *et al.* [34]. They showed that statistically, there was no significant difference between equal-loudness jnd's in the normal and impaired ears, whereas the corresponding SLs and SPLs were significantly different.

From the above presented considerations, it is to be issued that the influence of the cochlear impairment on the perception of sounds is not univocally determined and continues to be a subject of intensive research. Particularly interesting is a closer determination of that perception with reference to signals with amplitude varying in time. Sounds of speech and music are typical examples of these signals. This prompted us to start an investigation whose basic objective was to determine the detection theresholds and the loudness of AM signals, measured by normal and cochlear-impaired subjects.

2. Experiment I. Detection thresholds for AM signals

A. Method

1. *Apparatus and stimuli.* The AM stimuli were digitally generated by an IBM-PC computer and played through 16-bit digital-to-analog converter, at a sampling rate of 20 kHz, and were low-pass filtered at 8 kHz (Tucker-Davis Technology-TDT). The overall duration of each stimulus was 1000 ms, including 20 ms rise/fall times. The stimuli were arranged in pairs, and presented at a sensation level equal to 70 dB. The onset and offset phase of the modulation signal were equal to zero.

At each trial two successive stimuli were presented, one unmodulated-sinusoidal tone (called standard) and the other AM modulated (called signal). Standard and

signal in trial were presented in a random order, and were separated by a 400 ms interval.

The measurements of the AM detection thresholds were made for the sinusoidal carriers of 250, 1000 and 4000 Hz, amplitude modulated by another sinusoidal signal of frequencies 4, 8, 64, 128, 256, and 512 Hz. The entire experiment was computer controlled.

2. Procedure and subjects. Stimuli were presented in a two-interval, two-alternative, forced choice paradigm (2AFC). A two-down one-up adaptive procedure was used to obtain the 70.7% correct point on the psychometric function (LEVITT [21]). Trials started with the depth of modulation (modulation index m) well above the anticipated threshold (the initial m value was selected on the basis of the preliminary measurements). The depth of modulation was varied by changing the amplitude of the modulation signal. Depending on the correctness of the subject's responses, the depth of modulation was changed according to the two-down one-up rule during the run. The coefficient m was changed by 2.0 dB until four turnpoints were reached, and then by a factor of 0.5 dB for the rest of the run. For each threshold measurement, 16 turnpoints were obtained. The threshold estimate of the modulation index m was calculated as an arithmetic mean of the last 10 turnpoints. The final threshold value of m, for the determined measurement parameters, was counted as an average of at least five single threshold estimates (50 turnpoints). In the case when the standard deviation of the final threshold estimate exceeded 20% of the mean, two additional runs were performed and all estimates were averaged.

The subject's task was to indicate, by pushing an appropriate button, which of the stimuli in a pair was amplitude modulated. Stimuli were presented monaurally to the subjects through AGH 144 headphones. Feedback of the correct answer was provided immediately after each response by light on the response box.

Three subjects with normal hearing (S1, S2, S3), and three subjects with hearing loss (S4, S5, S6) of unknown etiology participated in the experiment. Two of them (S5, S6) had unilateral-like hearing loss. At the frequency region from 125 Hz to 6000 Hz, the thresholds for the better ears for these two subjects were better than 20 – 30 dB relative to the thresholds for the impaired ears. For these two subjects, AM detection thresholds and loudness estimation were determined separately for each ear. In this way it was possible to compare detection thresholds of AM signals for the better and impaired ear for the same subject. For the bilaterally impaired subject (S4), only the one ear was tested. Standard audiometric evaluations, bone-conduction thresholds, tympanometry, and acoustic reflex tests indicated that the hearing loss was of cochlear origin. Subjects were tested individually in a sound-treated chambers. Subjects with normal hearing were well experienced in the psychoacoustic experiments, but hearing-impaired subjects had no experience in this task. The masking noise was presented to the normal ear when testing the thresholds in the impaired ear. Audiograms for the two tested groups of subjects are included (Fig. 1). Hearing-impaired subjects were tested at the same SLs as normal-hearing subjects.

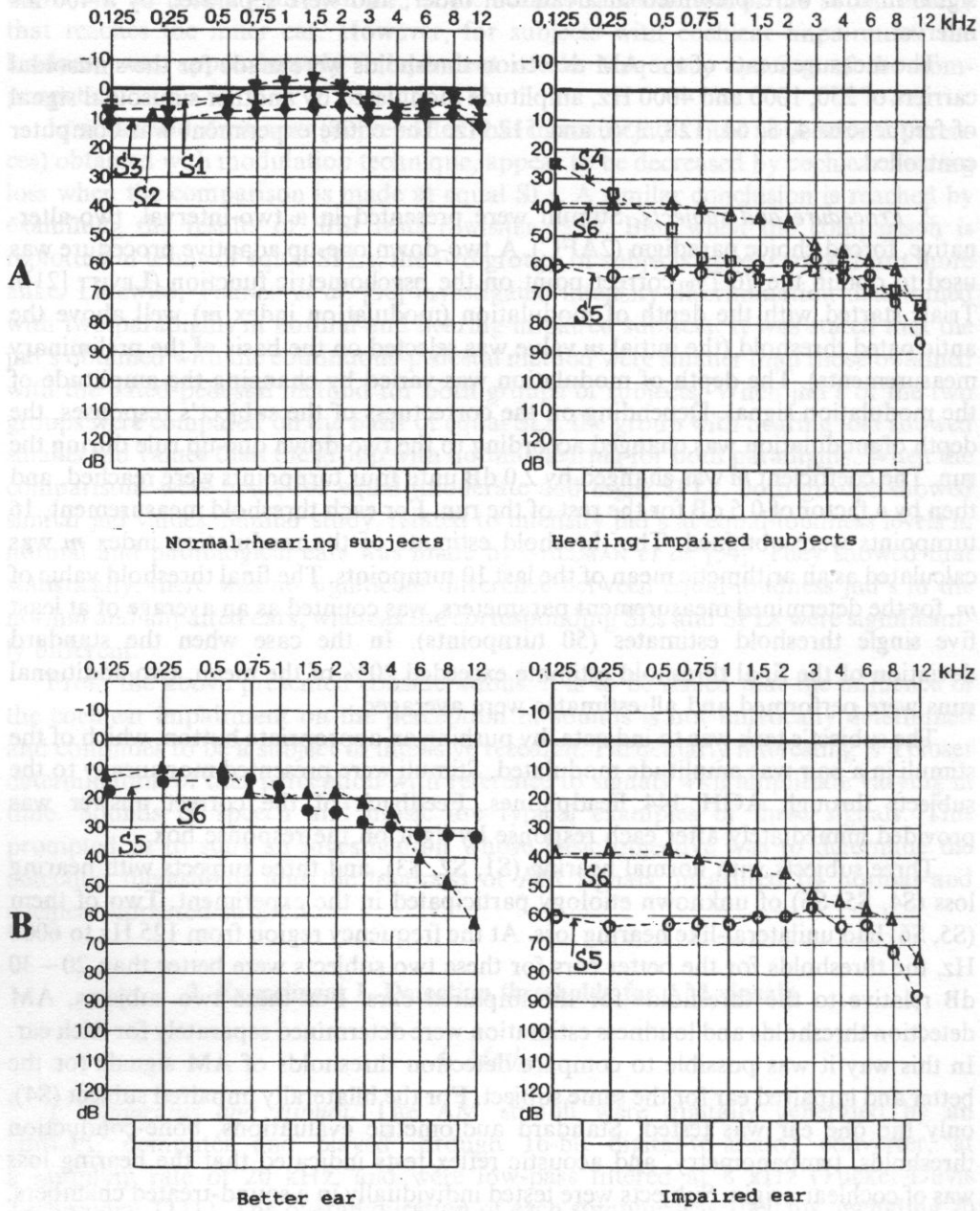

Fig. 1. Audiograms for normal and hearing-impaired subjects (A) and for two unilateraly hearing-impaired subjects (B)

B. Results

Figure 2 shows the comparison of the detection thresholds of the AM signals expressed as 20 log m, as a function of modulation frequency (f_m), obtained for three normal-hearing (A) and for three hearing-impaired subjects (B). The thresholds were determined for SL=70 dB. The parameter of the curves is the carrier frequency (f_c) equal to 250, 1000 and 4000 Hz. The increase of negative numbers on the ordinate axis indicates the better performance by the subject.

For each subject and each condition the arithmetic mean and standard deviation was calculated. Only mean values are shown in Fig. 2 and 3, and SD ranges are left out for clarity. The SD values for all conditions ranged between 1–3 dB and only for modulation frequency of 64 and 128 Hz, the SD values sometimes reached 5 dB.

As one can see, the AM thresholds for three normal-hearing subjects are roughly similar. The values of those thresholds for the low f_m are nearly constant, and depending on f_c and the subject, are contained in the limits of −26 to −37 dB. Whereas for higher f_m (exceeding 64 Hz) they get markedly decreased at the rate of 3–5 dB/oct, depending on the subject. These data are consistent with the investigations of ZWICKER [40] and VIEMEISTER [39]. The point the thresholds decrease from depends on the carrier frequency. The higher that frequency, the more shifted is that point towards higher modulation frequencies. Additionally to be noticed a certain dependence of the thresholds on the carrier frequency. The lower that frequency, the higher is the value of the threshold. However, a statistically significant fall of the thresholds about f_m=4 Hz, as suggested by ZWICKER [40, 41] and VIEMEISTER [39] could not be ascertained.

The time constant $\tau = 1/2\pi f_0$ (where f_0 is the cutoff frequency of the TMTF taken on the level of −3 dB of the TMTF) comprises in the range 2–4 ms for the carrier from 1000–4000 Hz. It continues to increase slightly as the carrier frequency increases. The data presented here indicate that there is some change in the shape of the TMTF depending on the carrier frequency.

Figure 2B shows the AM threshold for three hearing-impaired subjects. As can be seen, for $f_m < 64$ Hz the detection thresholds are approximately equal to the thresholds corresponding to the normal-hearing subjects within the limit of error. Characteristic, however, is the fact, that for $f_m < 64$ Hz, the detection thresholds for the hearing-impaired subjects increase (on an average of 5–8 dB/oct depending on f_c and the subject) along with the increase of f_m. Thus, they show a course, other than for normal-hearing subjects, for whom those thresholds, in that frequency range, were decreasing (on an average 3–5 dB/oct). BACON and VIEMEISTER [1] and FORMBY [11] found out that for high modulation frequency, the TMTF functions for sinusoidal AM noise always show decreasing tendency. The decreasing rate was higher for subjects with sensorineural hearing loss compared to normal-hearing subjects.

An analysis of variance was performed on the data presented in Fig. 2–3 to test the effect of modulation frequency. It was found out that the effect of modulation

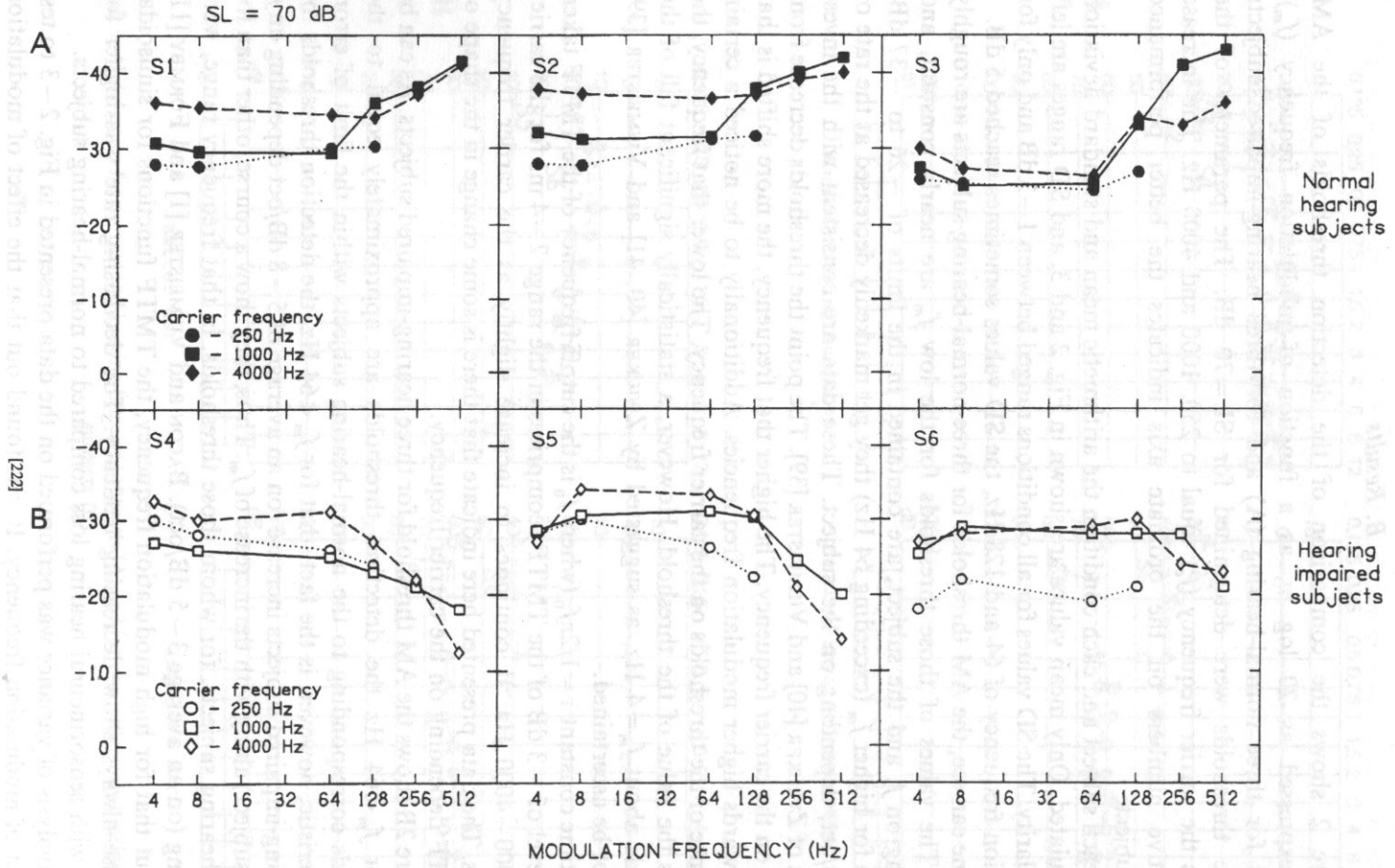

[222]

Fig. 2. AM detection thresholds for 3 normal-hearing subjects (A — filled symbols) and 3 hearing-impaired subjects (B — open symbols). Parameter of the curves is the carrier frequency equal: 250, 1000 and 4000 Hz. SL = 70 dB.

frequency was significant ($p<0.05$) and was decisively different for normal and hearing-impaired subjects.

In Fig. 3 the dependence of the AM detection thresholds on the modulation frequency for two subjects (S5 and S6) of differing hearing loss in the left and right ears is shown. Those thresholds were determined for SL = 70 dB. The parameter of the curves is the carrier frequency, Fig. 3A shows detection thresholds for the better ear, while Fig. 3B for the impaired ear, for the same subject (audiograms of the left and right ears for those subjects are given in Fig. 1). The thresholds shown in Fig. 3 have a shape approximating the thresholds presented in Fig. 2, which confirms the earlier drawn conclusions. As it is seen, for the low f_m the detection thresholds are approximately constant, and depending on f_c and the subject they are contained in the limits of −25 to −33 dB. For the impaired ear that dispersion is slightly larger. More

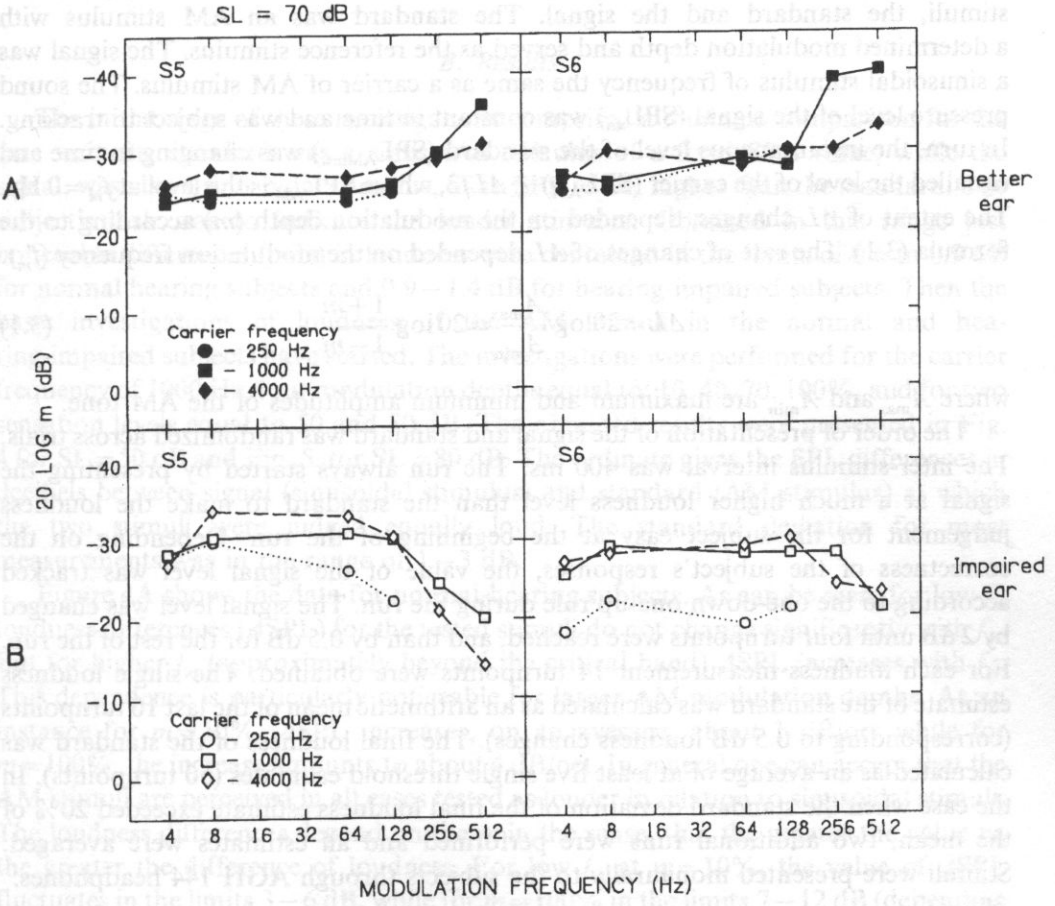

Fig. 3. AM detection thresholds for 2 hearing-impaired subjects , with one better ear (A — filled symbols) and the other one poorer (B — open symbols). Parameter of the curves is the carrier frequency equal: 250, 1000 and 4000 Hz. SL = 70 dB.

essential, however, is the fact, that for higher f_m the detection threshold lowers in the function of f_m for the better ear, whereas for the impaired ear that threshold in the function of f_m rises. Those dependences are analogical as in Fig. 2, which once again confirms the conclusion, that for the higher f_m the cochlear impairment changes the character of the detection threshold for AM sinusoidal carrier.

This fact may constitute an additional diagnostic clue in a clinical application to distinguish the character of the ear impairment.

3. Experiment II. Loudness of AM signal

A. Method

1. *Apparatus and stimuli.* A single trial consisted of a pair of successively presented stimuli, the standard and the signal. The standard was an AM stimulus with a determined modulation depth and served as the reference stimulus. The signal was a sinusoidal stimulus of frequency the same as a carrier of AM stimulus. The sound pressure level of the signal (SPL_{sin}) was constant in time and was subject to tracking. In turn, the instantaneous level of the standard (SPL_{AMinst}) was changing in time and equalled the level of the carrier (SPL_{AM}) $\pm \Delta L/2$, where SPL_{AM} is the level at $f_m = 0$ Hz. The extent of ΔL changes, depended on the modulation depth (m) according to the formula (3.1). The rate of changes of ΔL depended on the modulation frequency (f_m).

$$\Delta L = 20\log \frac{A_{max}}{A_{min}} = 20 \log \frac{1+m}{1-m} \tag{3.1}$$

where A_{max} and A_{min} are maximum and minimum amplitudes of the AM tone.

The order of presentation of the signal and standard was randomized across trials. The inter-stimulus interval was 400 ms. The run always started by presenting the signal at a much higher loudness level than the standard to make the loudness judgement for the subject easy at the beginning of the run. Depending on the correctness of the subject's responses, the value of the signal level was tracked according to the one-down one-up rule during the run. The signal level was changed by 2 dB until four turnpoints were reached, and than by 0.5 dB for the rest of the run. For each loudness measurement 14 turnpoints were obtained. The single loudness estimate of the standard was calculated as an arithmetic mean of the last 10 turnpoints (corresponding to 0.5 dB loudness changes). The final loudness of the standard was calculated as an average of at least five single threshold estimates (50 turnpoints). In the case when the standard deviation of the final loudness estimate exceeded 20% of the mean, two additional runs were performed and all estimates were averaged. Stimuli were presented monaurally to the subjects through AGH 144 headphones.

2. *Procedure and subjects.* Among many procedures which have been used over the years to obtain loudness balance one can distinguish traditional techniques comprising: magnitude balance and cross-modality technique (HELLMAN and ZWISLOCKI

[17]; HELLMAN [19]), the method of adjustment (FLETCHER and MUNSON [8]; ROSS [30]), the method of constant stimuli (ROBINSON and DADSON [29]), and recently used, efficient technique based upon adaptive procedures (LEVITT [21]; JESTEADT [20]). In this study, 2IFC adaptive procedure was used. The subject was asked to balance the loudness of the signal with the loudness of the standard, by tracking the signal SPL. In this way, loudness matching was achieved between standard and signal (with the accuracy of jnd in loudness).

The same three subjects as in experiment I participated in this experiment. Two of them (S5, S6) had unilateral-like hearing loss. At the frequency region from 125 Hz to 4000 Hz, the thresholds for the better ears for these two subjects were below, about 20 – 30 dB, the thresholds for impaired ears. The loudness was determined separately in the better and impaired ears for these two subjects. The subjects were tested individually in a sound-treated chambers.

B. Results

The initial stage of these investigations comprised a loudness comparison for the case were the standard was a sinusoidal stimulus of a fixed SPL value, while the signal, was also a sinusoidal stimulus, of an SPL value, higher than the standard. The subject's task was to indicate the louder stimulus. Obtained in this range just noticeable differences (jnds) in loudness were contained in the limits of 0.6 to 0.9 dB for normal hearing subjects and 0.9 – 1.4 dB for hearing-impaired subjects. Then the basic investigations of loudness of the AM stimuli in the normal and hearing-impaired subjects have started. The investigations were performed for the carrier frequency of 1000 Hz, four modulation depths equal to: 10, 40, 70, 100%, and for two sensation levels equal to 50 and 80 dB. The obtained results were presented in Fig. 4 for SL = 50 dB and Fig. 5, for SL = 80 dB. The ordinate gives the SPL differences in decibels between signal (sinusoidal stimulus) and standard (AM stimulus) at which the two stimuli were judged equally loud. The standard deviation for most measurements was in the range of 1 – 3 dB.

Figure 4A shows the data for normal-hearing subjects. As can be seen, for low f_m loudness differences (ΔSPL) for the tested stimuli do not change significantly with f_m. But for higher f_m (approximately beyond the critical band) ΔSPL increases with f_m. This dependence is particularly noticeable for larger AM modulation depths. As an instance for $m = 10\%$, ΔSPL increases, on an average, about 1 dB/oct while for $m = 100\%$, the increase amounts to about 4 dB/oct. In general one can accept that the AM stimuli are perceived in all cases tested as louder in relation to sinusoidal stimuli. The loudness differences depend on the m in the sense, that the greater the value m, the greater the difference of loudness. For low f_m at $m = 10\%$, the value of ΔSPL fluctuates in the limits 3 – 6 dB, while for $m = 100\%$ in the limits 7 – 12 dB (depending on the subject). Analogical dependences are to be observed also in Fig. 5A, for SL = 80 dB. The ΔSPL values are in this case also a certain linear function of the modulation depth. They are approximately constant for low f_m, whereas for higher f_m

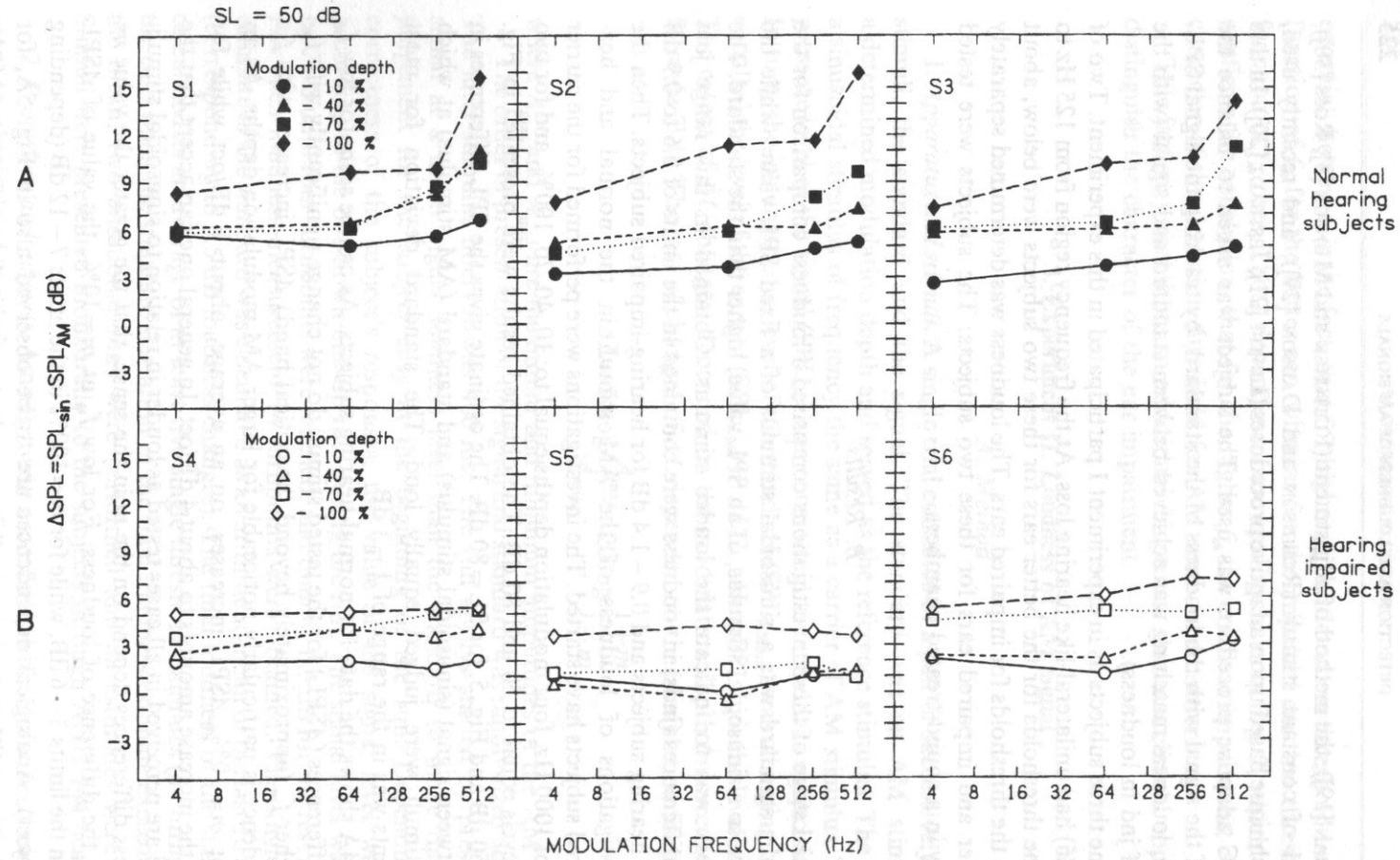

Fig. 4. SPL differences between signal and standard as a function of modulation frequency. The ordinate gives the difference in dB between SPL of the signal (sinusoidal stimulus) and SPL of the standard (AM stimulus) for the matched (balanced) signal to standard loudness. Matching was done by 3 normal-hearing subjects (A — filled symbols) and 3 hearing-impaired subjects (B — open symbols). Parameter of the curves is the modulation depth equal: 10, 40, 70 and 100%. Sensation level (SL) = 50 dB.

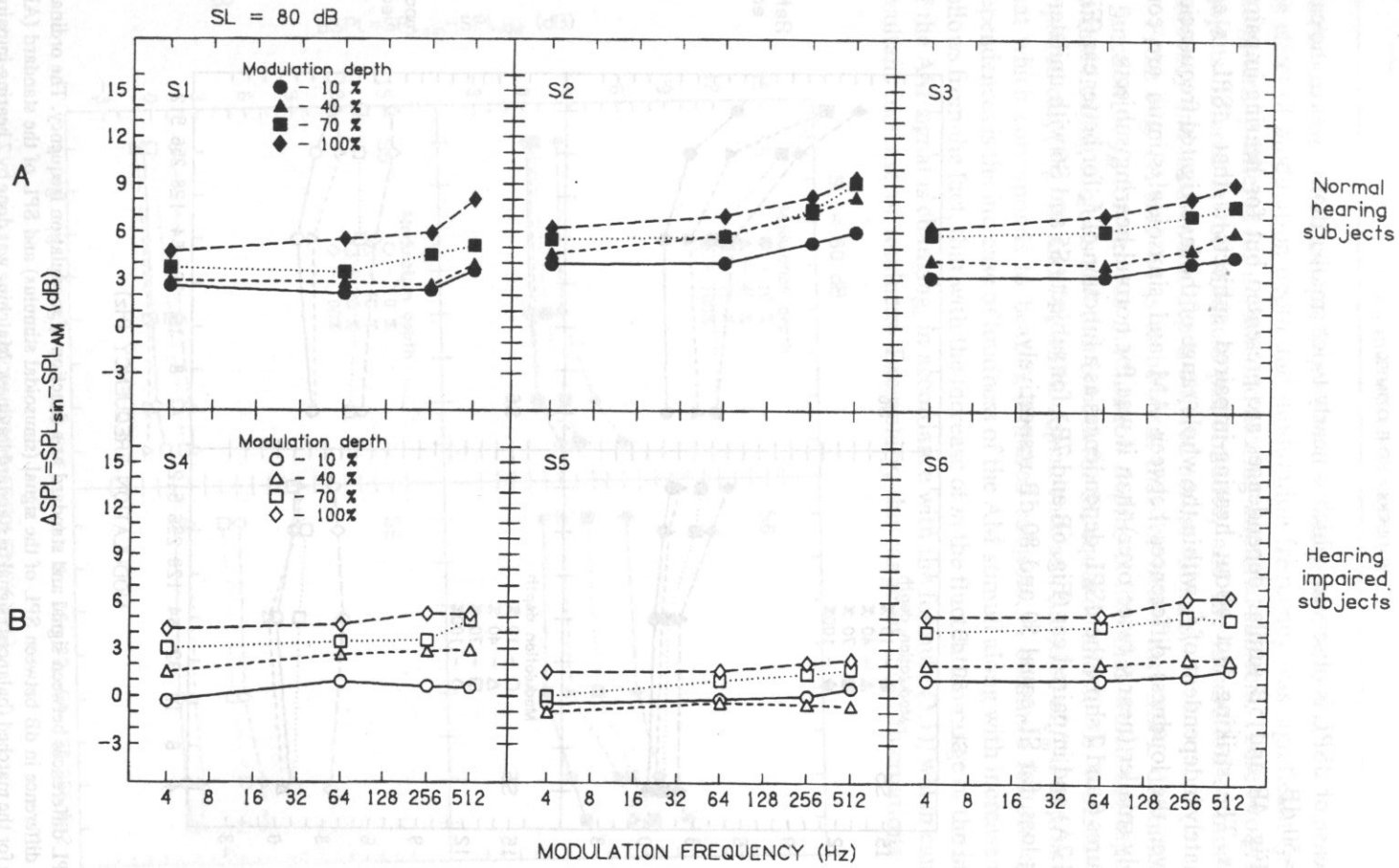

Fig. 5. As Fig. 4 but for SL = 80 dB.

an increase of ΔSPL is observed, which is nearly twice smaller than it was in the case of SL = 50 dB.

In Fig. 4B and 5B similar dependences are presented but for hearing-impaired subjects. The striking fact about hearing-impaired subjects is that ΔSPL is approximately independent of f_m within the whole range of the investigated frequencies. Moreover the loudness differences between AM and sinusoidal stimuli are considerably smaller (nearly twice over) than it was for normal-hearing subjects.

Figures 6 and 7 show the ΔSPL dependences as a function of f_m for better ear (Fig. 6A and 7A) and impaired ear (Fig. 6B and 7B), for subjects S5 and S6 with unilateral hearing loss, for SL equal 50 and 80 dB respectively.

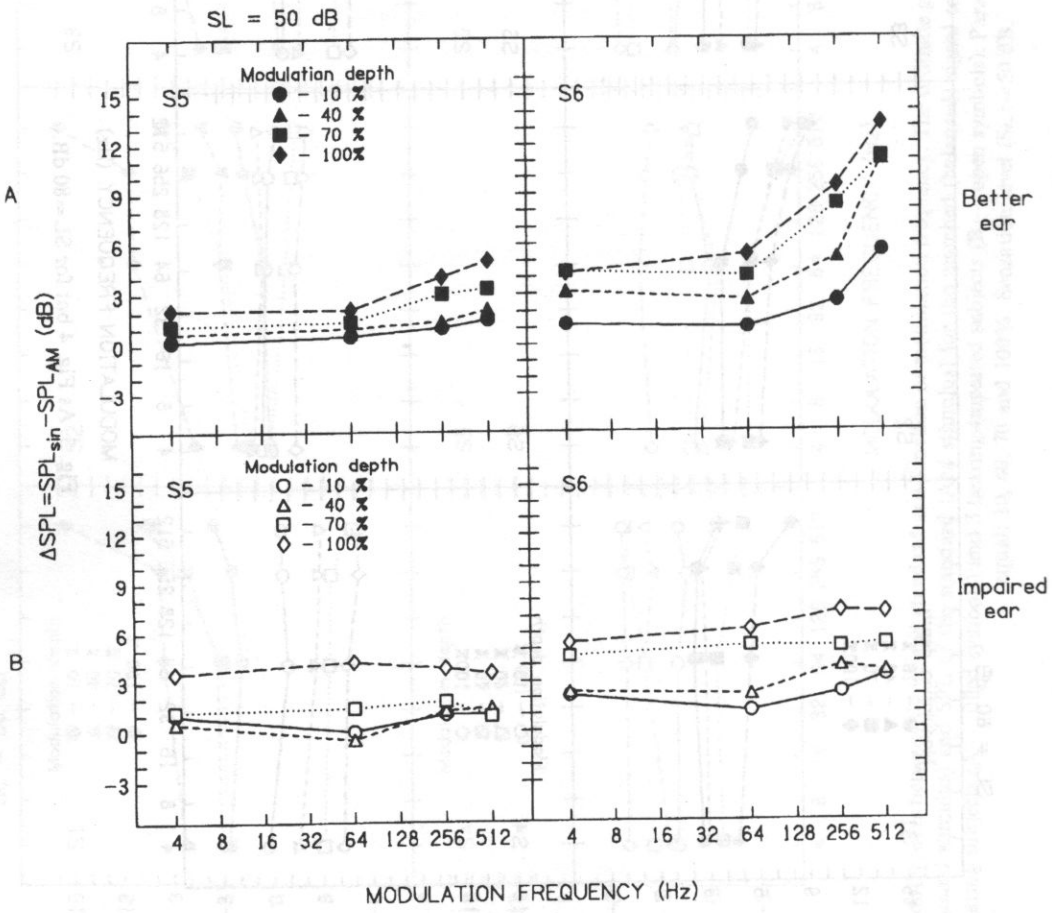

Fig. 6. SPL differences between signal and standard as a function of modulation frequency. The ordinate gives the difference in dB between SPL of the signal (sinusoidal stimulus) and SPL of the standard (AM stimulus) for the matched (balanced) signal to standard loudness. Matching was done by 2 hearing-impaired subjects, with one better ear (A — filled symbols) and the other one poorer (B — open symbols). Parameter of the curves is the modulation depth equal: 10, 40, 70 and 100%. Sensation level (SL) = 50 dB.

An analysis of variance performed on the data presented in Fig. 4–7 showed that the effect of modulation depth and modulation frequency was significant ($p<0.05$) and generally differed for normal and hearing-impaired subjects. These two groups of subjects differed in the loudness performance, and the interaction of modulation frequency and modulation depth differed across subjects.

From Fig. 6A and 7A is to be seen, that for better ear, ΔSPL dependences as a function of f_m for various modulation depths is like that which corresponds to normal-hearing subjects and that is both for SL equal 50 and 80 dB. Whereas for the impaired ear, (Fig. 6B and 7B) ΔSPL dependence as a function of f_m is approximately that which corresponds to hearing-impaired subjects. A common feature of those dependences is the increase of loudness of the AM stimuli along with increase of m. It follows from the fact, that with the increase of m the fluctuation range of the intensity of the AM signal is changing, in accordance with the formula (3.1), which causes the resultant increase of loudness. Exemplary, the range of those fluctuations for the

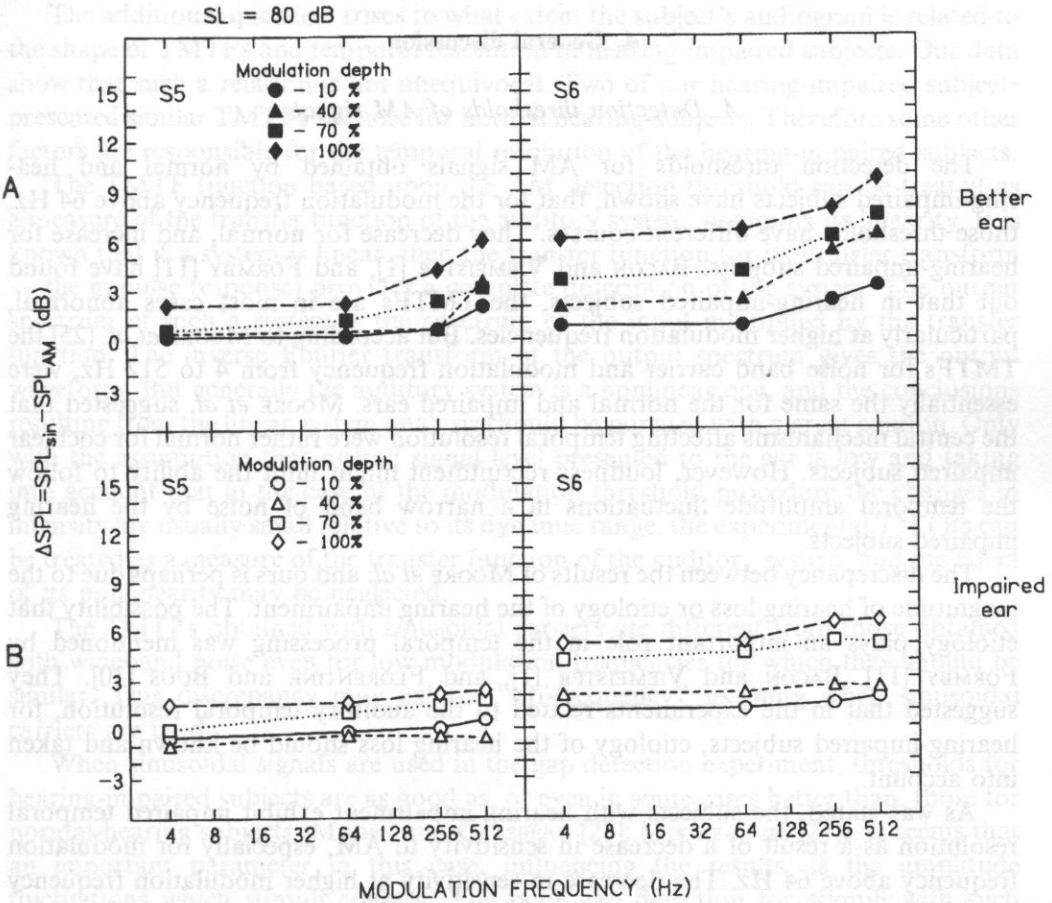

Fig. 7. As Fig. 6 but for SL = 80 dB.

successive modulation depths equal 10, 40, 70% amounts to: 1.7; 7.4 and 15.1 dB, respectively. Maximal intantaneous intensity level, for successive modulation depths (10, 40 and 70%), is equal to $SPL_{AM}+\Delta L/2$. For $SPL_{AM}=50$ dB, it gives as a result the values: 50.9; 53.7 and 57.5 dB. The calculated instantaneous increments of intensity level caused by amplitude modulation amounted to: 0.9; 3.7 and 7.5 dB. Thus, changes in instantaneous intensity of the AM signals, produced by modulation should be related to changes in the resultant loudness of the signal. The increments of loudness of the AM stimuli relative to sinusoidal signal obtained in the psychoacoustic experiment are shown in Fig. 4–7. As can be seen from those figures, for the normal-hearing subjects and SL=50 dB, increments of intensity levels for the AM the signal relative to sinusoidal one, determined subjectively, are larger than the increments calculated according to formula (3.1). A smaller discrepancy of the calculated and subjectively determined increments of intensity levels is observed for hearing-impaired subjects.

4. General discussion

A. Detection thresholds of AM signals

The detection thresholds for AM signals obtained by normal and hearing-impaired subjects have shown, that for the modulation frequency above 64 Hz, those thresholds have different courses. They decrease for normal, and increase for hearing-impaired subjects. BACON and VIEMEISTER [1], and FORMBY [11] have found out that in hearing-impaired subjects, the TMTFs are in most cases abnormal, particularly at higher modulation frequencies. But according to MOORE *et al.* [25] the TMTFs for noise band carrier and modulation frequency from 4 to 512 Hz, were essentially the same for the normal and impaired ears. MOORE *et al.* suggested that the central mechanisms affecting temporal resolution were rather normal for cochlear impaired subjects. However, loudness recruitment might limit the ability to follow the temporal amplitude fluctuations in a narrow band of noise by the hearing impaired subjects.

The discrepancy between the results of MOORE *et al.* and ours is perhaps due to the magnitude of hearing loss or etiology of the hearing impairment. The possibility that etiology plays an important role in the temporal processing was mentioned by FORMBY [11], BACON and VIEMEISTER [1], and FLORENTINE and BUUS [10]. They suggested that in the experiments related to the auditory temporal resolution, for hearing-impaired subjects, etiology of the hearing loss should be known and taken into account.

As was stated, the subjects with hearing impairment exhibit impaired temporal resolution as a result of a decrease in sensitivity to AM, especially for modulation frequency above 64 Hz. The decrease in sensitivity at higher modulation frequency results in steep high-frequency attenuation rate in a TMTF. For subjects with hearing impairment the rates can be twice those for normal hearing subjects (BACON and

VIEMEISTER [1]; FORMBY [11]). Abnormal TMTFs in the subjects with high-frequency hearing loss may reflect impaired temporal resolution or a restricted perceived bandwidth. It is also possible that the decrease in sensitivity to AM in hearing impaired subjects reflects a decrease in the SL of the carrier. It happens quite often that for subjects with high-frequency hearing impairment, energy at this frequency region, is just audible or even inaudible despite the high SL of the carrier. On the other hand, it is not possible to test these subjects at high SLs, because of the limited dynamic range of their hearing.

Some papers (PIERCE *et al.* [27]; HALL *et al.* [15]; HALL and GROSE [16]) suggest, that for high modulation rate, AM is not detected with time-domain cues but with combined spectro-temporal cues. The detection of AM at high modulation frequency may depend on across-frequency spectro-temporal cues rather than on time-based cues. It could account for the ability to detect high rates of modulation by the subject. But at a low modulation frequency, AM detection is mainly based on temporal cues. For intermediate modulation frequency the situation remains rather unclear.

The additional question arises to what extent the subject's audiogram is related to the shape of TMTFs and temporal resolution of hearing-impaired subjects. Our data show that such a relation is not unequivocal. Two of our hearing-impaired subjects presented similar TMTFs as those for normal hearing-subjects. Therefore some other factors are responsible for the temporal resolution of the hearing-impaired subjects.

The TMTF function based upon the AM detection threshold can be treated as a measure of the transfer function of the auditory system, assuming its linearity. It is known that if a system is linear, then the transfer function (or its Fourier transform — the impulse response) provides a complete description of the system. The output spectrum of such a system is the spectrum of the input multiplied by the transfer function. The inverse Fourier transform of the output spectrum gives the output waveform. But generally the auditory system is a nonlinear one, and the conclusions resulting from the linear system analysis should be pursued with a great caution. Only with the assumption that overall signal level presented to the ear is low and taking into account that in the case of the modulation threshold procedure the changes in intensity are usually small relative to its dynamic range, the experimental TMTFs can be treated as a measure of the transfer function of the auditory system, and the effect of its nonlinearity may be neglected.

The TMTFs obtained with sinusoidal carriers are different from those obtained with wideband noise even for low modulation frequencies for which they should be similar. This discrepancy may exhibit "off-frequency" listening when sinusoidal carriers are used.

When sinusoidal signals are used in the gap detection experiment, thresholds for hearing-impaired subjects are as good as, or even in some cases better than, those for normal-hearing subjects (MOORE and GLASBERG [23]; MOORE *et al.* [24]). It seems that an important parameter in this case, influencing the results, is the amplitude fluctuations which stimuli contain. The poor gap detection for stimuli with such fluctuations might result from the loudness recruitment.

B. Loudness of AM signal

Psychoacoustic data related to the estimation of loudness of the AM stimuli by normal and cochlear-impaired subjects indicated that the estimation, in the range of higher modulation frequency is different. The striking fact about hearing-impaired subjects is that ΔSPL is approximately independent of f_m in the whole range of the modulation frequencies tested. SCHARF and HELLMAN [32] also noticed a different loudness summation for normal and cochlear-impaired subjects. They investigated the loudness of complex sounds as a function of the frequency spacing (ΔF) between the lowest and highest components, and stated that loudness increased considerably with ΔF in the normal ear, whereas it remained independent of ΔF in the impaired ear. Thus, although an inner-ear pathology produces the same high thresholds and similar loudness functions for pure tone (HELLMAN and ZWISLOCKI [18]), they seem to affect the summation of loudness summation in the normal and cochlear impaired ear. Normally, increasing the bandwidth of a complex sound of fixed energy up to the critical band does not change its loudness, because the excitation pattern to which loudness is directly related, does not change. In this case the loudness depends only upon the overall SPL of the complex sound. But if the bandwidth increases out of the critical bandwidth, it involves a change in the excitation pattern, and the loudness of the complex sound starts to increase. This is the case for noise bands (ZWICKER *et al.* [42]) and complexes consisting of pure tones (SCHARF [31]). The similar rule may hold in cochlear pathology, the difference being that the critical bands are much wider for hearing-impaired subjects than for normal-hearing subjects (de BOER [3]; SCHARF and HELLMAN [32]). If the critical band is very wide in the impaired ear, narrow-band stimuli (e.g. AM signals with low modulation frequency) ought to produce the same large spread of excitation as wide-band stimuli (e.g. AM signals with high modulation frequency). So the total excitation remains approximately constant even as the stimulus bandwidth (modulation frequency) increases. Thus, if the critical-band mechanism did not analyze the excitation pattern in the cochlear-impaired ear, then the overall loudness of the AM stimulus would not depend on the stimulus bandwidth (modulation frequency), as was stated in this paper.

Perhaps in special cases of hearing loss, impairment of the critical-band mechanism may, without changing the excitation patterns, change the relation between loudness and excitation. Some impaired ears appear to be unable to integrate energy over intervals as long as those used by the normal ear (GENGEL and WATSON [12]). Also greater temporal masking in hearing-impaired listeners with large intrasubject variability has been reported (ELLIOTT [4]). Besides, hearing loss can also alter frequency selectivity of the auditory system and deform the auditory filter shapes (SOMMERS and HUMES [33], GLASBERG and MOORE [13]).

The loudness of AM signals, especially for low SPL, may also be affected by the loudness recruitment. It is known that for subjects with cochlear hearing loss, for low SPL, the loudness of sounds increases more rapidly with increasing SPL than for normal-hearing subjects. This rapid loudness growth continues until to a relatively

high SPL, and then reaches the normal increase. Thus, for hearing-impaired subjects, the instantaneous changes in intensity of AM signals might result in larger changes in instantaneous loudness compared with normal-hearing subjects. This hypothesis should be verified experimentally.

It is worth adding at the end, that perhaps the different mechanism of the loudness summation for normal and hearing-impaired subjects could be an additional diagnostic clue in a clinical application to distinguish the character of the ear impairment. It is also worth turning attention to the fact that as stated in the paper, for the cochlear-impaired subjects, the increase of the AM detection threshold in the range of higher modulation frequencies, and the likewise found for those subjects, loudness independence of amplitude changes rate of the signal, may appear to be useful at designing new hearing aids.

5. Conclusions

Detection threshold obtained with sinusoidal carriers AM modulated are roughly similar for normal and cochlear-impaired subjects but only for the low modulation frequency (below 64 Hz). However, for higher modulation frequency, the thresholds decrease for the normal-hearing subjects, whereas they tend to increase for the hearing-impaired subjects.

For modulation frequency f_m greater than the critical band, loudness of AM signals increased with f_m for the normal-hearing subjects, whereas it remained independent of f_m for the hearing-impaired subjects.

Acknowledgments

We thank Dr A. Sekula from the Audiology Department of the Swięcickiego Hospital in Poznań for providing the subjects with hearing loss. This work was supported by the Geers Hörgeräte Company from Germany and by the State Committee of for Scientific Research (KBN, grant no 2 00 71 9101).

References

[1] S.P. BACON and N.F. VIEMEISTER, *Temporal modulation transfer functions in normal-hearing and hearing-impaired listeners*, Audiology, **24**, 117–134 (1985).

[2] S.P. BACON and R.M. GLEITMAN, *Modulation detection in subjects with relatively flat hearing losses*, J. Speech Hear. Res., **35**, 642–653 (1992).

[3] E. de BOER, *Measurement of critical bandwidth in case of perception deafness*. Proc. Int. Congr. Acoust. 3rd, Stuttgart, Amsterdam, Elsevier, 100–102 (1959).

[4] L.L. ELLIOTT, *Temporal and masking phenomena in persons with sensorineural hearing loss*, Audiology Basel, **14**, 336–353 (1975).

[5] E.F. EVANS, *Cochlear nerve and cochlear nucleus*, in: *Handbook of Sensory Physiology. Behavioral Studies and Psychoacoustic*, [Eds.] W.D. Keidel and W.D. Neff Springer-Verlag, 1975, Berlin vol. 5, pt. 2, 4–108 (1974).

[6] P.J. FITZGIBBONS and F.L. WIGHTMAN, *Gap detection in normal and hearing-impaired listeners*, J. Acoust. Soc. Am., **72**, 761–765 (1982).
[7] P.J. FITZGIBBONS, *Temporal gap detection in noise as a function of frequency, bandwidth and level*, J. Acoust. Soc. Am., **74**, 67–72 (1983).
[8] H.F. FLETCHER and W.A. MUNSON, *Loudness, its definition, measurement and calculation*, J. Acosut. Soc. Am., 5, 82–108 (1933).
[9] M. FLORENTINE and S. BUUS, *Temporal resolution as a function of level and frequency*, Proc. 11th Int. Congr. Acoust., **3**, 103–106 (1983).
[10] M. FLORENTINE and S. BUUS, *Temporal gap detection in sensorineural and simulated hearing impairments*, J. Speech Hear. Res., **27**, 449–455 (1984).
[11] C. FORMBY, *Modulation detection by patients with eight-nerve tumors*, J. Speech Hear. REs., **29**, 413–419 (1986).
[12] J.L. GENGEL and C.S. WATSON, *Temporal integration. I. Clinical implications of a laboratory study. II Additional data from hearing-impaired subjects*, J. Speech Hear. Disord., **36**, 213–224 (1971).
[13] B.R. GLASBEG and B.C.J. MOORE, *Auditory filter shapes in subjects with unilateral and bilateral cochlear impairments*, J. Acoust. Soc. Am., **79**, 1020–1030 (1986).
[14] B.R. GLASBEG, B.C.J. MOORE and S.P. BACON, *Gap detection and masking in hearing-impaird and normal-hearing subjects*, J. Acoust. Soc. Am., **81**, 1546–1556 (1987).
[15] J.W. HALL, A.C. DAVIS, M.P. HAGGARD and H.C. PILLSBURY, *Spectro-temporal analysis in normal-hearing and cochlear-impaired listeners*, J. Acoust. Soc. Am., **84**, 1325–31 (1988).
[16] J.W. HALL and J.W. GROSE, *Spectro-temporal analysis in cochlear hearing impairment: effects of frequency selectivity, temporal resolution, signal frequency, and rate of modulation*, J. Acoust. Soc. Am., **85**, 2550–62 (1989).
[17] R.P. HELLMAN and J.J. ZWISLOCKI, *Some factors affecting the estimation of loudness*, J. Acoust. Soc. Am., **33**, 687–694 (1961).
[18] R.P. HELLMAN and J.J. ZWISLOCKI, *Loudness function of a 1000-cps tone in the presence of a masking noise*, J. Acoust. Soc. Am., **36**, 1618–1627 (1964).
[19] R.P. HELLMAN, *Dependence of loudness growth on skirts of excitation patterns*, Acoust. Soc. Am., **63**, 1114–1119 (1978).
[20] W. JESTEADT, *An adaptive procedure for subjective judgments*, Percept. and Psychoph. **28**, 85–88 (1980).
[21] H. LEVITT, *Transformed up-down methods in psychoacoustics*, J. Acoust. Soc. Am., **49**, 467–477 (1971).
[22] E. LÜSCHER and J.J. ZWISLOCKI, *A simple method for indirect monaural determination of the recruitment phenomena. (Difference limen in intensity in different types of deafness)*, Acta Oto-laryngol. Suppl., **78**,156–167 (1949).
[23] B.C.J. MOORE and B.R. GLASBERG, *Gap detection with sinusoids and noise in normal, impaired and electrically stimulated ears*, J. Acoust. Soc. Am., **83**, 1093–1101 (1988).
[24] B.C.J. MOORE, B.R. GLASBERG, E. DONALDSON, T. MCPHERSON and C.J. PLACK, *Detection of temporal gaps in sinusoids by normally hearing and hearing-impaired subjects*, J. Acoust. Soc. Am., **85**, 1266–1275 (1989).
[25] B.C.J. MOORE, M.J. SHAILER and G.P. SCHOONEVELDT, *Temporal modulation transfer functions for band-limited noise in subjects with cochlear hearing loss*, Brit. J. Audiol., **26**, 229–237 (1992).
[26] J.O. PICKLES, *The neurophysiological basis of frequency selectivity. Frequency selectivity in hearing*. B.C.J. Moore (Ed.) (pp. 51–121), Academic Press, London 1986.
[27] J.R. PIERCE, R. LIPES and C. CHEETHAM, *Uncertainty concerning the direct use of time information in hearing: Place cues in white spectra stimuli*, J. Acoust. Soc. Am., **61**, 1609–21 (1977).
[28] M. RODENBURG, *Investigation of temporal effects with amplitude modulated signals*. in: *Psychophysics and Physiology of Hearing*, [Eds.] E.F. Evans and J.P. Wilson, Academic, London 1977, pp. 429–437.
[29] D.W. ROBINSON and R.S. DADSON, *A re-determination of the equal-loudness relations for pure tones*, Brit. J. App. Physics, **7**, 166–181 (1956).
[30] S. ROSS, *Matching functions and equal-sensation contours for loudness*, J. Acoust. Soc. Am., **42**, 778–793 (1967).

[31] B. SCHARF, *Complex sounds and critical bands*, Psychol. Bull., **58**, 205–217, (1961).
[32] B. SCHARF and R. HELLMAN, *Model of loudness summation applied to impaired ears*, J. Acoust. Soc. Am., **40**, 71–78 (1966).
[33] M.S. SOMMERS and L.E. HUMES, *Auditory filter shapes in normal-hearing, noise-masked normal, and elderly listeners*, J. Acoust. Soc. Am., **93**, 2903–2914 (1993).
[34] J.A. STILLMANN, J.J. ZWISLOCKI, M. ZHANG and L.K. CEFARATTI, *Intensity just-noticeable differences at equal-loudness levels in normal and pathological ears*, J. Acoust. Soc. Am., **93**, 425–434 (1992).
[35] L. SWISHER, *Response to intensity change in cochlear pathology*, Laryngoscope, **76**, 1706–1713 (1966).
[36] C.W. TURNER, J.J. ZWISLOCKI and P.R. FILION, *Intensity discrimination determined with two paradigms in normal and hearing-impaired subjects*, J. Acoust. Soc. Am., **86**, 109–115 (1989).
[37] R.S. TYLER, *Frequency resolution in hearing-impaired listeners*, in: *Frequency selectivity in hearing*, B.C.J. MOore (Ed). (pp. 309–371), Academic Press, London 1986.
[38] N.F. VIEMEISTER, *Temporal factors in audition: a systems analysis approach*, in *Psychophysics and Physiology of Hearing*, [Eds.] E.F. Evans and J.P. Wilson, Academic, London 1977, pp. 419–428.
[39] N. F. VIEMEISTER, *Temporal modulation transfer function based upon modulation thesholds*, J. Acoust. Soc. Am., **66**, 1364–1380 (1979).
[40] E. ZWICKER, *Die Grenzen der Hörbarkeit der Amplitudenmodulation und der Frequenzmodulation eines Tones*, Acustica, **2**, 125–133 (1952).
[41] E. ZWICKER, *Die elementaren Grundlagen zur Bestimmung der Informationskapazitnt des Gehörs*, Acustica, **6**, 365–381 (1956).
[42] E. ZWICKER,G. FLOTTORP and S.S. STEVENS, *Critical bandwidth in loudness summation*, J. Acoust. Soc. Am., **29**, 548–557 (1957).
[43] E. ZWICKER and H. FELDTKELLER, *Das Ohr als Nachrichtenempfänger*, S. Hirzel Verlag, Stuttgart 1967.
[44] J.J. ZWISLOCKI, *Temporal summation in loudness*, J. Acoust. Soc. Am., **46**, 431–441 (1969).

ARCHIVES OF ACOUSTICS
20, 3, 237–246 (1995)

TEMPERATURE INCREASE IN A TWO-LAYER OBSTETRIC MODEL OF TISSUES IN THE CASE OF LINEAR AND NONLINEAR PROPAGATION OF A CONTINUOUS ULTRASONIC WAVE

L. FILIPCZYŃSKI and J. WÓJCIK

Department of Ultrasonics
Institute of Fundamental Technological Research
Polish Academy of Sciences
(00-049 Warszawa, Świętokrzyska 21)

The object of the present study was the analysis of temperature effects which arise in a two-layer tissue model applied in obstetrics, from the point of view of continuous wave radiation of a focussed Gaussian ultrasound beam. In particular, the authors considered nonlinear propagation using the weak shock theory and compared the results of the analysis with those obtained assuming linear propagation. It was demonstrated that for 3 MHz, 10 cm focal length of the beam, the transducer diameter of 1 cm and the intensity of 0.1 W/cm^2 the schock parameter does ot then exceed 1.66^0 cm. For a radiated intensity equal to 1 W/cm^2 the shock coefficient is higher than unity, causing losses related to nonlinear propagation. The temperature distributions were determined along the beam axis using both the weak shock theory and the linear propagation procedure.

1. Introduction

In the past years the first of the authors showed that ultrasonic Doppler equipment could cause a temperature increase on the body surface up to about 10°C [6, 7]. The measurements were taken using thermographic equipment showing decidedly that ultrasonic diagnostic equipment could cause relatively large temperature increase.

It is an important problem from the point of view of a threat caused by ultrasound to a foetus. In keeping with recommendation of the World Federation for Ultrasound and Biology [13], the permissible increase of the foetus temperature is 1.5°C above the physiological temperature of 37°. If the temperature rises to 41°C higher the nervous system of the child being born can be endangered, with e.g. tragic effects for it (teratism).

For ethical reasons direct measurements in the pregnant woman's uterus are impossible. Therefore, for several years attempts have been made to determine temperature increase analytically.

The purpose of this study is to determine temperature increases for diagnostic c.w. ultrasound beams. In obstetrics c.w. equipment is very broadly used to monitor and alert physicians in the case of a threat to a foetus in his mother's womb. According to Japanese data [11], intensities applied in c.w. diagnostic Doppler equipment vary between 10 and 330 mW/cm^2. In the present study both linear and nonlinear types of propagation are considered; the purpose is to find a limiting ultrasound intensity at which relatively simple and proven calculation methods developed for linear propagation may still be used.

2. A diagnostic ultrasound beam and a two-layer tissue model

In a previous work [9] the authors calculated temperature increases in a two-layer tissue for 6 ultrasonic probes. The frequencies of these probes were 3, 5 and 7.5 MHz the focal lengths were 10, 5, 4, 3 i 2 cm, and the transducer diameters were 20, 13, 9.6 and 6 mm. The calculated results showed that the greatest temperature increases occurred when a 3 MHz beam was applied, one which was generated by a piezoelectric transducer with radius $d=1$ cm and a focal length of 10 cm. Therefore, our further considerations will be restricted to such an ultrasonic beam which is the worst case.

Just as in the study cited above, the Gaussian beam model was assumed. It was for such a beam that such temperature increases as occurred for a continuous wave were published [14]. Moreover, the Gaussian beam is convenient because of the simplicity of mathematical transformations; additionally, it gives results which, as Wu and Nyborg showed, are very close to the real beams [15].

A temperature increase depends on the absorption and thermal conductivity of tissues as well on the heat generated by the ultrasonic probe. The latter may be ignored, for it has only a superficial effect, whereas the heat sources caused by absorption are volumetric. The cooling effect of blood is also neglected so as to consider the worst patient case.

The tissue model under consideration consists of two layers. The first one is water, analogous to the physiological liquids which fill the space between the body surface and the foetus. The other layer is the soft tissue of the foetus itself. It was shown in study [9] that in the case of a continuous wave there was the highest temperature increase in the beam focus (see Fig. 6.1 in the study cited above). It is a result of no attenuation of ultrasonic beam in the first (liquid) layer.

Moreover, it is assumed here that the thickness z_l of the first liquid layer is equal to the physical focal length $z_f=10$ am. It is than that an almost maximum temperature increase occurs (see Fig. 4 of study [15]).

3. Basic formulae

Given the beams and tissues thus selected, the nonhomogenous equation of thermal conductivity can be solved in a form which neglects the cooling blood flow (perfusion)

$$\partial T/\partial t = a \nabla^2 T + Q/\rho c_s, \tag{3.1}$$

where T is the tissue temperature, t is time, $a=\lambda_c/\rho$ is a thermal conductivity coefficient, ∇^2 is the Laplace operator, ρ is the tissue density, c_s is the specific heat, Q is the power density of the heat sources, depending on the attenuation coefficient α, which is a function of frequency and the intensity I, according to the relation

$$Q = 2\alpha(f)\, I(x, y, z). \tag{3.2}$$

This relation is valid only for linear wave propagation. In a general nonlinear case the coefficient α is replaced by the attenuation parameter α_r, which is defined using the general relation [4]

$$\alpha_p = -(\operatorname{div} \mathbf{I})/2\,\mathrm{I}, \tag{3.3}$$

where $\mathbf{I}$, I are respectively the vector and value of a local wave intensity.

The power density of the heat sources (the power density absorbed in tissues) has the general form [3], [12] of

$$Q = -\operatorname{div} \mathbf{I}. \tag{3.4}$$

The intensity vector in a focussed Gaussian beam in a cylindrical coordinate system z, r is in the form (see equation A4 in [4]) of

$$\mathbf{I}(z, r) = \mathbf{I}(o, o) G^2 \exp[-2r^2/a_e^2(1+R^2)]\{e_r rR/r_0(1+R^2)^2 + e_z 1/(1+R^2))\times \tag{3.5}$$

$$\sum_{n=1}^{\infty} B_n^2[\sigma(z, r)] = \mathrm{I}'(z, r) \sum_{n=1}^{\infty} B_n^2[\sigma(z, r)],$$

where z, r — coordinates of the cylindrical system, $R=(z-z_f)h^{1/2}$, z_f — physical focal length, k-$2\pi f/c_0$ — wave number, $h=(kR_0^2/2z_a)^2$, c_0 — wave velocity of low amplitude waves, σ — shock parameter [1], $a_0^2=R_0^2/(1+h)$ — beam radius at the focus for the amplitude level $\exp(-1)$, R_0 — radius for which the vibration velocity on the transducer surface falls to $e^{-1} \cong 0.37$ of its maximum amplitude [8], $r_0=ka_0^2/2$, e_r, e_z — respective unit vectors of the cylindrical coordinate system, G — amplitude gain in the focus.

In the geometrical focus the amount of the gain in a Gaussian beam can be determined from formula (23) in study [8]. Then

$$G_g = \mid p,(z_0, 0)/p(0,0) \mid = kR_0^2/2z_0, \tag{3.5a}$$

p is the acoustic pressure in the beam. The gain in the physical focus, where the maximum amplitude occurs, is a slightly larger

$$G = (h+1)^{1/2} = G_f = \mid p(z_g, 0)/p(0,0) \mid > G_g. \tag{3.5b}$$

It can be calculated by determining the value of z_f given by formula (5a) in study [9]

$$z_f = z_g[1+4z_g^2/k^2R_0^4)]^{-1} = z_g h/(1+h) \cong z_g. \tag{3.5c}$$

In study [4] the authors assumed a different value of the amplitude gain

$$G_D = d/a = dkR_0/2z_g, \tag{3.5d}$$

which seems to be doubtfull since for the Gaussian beams exact are the values given by (3.5a), (3.5b), (3.5c).

According to [4], the last term of expression (3.5) is determined in terms of the weak shock theory proposed by BLACKSTOCK [1]. B_n is the harmonic coefficient of the distorted wave.

$$B_n[\sigma(z\,r)] = 2[n\pi\sigma]^{-1}\left\{\Phi_{\min} + \int_{\Phi_{\min}}^{\pi} \cos n[\Phi - \sigma\sin\Phi]d\Phi\right\}, \tag{3.6}$$

$\Phi_{\min}$ is the root of the equation $\Phi = \sigma(z,r)\,\sin\Phi_{\min}$ for $\sigma > 1$; $\Phi_{\min} = 0$ for $\sigma < 1$.

In a two-layer model with attenuation occurring for $z \geqslant z_l$ the intensity vector is

$$\mathbf{I}(z,r) = \mathbf{I}'(z\,r)\begin{cases} \sum_{n=1}^{\infty} B_n^2(z,r) & \text{for } z < z_l, \quad (3.7a) \\ \sum_{n=1}^{\infty} B_n^2(z,r)\exp[-2\sigma(n)(z-z_l)] & \text{for } z \geqslant z_l, \quad (3.7b) \end{cases}$$

where the vector field $I'(z,r)$ is lossless. The attenuation of the beam is represented in the second right term of Eq. (3.7 b). The attenuation coefficient α (for low amplitudes) is proportional to the (harmonic) frequencies $a(n) = n\alpha$.

The shock parameter σ for the Gaussian beam equals [4]

$$\sigma(z,r) = \beta\varepsilon k z_0 G\,(G^2-1)^{-1/2}\{\ln[G + (G^2-1)^{1/2})\,(R + (1+R^2)^{1/2})]\} \times \exp[-r^2/a_0^2(1+R^2)], \tag{3.8}$$

where $\beta = 1 + B/2A$, B/A — coefficient of nonlinearity equal for the muscle tissue and liver 7.5, for fat 11, for water 5.5, $\varepsilon = (2I_0/\rho c_0^3)^{1/2}$ — ratio of the particle velocity to c_0, $I_0 = I(0,0)$.

The value of Q can now be determined

$$Q = -\operatorname{div} I(z,r). \tag{3.9}$$

The vector $\mathbf{I}'$ in expressions (3.5) and (3.7 a, b) is a quantity formulated on the basis of the linear theory of the Gaussian beam, without any losses. Therefore, due to the energy conservation and Gauss laws

$$\int \mathbf{I}'d\mathbf{s} = \int \operatorname{div}\mathbf{I}'\,dv = 0, \tag{3.10}$$

where ds and dv are surface and volumen elements. Hence $\operatorname{div}\mathbf{I}' = 0$. On the other hand, the expression under the summation sign in Eq. (3.7) is a scalar U. Using then the vector relation one obtains

$$\operatorname{div} U\mathbf{I}' = U \operatorname{div} \mathbf{I}' + \mathbf{I}' \operatorname{grad} U = \mathbf{I}' \cdot \operatorname{grad} U. \tag{3.10b}$$

Therefore one obtains from relations (3.10b), (3.8), (3.7) and (3.5)

$$\text{for } z < z_l \quad \text{the value} \quad Q = Q_1, \tag{3.11a}$$

where

$$Q_1 = -C \exp\{-3r^2/a_0^2[1+R^2(z)]\}[1+R^2(z)]^{-1/2} \times \tag{3.11b}$$
$$\times \sum_{n=1}^{\infty} B_n[\sigma(z,r)] BP_n[\sigma(z,r)]$$

$$\text{for} \quad z \geqslant z_l \quad \text{the value} \quad Q = Q_L + Q_2, \tag{3.12a}$$

where

$$Q_L = 2I'^2 G^2 [1+R^2(z)]^{-1} \exp\{-2r^2/a_0^2[1+R^2(z)]\} \times \tag{3.12b}$$
$$\times \sum_{n=1}^{\infty} \sigma_n B_n^2[\sigma(z,r)] \exp[-2\alpha(n)(z-z_l)],$$

$$Q_2 = -C \exp\{-3r^2/a_0^2[1+R^2(z)]\}[1+R^2(z)]^{-1/2} \times \tag{3.12c}$$
$$\times \sum_{n=1}^{\infty} B_n[\sigma(z,r)] BP_n[\sigma(z,r)] \exp[-2\sigma(n)(z-z_l)],$$

and

$$C = 2I_0 \beta \varepsilon k G^3; \quad BP_n = B_{1n} - B_n/\sigma(z,r), \tag{3.12d, e}$$

$$B_{1n} = 2(\pi\sigma)^{-1} \int_{\Phi_{\min}}^{\pi} \sin[n(\phi - \sigma \sin(\phi))] \sin(\phi) d\phi. \tag{3.12f}$$

In the case of a plane wave the following dependence should then be satisfied

$$\beta \varepsilon k \gg \alpha. \tag{3.13}$$

When relation (3.13) is not valid shock can be neglected [1]. Study [10] also makes a similar suggestion. It demonstrates that for a plane wave in soft tissues, harmonic frequencies are very rapidly attenuated, preventing shock [12]. In a weakly focussed Gaussian beam this phenomenon must occur in a similar way when attenuation is strong, which, as in other studies, is assumed to be 5 Np/(m.MHz); particularly in the focal area, where the wave is close to a plane one. The solution of equation (3.1) under the initial conditions

$$T(x,y,z,t) = 0 \quad \text{for } t = 0, \tag{3.14}$$

and the boundary ones

$$\partial T/\partial z = 0 \quad \text{for } z = 0, \tag{3.15}$$

which are the same as in the previous author's study [9], a general solution is obtained in the form given there (3.14)

$$T=(4\pi\rho c_s)^{-1/2}\int_{-\infty}^{\infty}d\zeta\int_{-\infty}^{\infty}d\eta\int_{-\infty}^{\infty}d\zeta\int_{0}^{t}d\tau\,[4\pi a^3(t-\tau)^3]^{1/2}\cdot \exp[-\gamma^2(\zeta,\zeta,\eta)/4a(t-\tau)]\cdot Q(\zeta,\eta,|\zeta|), \tag{3.16}$$

where

$$\gamma^2=(x-\zeta)^2+(y-\eta)^2+(z-\zeta)^2. \tag{3.17}$$

After integration with respect to τ (see equation A6 in study [9]) and considering the relation erfc(0)=1 for t which tends to infinity, equation (3.16) becomes

$$T=(4\pi a\rho c_s)^{-1}\int_{-\infty}^{\infty}d\zeta\int_{-\infty}^{\infty}d\eta\int_{-\infty}^{\infty}d\zeta\,\gamma^{-1}Q(\zeta,\eta,|\zeta|). \tag{3.18}$$

Integral (3.18) can be expressed in a cylindrical coordinate system introducing the dependencies

$$\zeta=r'\cos\phi',\quad \eta=r'\sin\phi',\quad x=r\cos\phi,\quad y=r\sin\phi \tag{3.19}$$

then

$$r'^2=\zeta^2+\eta^2,\quad r^2=x^2+y^2,\quad d\zeta d\eta=r'dr'd\phi'. \tag{3.20}$$

The temperature distribution on the beam axis ($r=0$) is taken into account. Then, considering (3.19) and (3.20) in expression (3.18) integration is carried out with respect to ϕ' within the limits of 0, 2π, finally to give the form

$$T(r',\zeta,t=\infty)=(2a\rho c_s)^{-1}\int_{-\infty}^{\infty}d\zeta\int_{0}^{\infty}[r'^2+(z-\zeta)^2]^{-1}Q(r',|\zeta|)r'dr'. \tag{3.21}$$

Integral (3.21) was solved numerically for the following data: $I_0(0,0)=0.01$, 0.1, 1 W/cm, 3 W/cm, 5 W/cm, 6=5 Np/(m·MHz), $c=1500$ m/s, $c_s=4190$ J/(kg°C), $a=0.0015$ cm/s, $f=3$ MHz, $G=G_f=3.67$ ($G_g=3.53$), $d=1$ cm (the transducer radius), $R_0=0.75$ cm (see [9]), $z_f=10$ cm and $t=\infty$.

Table 1 shows the results of current calculations of the temperature increases T and the results determined for T_L using the previous linear procedure as applied in study [9]. These calculations were carried out for a two-layer TL model, where the

Table 1. Comaprison of temperature increases determined for a two-layer model in the cases of nonlinear T and linear T_L propagation

$I(z=0, r=0)$	W/cm²	0.01	0.1	1	3	5
T	°C	0.166	1.66	18.0	61.5	104.4
T_L	°C	0.166	1.66	16.6	49.8	83.0
T/T_L		1	1	1.08	1.23	1.26

first 10 cm thick layer was a liquid ($\alpha=0$) and the other was soft tissue ($a=5$ Np/(mMHz). The table also shows the maximum temperature found on the beam axis ($r=0$) close to the focus ($z\cong z_f$).

The linear procedure made it possible to apply simple extrapolation of temperature to any intensities I(0,0). For in the case of linear propagation a temperature increase is proportional to the intensity generated by the transducer (see Eq. (3.18) and A22 in study [9]). The temperature values determined in this way were denoted as T_L.

Figure 1 shows the distributions of the temperature increases T along the beam axis, determined by the weak shock method and based on formula (3.21) for the intensities $I(0,0)=0.1$ W/cm² and 1 W/cm².

Figure 2 shows analogous distributions of temperature increases T_L determined for the intensity $I(0,0)=0.1$ W/cm², assuming linear propagation (see Fig. 6.1 in study [9]).

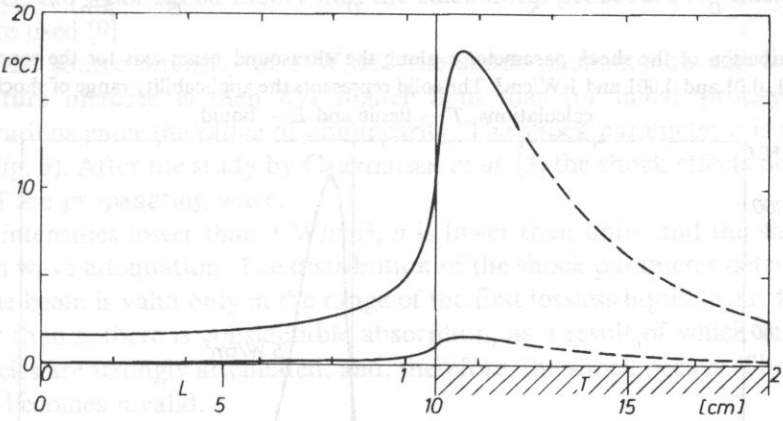

Fig. 1. Distribution of the increase in the temperature T along the axis of the ultrasound beam determined using the weak shock theory for the source intensity $I(0,0)=0.1$ and 1 W/cm². The solid line represents the applicability range of the weak shock theory. T denotes tissue and L — liquid.

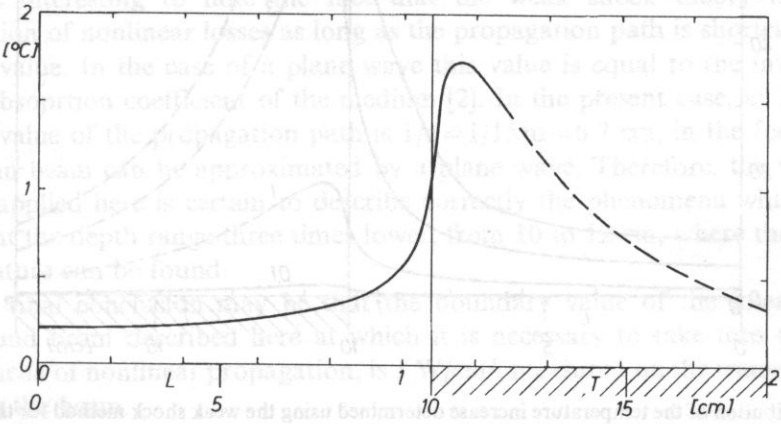

Fig. 2. Distribution of the increase in the temperature T along the axis determined using the linear procedure at the source intensity $I(0,0)=0.1$ and 1 W/cm². T — tissue and L — liquid.

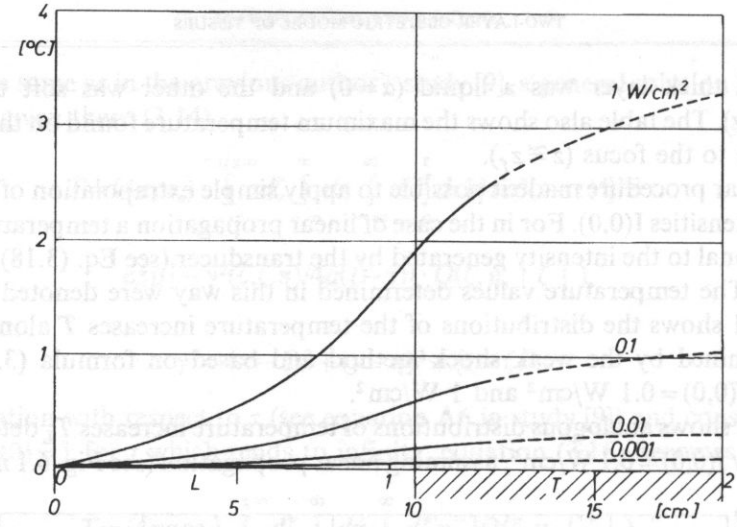

Fig. 3. Distribution of the shock parameter σ along the ultrasound beam axis for the source intensity $I(0,0)=1$, 0.1, 0.01 and 0.001 and 1 W/cm². The solid represents the applicability range of shock parameter calculations. T — tissue and L — liquid.

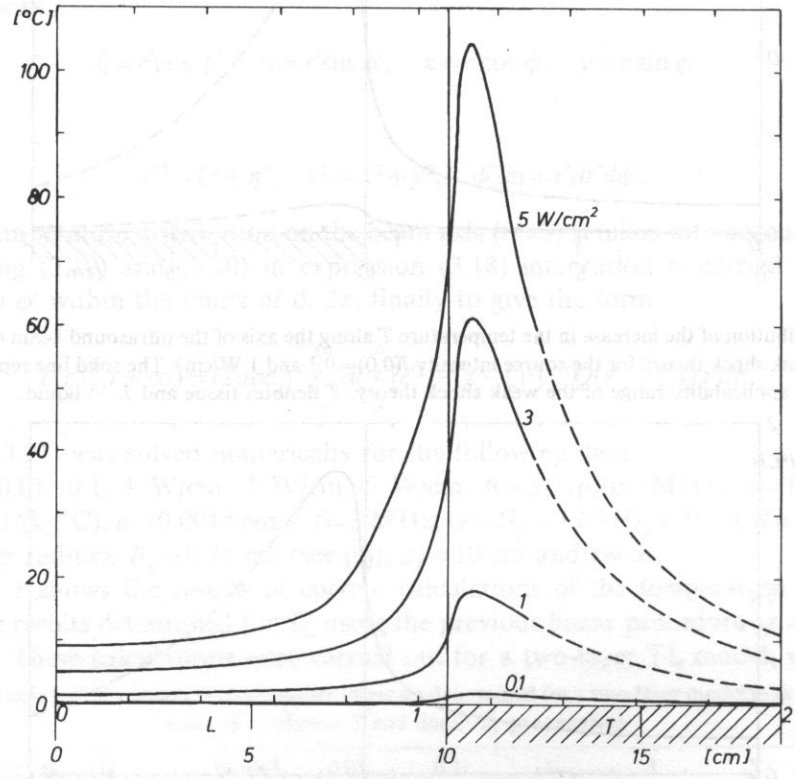

Fig. 4. Distribution of the temperature increase determined using the weak shock method for the intensities $I(0,0)=0.1$, 1, 3 and 5 W/cm². The solid represents the applicability range of the weak shock theory. T — tissue and L — liquid.

Figure 3 shows the distribution of the shock parameter along the beam axis, calculated from expression (3.12).

Figure 4 shows comparison of the distributions of temperature increases determined using the weak shock method for the intensities $I(0,0)=0.1$, 1, 3 and 5 W/cm^2.

4. Discussion and conclusion

The present analysis shows that in the case of ultrasonic diagnostic probes which generates the highest potential temperature increases, when working at a continuous wave, temperature increases determined with the assumption of linear and nonlinear propagation are the same for source intensities lower than 1 W/cm^2 (see Table). This result was obtained assuming a two-layer tissue model which is applied in obstetrics. Moreover, the weak shock theory and the calculation procedure for linear propagation were used [9].

For the source intensity of 1 W/cm^2 the shock phenomenon can be seen. The temperature increase is then 8% higher than that for linear propagation. The considerations enter the range of nonlinearity. The shock parameter σ is higher than unity (Fig. 3). After the study by CARSTENSEN *et al.* [3] the shock effects decidedly the losses of the propagating wave.

For intensities lower than 1 W/cm^2, σ is lower than unity and the shock has no effect on wave attenuation. The distribution of the shock parameter determined here along the beam is valid only in the range of the first lossless liquid layer. In tissue for z higher than z_l there is considerable absorption, as a result of which the harmonic frequencies are strongly attenuated, and, therefore, the shock decays. Then the curve $\sigma=\sigma(z)$ becomes invalid.

The temperature distributions on the beam axis determined using the weak shock theory (Fig. 1) and the linear procedure (Fig. 2) are very close to each other. It seems to confirm the validity of both methods.

It is interesting to note the fact that the weak shock theory is a correct description of nonlinear losses as long as the propagation path is shorter than some critical value. In the case of a plane wave this value is equal to the inverse of the linear absoprtion coefficient of the medium [2]. In the present case, at 3 MHz, the critical value of the propagation path is $1/\alpha=1/15\,\mathrm{m}=6.7$ cm, in the focal area the Gaussian beam can be approximated by a plane wave. Therefore, the weak shock theory applied here is certain to describe correctly the phenomena which occur in tissues at the depth range three times lower, from 10 to 12 cm, where the maximum temperature can be found.

The final conclusion may be that the boundary value of the intensity of the ultrasound beam described here at which it is necessary to take into account the phenomena of nonlinear propagation, is 1 W/cm^2, measured on the transducer which radiates the beam.

What is important for clinical applications is the result that the intensity $I(z=0, r=0)$ should be lower than 0.1 W/cm^2 for the temperature increase of the probe in

question to be less than 1.66°C. In this case, the temperature increases are unlikely to grow as a result of nonlinear propagation.

Acknowledgment

The authors would like to thank Dr D. Dalecki for commenting on some details connected with the weak shock theory.

References

[1] D. BLACKSTOCK, *Connecting between the Fay and Fubini solutions for plane sound waves of finite amplitude*, J. Acoust. Soc. Am., **39**, 1019–1026 (1965).

[2] D. BLACKSTOCK, *On the absorption of finite-amplitude sound. Frontiers of nonlinear acoustics*, Proc. of 12th ISNA [Eds.] M. Hamilton and D. Blackstock, Elsevier, London 1990, pp. 119–124.

[3] E. CARSTENSEN, N. MCKAY and D. DALECKI, *Absorption of finite amplitude ultrasound in tissues*, Acustica, **51**, 116–123 (1982).

[4] D. DALECKI, E. CARSTENSEN, K. PARKER and D. BACON, *Absorption of finite amplitude focussed ultrasound*, J. Acoust. Soc. Am., **89**, 2435–2447 (1971).

[5] D. DALECKI, C. RAEMAN and E. CARSTENSEN, *Effects of pulsed ultrasound on the frog heart: II. An investigation of heating as a potential mechanism*, Ultrasound Med. Biol., **19**, 391–398 (1993).

[6] L. FILIPCZYŃSKI, *Measurement of the temperature increases generated in soft tissues by ultrasonic diagnostic Doppler equipment*, Ultrasound Med. Biol., **4**, 151–155 (1978).

[7] L. FILIPCZYŃSKI, *Experimental research and estimation of the temperature effect caused by ultrasound generated in soft tissue using ultrasonic Doppler diagnostic equipment* (in Polish), Archiwum Akustyki, **13**, 215–222 (1978).

[8] L. FILIPCZYŃSKI and J. ETIENNE, *Theoretical study and experiments on spherical focusing transducers with Gaussian surface velocity distribution*, Acustica, **28**, 121–128 (1973).

[9] L. FILIPCZYŃSKI, T. KUJAWSKA and J. WWÓJCIK, *Temperature elevation in focused Gaussian ultrasonic beams at various insonation times*, Ultrasound Med. Biol., **19**, 667–679 (1993).

[10] M. HARAN and B. COOK, *Distortion of finite amplitude ultrasound in lossy media*, J. Acoust. Soc. Am., **73**, 774–779 (1983).

[11] M. IDE, *Acoustic data of Japanese ultrasonic diagnostic equipment*, Ultrasound Med. Biol., **19**, Suppl. 1, 49–53 (1989).

[2] *NCRP (National Council on Radiation Protection). Exposure criteria for medical diagnostic ultrasound. I. Criteria based on thermal mechanisms*, Bethesda, Md: NCRP Publications 1992.

[13] *World Federation for Ultrasound in Medicine and Biology. Symposium on Safety and Standarisation in Medical Ultrasound.*

[14] J. WU, G. DU, *Temperature rise generated by a focussed Gaussian beam of ultrasound*, Ultrasound Med. Biol., **16**, 489–498, (1990).

[15] J. WU and W. NYBORG, *Temperature rise generated by a focused Gaussian beam in a two layer medium*, Ultrasound Med. Biol., **18**, 293–301 (1992).

ARCHIVES OF ACOUSTICS
20, 3, 247–269 (1995)

PROPAGATION AND SCATTERING OF APM IN THE PIEZOELECTRIC PLATE WITH PERIODICALLY CORRUGATED SURPHACES

D. BOGUCKI
Institute of Fundamental Technological Research
Polish Academy of Sciences
(00–049 Warszawa, Świętokrzyska 21)

Bragg reflection of acoustic plate modes (APM) in piezoelectric plate with periodically grooved surfaces is analysed. Reflectional mode conversion and phenomena of APM propagation along the grooves are also taken into account. Influence of phase shift between the grooves on dispersion relations is also analysed. Presented results may be applied in the analysis of APM sensors and signal processing devices.

1. Introduction

Phenomena of SAW propagation in a piezoelectric substrate with periodically corrugated surface were analysed in details in literature [5], [8], [11]. Corrugation has, usually, a form of shallow, periodic grooves. In this case, in substrate propagates one surface mode [5], [9] and the Bragg condition has the form $K=2k_v$, where K is wavenumber of grooves system and k_v is SAW wavenumber.

Corresponding phenomena in the piezoelectric plate are more complicated because of multimodal propagation of acoustic plate modes (APM) [2], [3], [4]. Different modes may be coupled by formula:

$$\mathbf{K}=\mathbf{k}_f=\mathbf{k}_b,$$

where: $\mathbf{k}_f$ — wavevector of forwards propagating mode, $\mathbf{k}_b$ — is wavevector of backwards propagating mode. In the coupling of different modes we have also phenomena of reflectional mode conversion.

If the plate is corrugated on both sides, then reflection of different modes, depends on grooves amplitude and their phase shift.

Different phenomenon is APM propagation along the grooves. There is no Bragg reflection in this case — propagation has a form of waveguiding by grooves of corrugation. This effect is similar to a SAW propagation along the grooves deposited on the isotropic halfspace analysed by A.A. MARADUDIN *et al.* in [11] and [12].

APM propagation in the isotropic corrugated plates was analysed by author in [10].

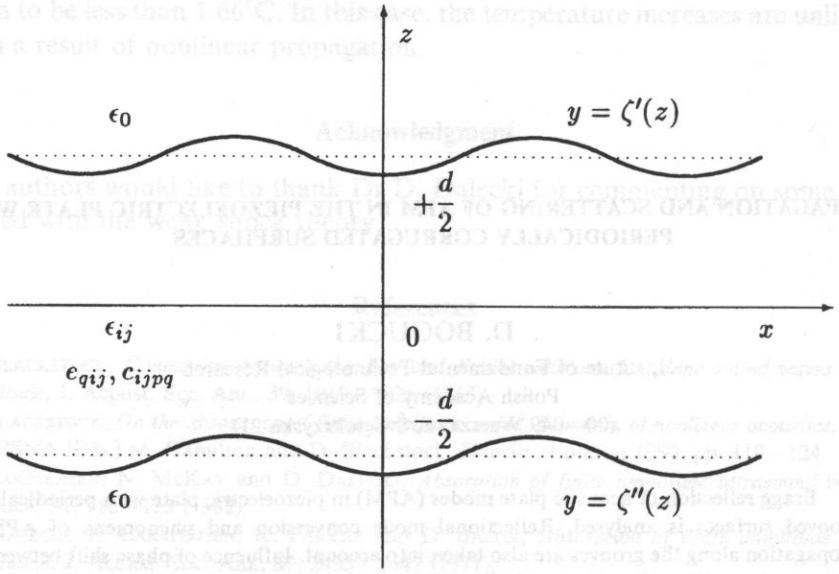

Fig. 1. Piezoelectric plate corrugated on both surfaces

In this paper APM propagation in the piezoelectric plate with both surfaces periodically corrugated is analysed. Solution for plate with corrugated one surface may be easily obtained from this generalized case. We consider slant propagating wave (with reference to groove system) and propagation of APM along the grooves in infinite piezoelectric plate d — thick (Fig. 1). Piezoelectric plate is characterised by ρ-mass density and material tensors ϵ_{ij}, e_{qij}, c_{ijpq}. Below and above the plate there is vacuum (ϵ_0). Periodic corrugation may be described as follows:

$$\zeta'(z) = h_1 e^{-jKz} + h_1^* e^{jKz}, \tag{1.1}$$

$$\zeta''(z) = h_2 e^{-jKz} + h_2^* e^{jKz}, \tag{1.2}$$

where $\Lambda = 2\pi/K$ is a period of corrugation. Corrugation amplitudes h_1, h_2 may be different, they especially may be phase shifted. Corrugation is assumed to be small, so a perturbation theory may be applied:

$$\left|\frac{h_i}{\Lambda}\right| \ll 1, \quad \left|\frac{h_i}{d}\right| \ll 1 \quad i = 1, 2. \tag{1.3}$$

We consider waves propagating in any direction on a (x, z) plane. According to the Floquet theorem [6], solutions for displacements and stresses in the structure may be written in the form:

$$T_{il} = \sum_n T_{il}^{(n)} e^{-j(s+nK)z} e^{-jrx} e^{j\omega t}, \tag{1.4}$$

$$u_i = \sum_n u_i^{(n)} e^{-j(s+nK)z} e^{-jrx} e^{j\omega t}, \tag{1.5}$$

where $i, j = x, y, z$ and $r > 0$, $s > 0$ — wave vector components of the incident wave in x and z axis direction respectively (Fig. 2). Analogous assumptions are made for electric field flux density and electric potential inside the plate:

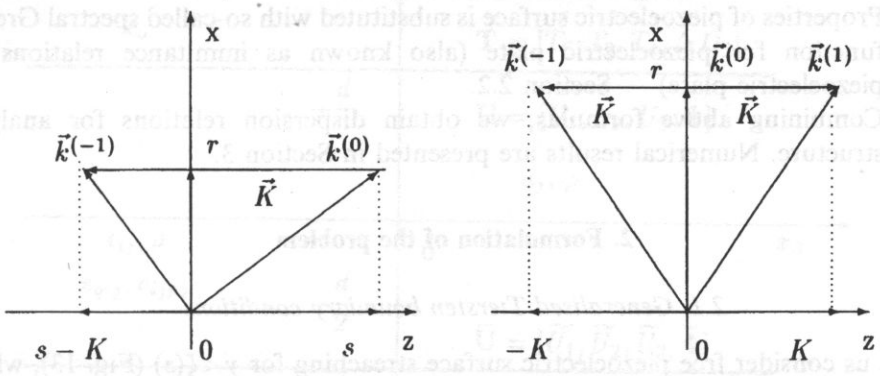

Fig. 2. Wavevectors taken into consideration in analysis: left — for oblique incidence, right — for propagation along the grooves.

$$D_i = \sum_n D_i^{(n)} e^{-j(s+nK)z} e^{-jrx} e^{j\omega t}, \tag{1.6}$$

$$\varphi = \sum_n \varphi^{(n)} e^{-j(s+nK)z} e^{-jrx} e^{j\omega t}, \tag{1.7}$$

Electric potential over and below the plate must additionally dissapear in $+\infty$ and in $-\infty$ respectively:

$$\varphi' = \sum_n \varphi'^{(n)} e^{-j(s+nK)z} e^{-jrx} e^{-k(n)y} e^{j\omega t}, \tag{1.8}$$

$$\varphi'' = \sum_n \varphi''^{(n)} e^{-j(s+nK)z} e^{-jrx} e^{-k(n)y} e^{j\omega t}, \tag{1.9}$$

where $k^{(n)} = \sqrt{r^2 + (s+nK)^2}$. In the case of slant propagating waves (with reference to the groove system) only the lowest harmonic components, coupled by Bragg condition are taken into account i.e. $n = 0, -1$. For propagation along the grooves (eg. for $s = 0$), it is necessary to account components $n = -1, 0, 1$, because $k^{(1)} = k^{(-1)}$.

This simplification is allowed in presented perturbation analysis ($h_i \to 0$). For $|n| \to \infty$ solutions for u_i and φ describe leaky modes exponentially attenuated with distance from plate surfaces. These modes gives ommitable contribution in total energy and can be neglected.

In this paper are analysed dispersion relations i.e. relations between ω and wavevector components s, r. Method of solution is the same for plate corrugated on one or on both surfaces:

1. Structure is decomposed onto three (two) parts:
   - Piezoelectric plate d-thick

- Thin, corrugated piezoelectric layers h_i — thick.

2. Influence of corrugated surfaces is substituted with so-called generalized Tiersten boundary conditions — Section 2.1.
3. Properties of piezoelectric surface is substituted with so-called spectral Green's function for piezoelectric plate (also known as immitance relations for piezoelectric plate) — Section 2.2.
4. Combining above formulas, we obtain dispersion relations for analysed structure. Numerical results are presented in Section 3.

2. Formulation of the problem

2.1. Generalised Tiersten boundary conditions

Let us consider free piezoelectric surface streaching for $y<\zeta(z)$ (Fig. 13), where

$$\zeta(z)=he^{-jKz}+h^*e^{jKz} \tag{2.1}$$

describes sinusoidally grooved surface with period $\Lambda=2\pi/K$ and amplitude $h\ll\Lambda$ (grooves are parallel to the x-axis). In [8] were presented so-called generalized Tiersten boundary conditions. They were exploited in the analysis of periodically corrugated isotropic plate in [10].

Generalised Tiersten boundary conditions have the form of additional stresses and electric charges subjected to mean surface $y=0$, in the function of known displacements and electric potential on the same surface. On the other hand, generalized Tiersten boundary conditions replace homogeneous boundary conditions on corrugated surface by inhomogeneous boundary conditions on mean surface (in simplification of small corrugation). In our case they have general form (denotation of complex amplitudes is analogous to (1.4)–(1.7).

$$\mathbf{T}^{(n)}=h\mathbf{g}^{(n,n-1)}\cdot\mathbf{U}^{(n-1)}+h^*\mathbf{g}^{(n,n+1)}\cdot\mathbf{U}^{(n+1)}, \tag{2.2}$$

where

$$\mathbf{T}^{(n)}\equiv[T_6^{(n)};T_2^{(n)};T_4^{(n)};\Delta D_2^{(n)}] \quad \text{and} \quad \mathbf{U}^{(n)}\equiv[u_1^{(n)};u_2^{(n)};u_3^{(n)};\varphi^{(n)}].$$

It is worth to note that in above formulas, matrices $\mathbf{g}^{(n,n+1)}$ and $\mathbf{g}^{(n,n-1)}$ couple waves propagating with different wavenumbers (for example wave $n=0$ with $n=\pm1$). This effect disapears with $h\to0$.

Method of evaluation of mentioned relationships for piezoelectric material and two-dimensional corrugation (periodic dots) is presented in the Appendix A.

2.2. Immitance relations for piezoelectric plate

Let us consider infinite piezoelectric plate bounded by planes $x_2=\pm d/2$ (Fig. 3) made of material characterized by ρ — mass density and material constants ϵ_{ij}, e_{qij}, c_{ijpq}. Vacuum (ϵ_0) is outside the plate. We consider harmonic waves propagating in

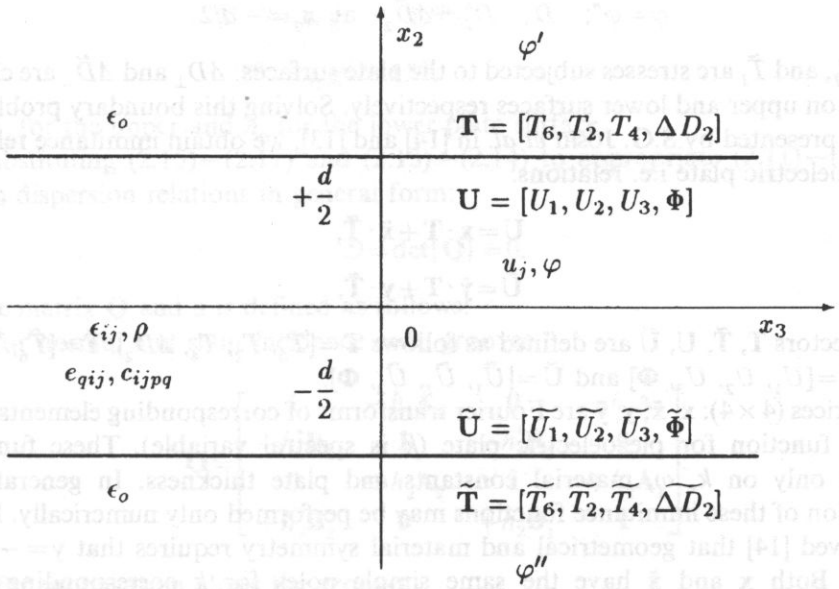

Fig. 3. Piezoelectric plate with forces on both surfaces.

x_3-axis direction proportional to $\exp(j\omega t - jkx_3)$, where k is wavenumber and ω is angular frequency.

In the piezoelectric material, the coupled acoustic wave equations are (in quasi-static approximation):

$$\begin{aligned} \rho\omega^2 u_i &= c_{ijpq}\, u_{p,jq} + e_{qij}\varphi_{,jq}, \\ 0 &= e_{jpq}\, u_{p,jq} - \epsilon_{jq}\, \varphi_{,jq}, \end{aligned} \tag{2.3}$$

where u_p is the particle displacement in the p-axis direction and φ is the electric potential inside the plate. Electric potential above (φ') and below (φ'') the plate satisfy Laplace's equation in the vacuum:

$$\begin{aligned} 0 &= \varphi'_{,jj}, \\ 0 &= \varphi''_{,jj}. \end{aligned} \tag{2.4}$$

Appropriate electrical and mechanical conditions must be satisfied on both plate surfaces. The mechanical boundary conditions are

$$T_{2i} = T_I \quad \text{at } x_2 = +d/2, \tag{2.5}$$

$$T_{2i} = T_I \quad \text{at } x_2 = -d/2, \tag{2.6}$$

and the electrical ones:

$$\varphi = \varphi'; \quad D_2 - D'_2 = \Delta D_2 \quad \text{at } x_2 = +d/2, \tag{2.7}$$

$$\varphi=\varphi''; \quad D_2-D_2''=\Delta\tilde{D}_2 \quad \text{at } x_2=-d/2, \tag{2.8}$$

where T_I, and $\tilde{T}_I$ are stresses subjected to the plate surfaces. $\Delta D_\perp$ and $\Delta\tilde{D}_\perp$ are charges induced on upper and lower surfaces respectively. Solving this boundary problem, in the way presented by S.G. Joshi *et al.* in [14] and [13], we obtain immitance relations for piezoelectric plate i.e. relations:

$$\mathbf{U}=\mathbf{x}\cdot\mathbf{T}+\tilde{\mathbf{x}}\cdot\tilde{\mathbf{T}}, \tag{2.9}$$

$$\tilde{\mathbf{U}}=\tilde{\mathbf{y}}\cdot\mathbf{T}+\mathbf{y}\cdot\tilde{\mathbf{T}}, \tag{2.10}$$

where vectors $\mathbf{T}$, $\tilde{\mathbf{T}}$, $\mathbf{U}$, $\tilde{\mathbf{U}}$ are defined as follows $\mathbf{T}=[T_6, T_2, T_4, \Delta D_2]$, $\tilde{\mathbf{T}}=[\tilde{T}_6, \tilde{T}_2, \tilde{T}_4, \Delta\tilde{D}_2]$, $\mathbf{U}=[U_1, U_2, U_3, \boldsymbol{\Phi}]$ and $\tilde{\mathbf{U}}=[\tilde{U}_1, \tilde{U}_2, \tilde{U}_3, \boldsymbol{\Phi}]$.

Matrices (4×4): $\mathbf{x}$, $\tilde{\mathbf{x}}$, $\mathbf{y}$, $\tilde{\mathbf{y}}$ are Fourier transforms of corresponding elements of the Green's function for piezoelectric plate (k is spectral variable). These functions depends only on k, ω, material constants and plate thickness. In general case, calculation of these immitance functions may be performed only numerically. It may be prooved [14] that geometrical and material symmetry requires that $\mathbf{y}=-\mathbf{x}$ and $\tilde{\mathbf{y}}=-\tilde{\mathbf{x}}$. Both $\mathbf{x}$ and $\tilde{\mathbf{x}}$ have the same simple poles for k corresponding APM wavenumber. Matrix $\mathbf{x}$ is hermitian ($x_{ij}=x_{ji}^*$), and $\tilde{\mathbf{x}}$ is symmetrical ones ($x_{ij}=x_{ji}$) [14], [13].

Matrices $\mathbf{x}$ and $\tilde{\mathbf{x}}$ for isotropic plate were presented in [10]. It is worth to note that only for piezoelectric materials elements x_{i4} and $\tilde{x}_{i4}$ are non equal to zero, because they describe coupling between mechanical displacements and electric field.

2.3. *Dispersion relations*

Let us introduce for each n new coordinate system such that axis $y\equiv x_2^{(n)}$ and $x_3^{(n)}\equiv k^{(n)}$ (Figure 2). Immitance relations for each n have the form:

$$\mathbf{U}^{(n)}=\mathbf{x}^{(n)}\cdot\mathbf{T}^{(n)}+\tilde{\mathbf{x}}^{(n)}\cdot\tilde{\mathbf{T}}^{(n)}, \tag{2.11}$$

$$\tilde{\mathbf{U}}^{(n)}=-\tilde{\mathbf{x}}^{(n)}\cdot\mathbf{T}^{(n)}-\mathbf{x}^{(n)}\cdot\tilde{\mathbf{T}}^{(n)}. \tag{2.12}$$

Transforming in the same way generalized Tiersten conditions and taking into account only the lowest harmonic components, coupled by Bragg condition we obtain (Section 1):

- for normal nad slant incidence onto grooves i.e. taking into account $n=0, -1$ we have:

$$\mathbf{T}^{(0)}=h_i\,\mathbf{g}^{(0,-1)}\cdot\mathbf{U}^{(-1)}, \tag{2.13}$$

$$\mathbf{T}^{(-1)}=h_i^*\,\mathbf{g}^{(-1,0)}\cdot\mathbf{U}^{(0)}, \tag{2.14}$$

- propagation along the grooves i.e. taking into account $n=1, 0, -1$ we have:

$$\mathbf{T}^{(0)}=h_i\,\mathbf{g}^{(0,-1)}\cdot\mathbf{U}^{(-1)}+h_i^*\,\mathbf{g}^{(0,1)}\cdot\mathbf{U}^{(1)}, \tag{2.15}$$

$$\mathbf{T}^{(-1)}=h_i^*\,\mathbf{g}^{(-1,0)}\cdot\mathbf{U}^{(0)}, \tag{2.16}$$

$$\mathbf{T}^{(1)}=h_i\,\mathbf{g}^{(1,0)}\cdot\mathbf{U}^{(0)}, \tag{2.17}$$

h_i is h_1 for the upper and h_2 for the lower plate surface.

Substituting (2.15)–(2.17) and (2.13)–(2.14) to appropriate (2.11)–(2.12) we obtain dispersion relations in general form:

$$D=\det\{\mathbf{Q}\}=0. \tag{2.18}$$

Where matrix $\mathbf{Q}$ and $\mathbf{u}$ is defined as follows:

• for normal and slant incidence onto grooves

$$\mathbf{Q}=\begin{bmatrix} \mathbf{I} & -h_1\mathbf{A}_1 & \mathbf{0} & -h_1\mathbf{A}_2 \\ -h_1^*\mathbf{B}_1 & \mathbf{I} & -h_1^*\mathbf{B}_2 & \mathbf{0} \\ \mathbf{0} & +h_2\mathbf{A}_2 & \mathbf{I} & +h_2\mathbf{A}_1 \\ +h_2^*\mathbf{B}_2 & \mathbf{0} & +h_2^*\mathbf{B}_1 & \mathbf{I} \end{bmatrix}. \tag{2.19}$$

• for propagation along the grooves

$$\mathbf{Q}=\begin{bmatrix} \mathbf{I} & -h_1\mathbf{C}_1 & \mathbf{0} & \mathbf{0} & -h_1\mathbf{C}_2 & \mathbf{0} \\ -h_1^*\mathbf{D}_1 & \mathbf{I} & -h_1\mathbf{A}_1 & -h_1^*\mathbf{D}_2 & \mathbf{0} & -h_1^*\mathbf{A}_2 \\ \mathbf{0} & -h_1^*\mathbf{B}_1 & \mathbf{I} & \mathbf{0} & -h_1^*\mathbf{B}_2 & \mathbf{0} \\ \mathbf{0} & +h_2\mathbf{C}_2 & \mathbf{0} & \mathbf{I} & +h_2\mathbf{C}_1 & \mathbf{0} \\ +h_2^*\mathbf{B}_2 & \mathbf{0} & +h_2\mathbf{A}_2 & +h_2^*\mathbf{D}_1 & \mathbf{I} & +h_2\mathbf{A}_1 \\ \mathbf{0} & +h_2^*\mathbf{B}_2 & \mathbf{0} & \mathbf{0} & +h_2\mathbf{B}_1 & \mathbf{I} \end{bmatrix}. \tag{2.20}$$

$\mathbf{I}$ is unitary matrix and $\mathbf{A}_I$, $\mathbf{B}_I$, $\mathbf{C}_I$, $\mathbf{D}_I$ are 4×4 matrices defined as follows:

$$\mathbf{A}_1=\mathbf{x}^{(0)}\cdot\mathbf{g}^{(0,-1)}, \qquad \mathbf{A}_2=\tilde{\mathbf{x}}^{(0)}\cdot\mathbf{g}^{(0,-1)}, \tag{2.21}$$

$$\mathbf{B}_1=\mathbf{x}^{(-1)}\cdot\mathbf{g}^{(-1,0)}, \qquad \mathbf{B}_2=\tilde{\mathbf{x}}^{(-1)}\cdot\mathbf{g}^{(-1,0)}, \tag{2.22}$$

$$\mathbf{C}_1=\mathbf{x}^{(1)}\cdot\mathbf{g}^{(1,0)}, \qquad \mathbf{C}_1=\tilde{\mathbf{x}}^{(1)}\cdot\mathbf{g}^{(1,0)}, \tag{2.23}$$

$$\mathbf{D}_1=\mathbf{x}^{(0)}\cdot\mathbf{g}^{(0,1)}, \qquad \mathbf{D}_2=\tilde{\mathbf{x}}^{(0)}\cdot\mathbf{g}^{(0,1)}. \tag{2.24}$$

Dispersion relation for piezoelectric plate corrugated on one side may be obtained by substitution $h_2=0$ in presented above formulas.

3. Numerical results

In numerical results presented in this section it is assumed that:

• $s\in(0,K)$ i.e. s is in the first Brillouin zone;

• angular frequency ω is normalised to $\Omega=\omega/V$ and $V=\sqrt{c_{44}/\rho}$, so $\Omega\in(0,K)$;

• it is assumed that $h_i=0.01\,\Lambda$;

- place thickness d is normalised: $d=m\cdot\Lambda/2\pi$; We analyse relatively thin plates with $m=1$ because for $m>3$ higher APM may propagate and corresponding dispersion relations are much more complicated;
- $r\in(0,K)$ for the waves propagating aiong the grooves and for slowness curves.
- amplitudes of corrugation on both sides are: $h_1=h\exp\left\{-j\frac{\psi}{2}\right\}$ and $h_2=h\exp\left\{+j\frac{\psi}{2}\right\}$ i.e. are phase-shifted by ψ.

It may be easily prooved that highest frequency $f_{\max}$ of model correctness is given:

$$f_{\max}=\frac{V}{\Lambda}. \tag{3.1}$$

For $f>f_{\max}$ we must take into account more n in the series (1.4)–(1.7).

3.1. Normal and slant incidence onto grooves

We analyse equation (2.18) in a two ways:

1. For normal incidence onto the grooves i.e. for $r=0$, the most natural is to analyse dispersion relation $D(r, s, \Omega)=0$ on (s,Ω) plane.
2. For slant incidence onto the grooves more useful is to analyse slowness curves i.e. for $\Omega=$const on (r,s) plane.

Numerical results for popular piezoelectric materials (BGO, SiO_2, $LiNbO_3$) are presented on Figures 4–10. Upper part of Figures 4–9 show dispersion curves for piezoelectric plate corrugated on one side. Dotted lines are dispersion curves for free (uncorrugated $h=0$) plate. Lower part of figures, presents dispersion curves for plates with corrugates both sides.

For APM propagation in the corrugated plates, existence of forbidden frequency bands (marked with letters on Figures 4–9, see table below).

letter	reflection	letter	reflection
a	$SH_0\leftrightarrow SH_0$	d	$A_0\leftrightarrow S_0$
b	$A_0\leftrightarrow A_0$	e	$A_0\leftrightarrow SH_0$
c	$S_0\leftrightarrow S_0$	f	$S_0\leftrightarrow SH_0$

Inside those bands wavenumber has complex values — which is connected with effects of Bragg reflection. There are two kind os stopbands:

- associated with backward mode reflection (a, b, c) inside those bands $Re\{s\}=K/2=$const
- connected with reflection associated with mode conversion. In this case $Re\{s\}\neq K/2\neq$const because of different velocities of coupled modes.

Let us note that, if crystal cut of the plate is such that in analysed plate displacements in saggital plane (u_2, u_3) and u_1 are independent each other, then for

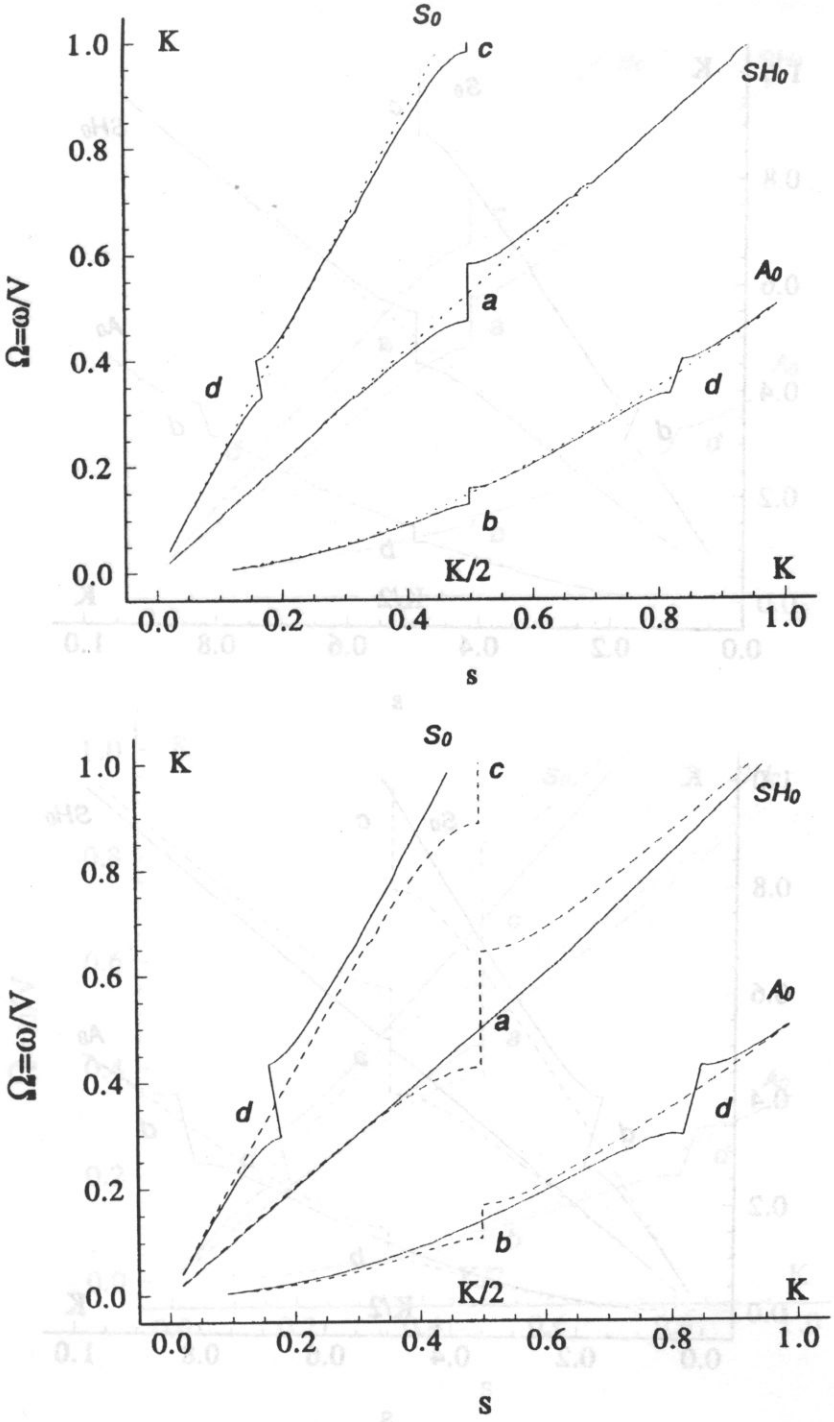

Fig. 4. BGO YZ plate $m=1$ thick, dispersion curves at $r=0$. Above: corrugated one side, dotted line — uncorrugated plate. Below: two-side corrugations phase-shifted by: a) $\psi=0$ — solid line and b) $\psi=\pi$ — dashed line.

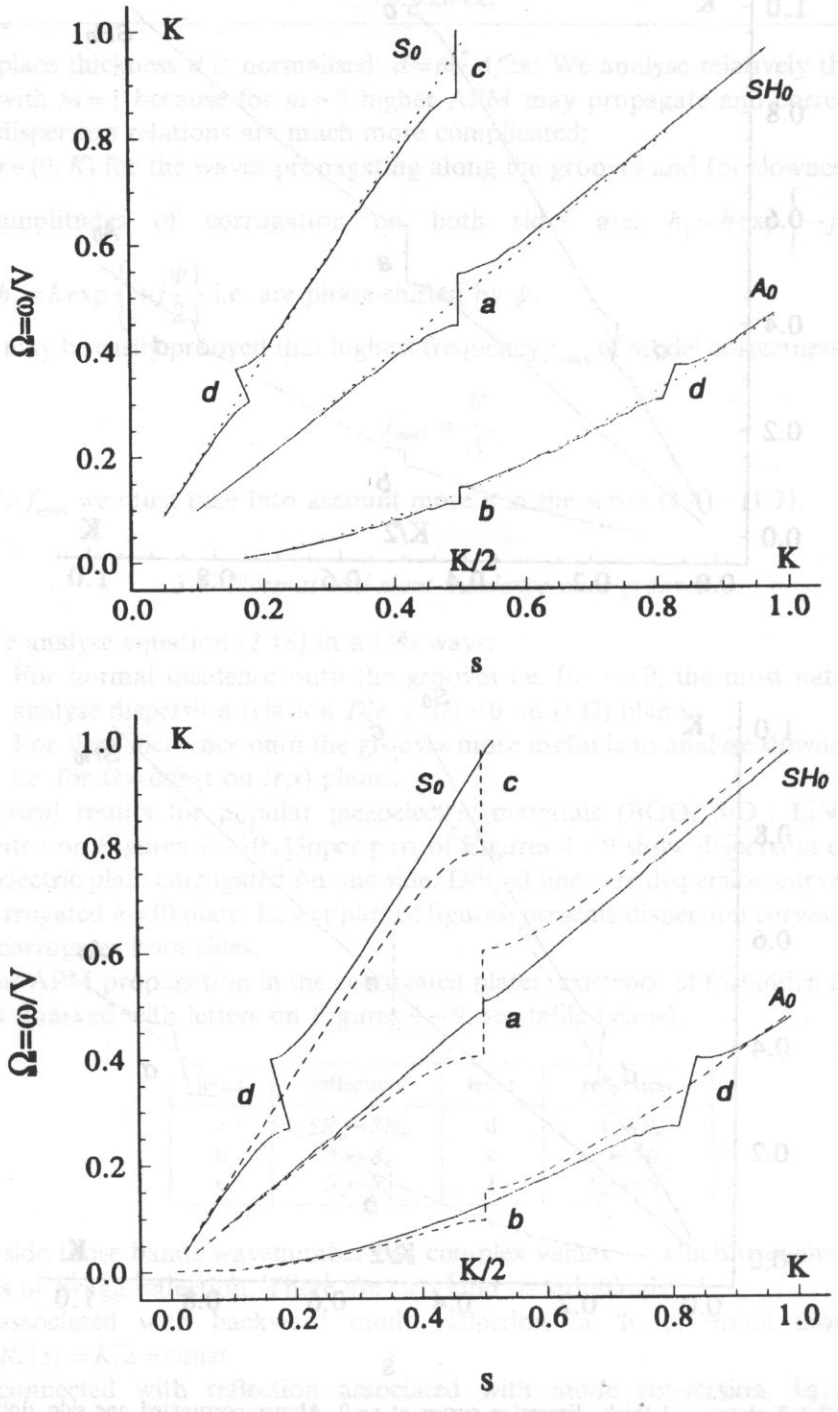

Fig. 5. $LiNbO_3$ YZ plate $m=1$ thick, dispersion curves at $r=0$. Above: corrugated one side, dotted line — uncorrugated plate. Below: two-side corrugations phase-shifted by: a) $\psi=0$ — solid line and b) $\psi=\pi$ — dashed line.

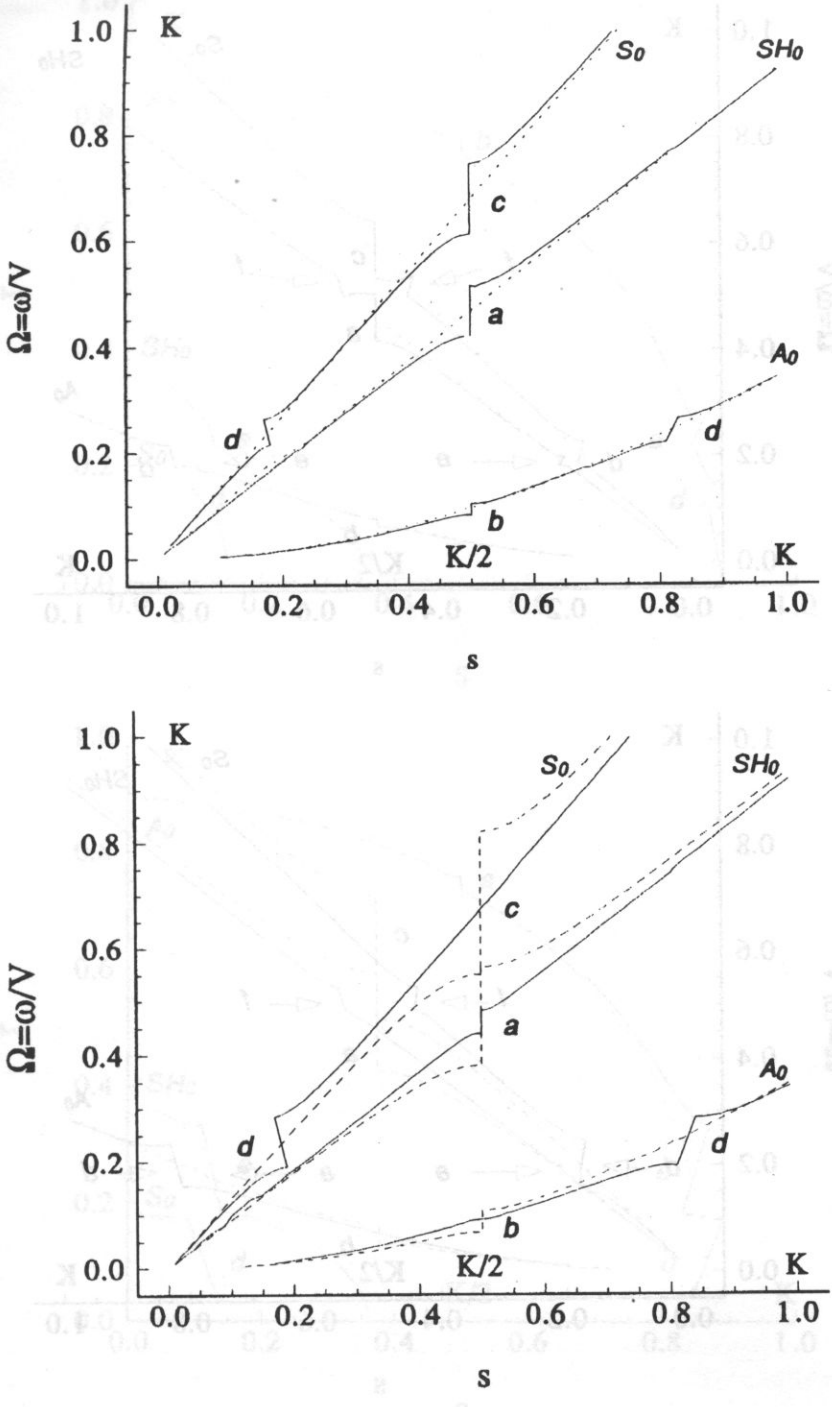

Fig. 6. SiO_2 YZ plate $m=1$ thick, dispersion curves at $r=0$. Above: corrugated one side, dotted line — uncorrugated plate. Below: two-side corrugations phase-shifted by: a) $\psi=0$ — solid line and b) $\psi=\pi$ — dashed line.

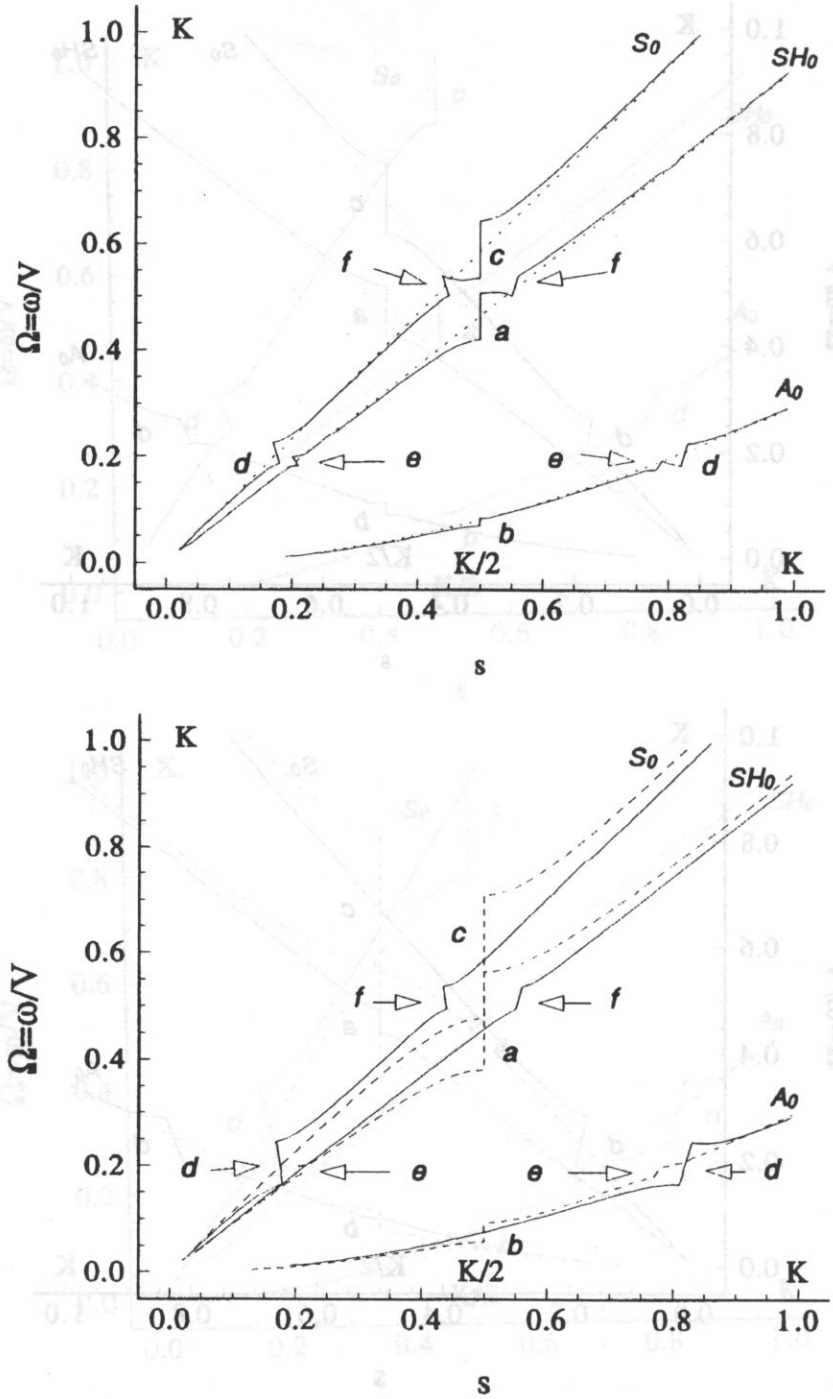

Fig. 7. SiO_2 YX plate $m=1$ thick, dispersion curves at $r=0$. Above: corrugated one side, dotted line — uncorrugated plate. Below: two-side corrugations phase-shifted by: a) $\psi=0$ — solid line and b) $\psi=\pi$ — dashed line.

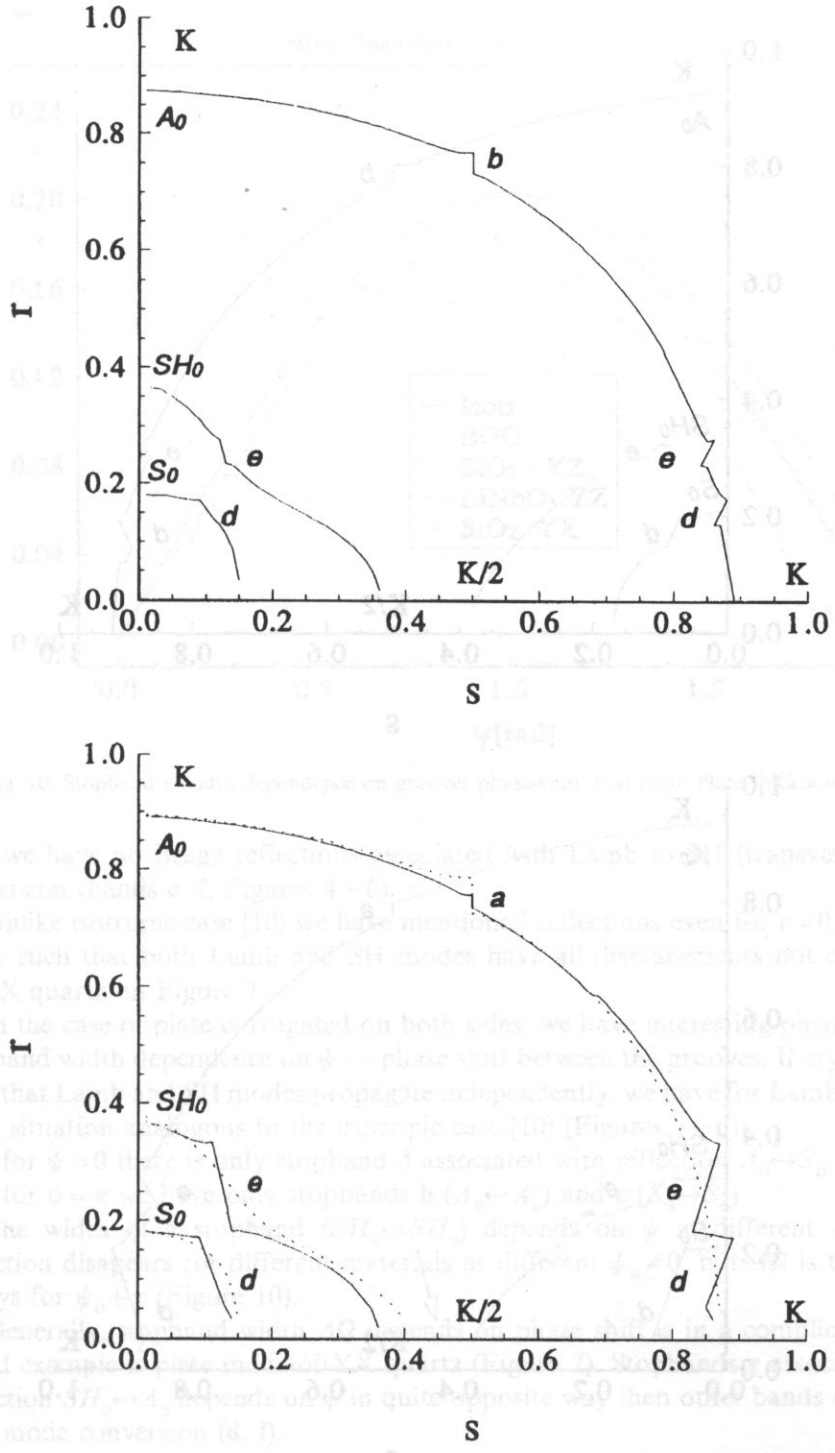

Fig. 8. Slowness curves at $\Omega=0.4$ *K*. BGO YZ plate $m=1$ thikc. Above: plate corrugated on one side. Below: two-side corrugations phase-shifted by: a) $\psi=0$ — (solid line) and b) $\psi=\pi$ — (dashed line).

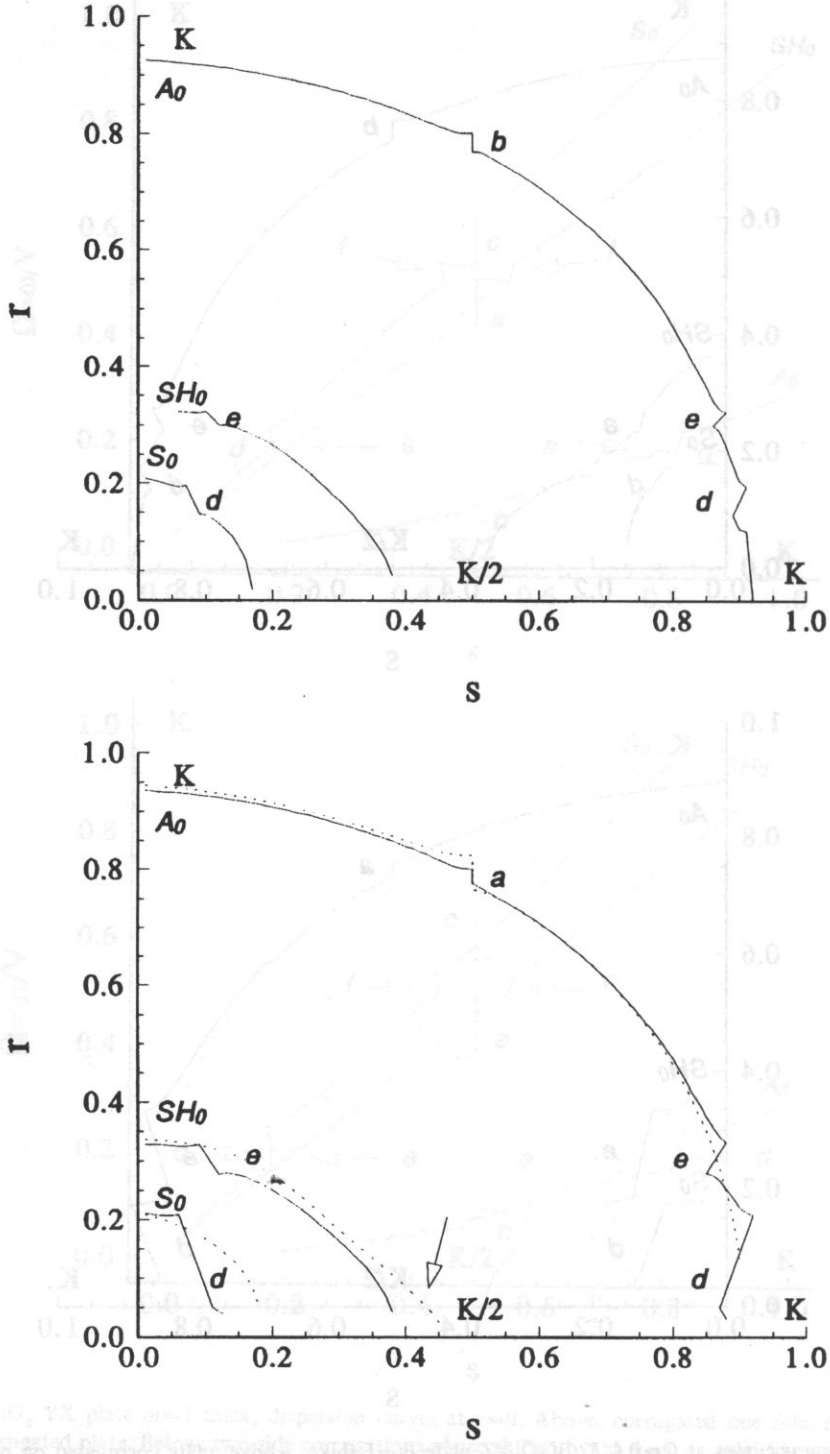

Fig. 9. Slowness curves at $\Omega = 0.4$ *K*. $LiNbO_3$ YZ plate $m = 1$ thick. Above: plate corrugated on one side. Below: two-side corrugations phase-shifted by: a) $\psi = 0$ — (solid line) and b) $\psi = \pi$ — (dashed line).

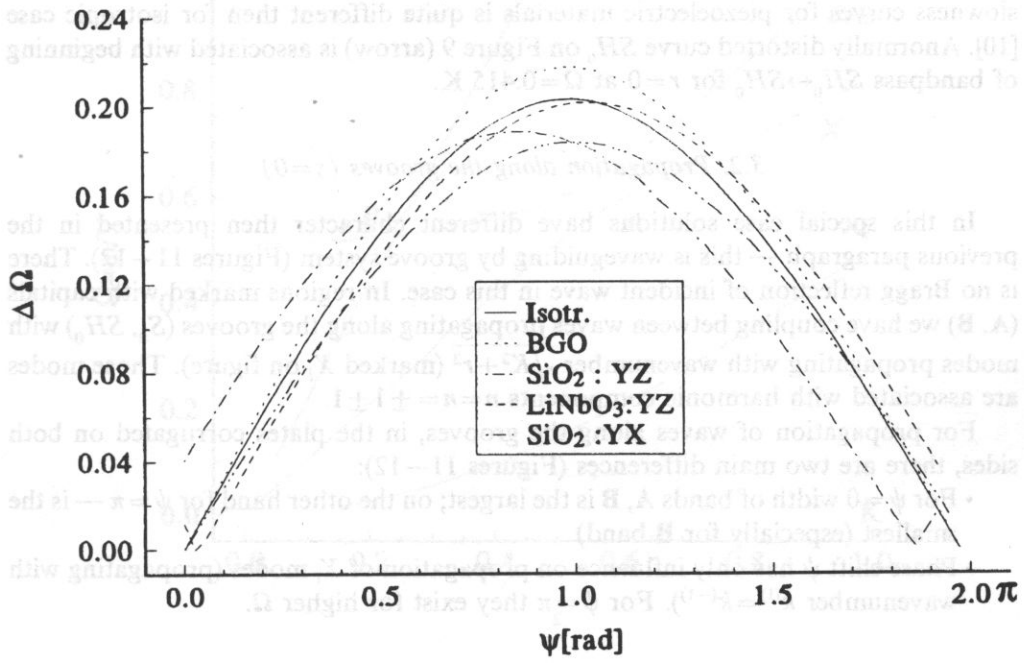

Fig. 10. Stopband a width dependence on grooves phase-shift ψ at $r=0$. Plate thickness: $m=1$.

$r=0$ we have no Bragg reflections associated with Lamb to SH (transverse) mode conversion (bands **e**, **f**, Figures 4–6).

Unlike isotropic case [10] we have mentioned reflections even for $r=0$, if crystal cut is such that both Lamb and SH modes have all displacements not equal zero — YX quartz on Figure 7.

In the case of plate corrugated on both sides, we have interesting phenomena of stopband width dependence on ψ — phase shift between the grooves. If crystal cut is such that Lamb and SH modes propagate independently, we have for Lamb modes at $r=0$, situation analogous to the isotropic case [10] (Figures 4–6):

- for $\psi=0$ there is only stopband **d** associated with reflection $A_0 \leftrightarrow S_0$
- for $\psi=\pi$ we have only stopbands **b** ($A_0 \leftrightarrow A_0$) and **c** ($S_0 \leftrightarrow S_0$)

The width of **a** stopband ($SH_0 \leftrightarrow SH_0$) depends on ψ in different way. This reflection disapears for different materials at different $\psi_0 \neq 0$, but $\Delta\Omega$ is the largest always for $\psi_0+\pi$ (Figure 10).

Generally, stopband width $\Delta\Omega$ depends on phase shift ψ in a complicated way. Good example is plate made of YX quartz (Figure 7). Stopbands **e** associated with relfection $SH_0 \leftrightarrow A_0$ depends on ψ in quite opposite way then other bands associated with mode conversion (**d**, **f**).

Numerical results for slant incidence of wave onto the grooves are presented on Figures 8, 9. In this case, analogously isotropic case [10] we have always stopbands **e**, **f** associated with reflection of SH to Lamb modes. On the other hand, the shape of

slowness curves for piezoelectric materials is quite different then for isotropic case [10]. Anormally distorted curve SH_0 on Figure 9 (arrow) is associated with beginning of bandpass $SH_0 \leftrightarrow SH_0$ for $r=0$ at $\Omega=0.415$ K.

3.2. Propagation along the grooves ($s=0$)

In this special case solutions have different character then presented in the previous paragraph — this is waveguiding by groove system (Figures 11 – 12). There is no Bragg reflection of incident wave in this case. In regions marked with capitals (**A**, **B**) we have coupling between waves propagating along the grooves (S_0, SH_0) with modes propagating with wavenumber $\sqrt{K^2+r^2}$ (marked X_i on figure). Those modes are associated with harmonic components $n=n=\pm 1 \pm 1$.

For propagation of waves along the grooves, in the plates corrugated on both sides, there are two main differences (Figures 11 – 12):

- For $\psi=0$ width of bands **A**, **B** is the largest; on the other hand for $\psi=\pi$ — is the smallest (especially for **B** band)
- Phase shift ψ has only influence on propagation of X_i modes (propagating with wavenumber $k^{(1)}=k^{(-1)}$). For $\psi=\pi$ they exist for higher Ω.

4. Conclusions

1. In piezoelectric plate with periodically corrugated surfaces, we have Bragg reflection phenomena associated with mode conversion — in this case $Re\{s\} \neq \text{const}$ inside forbidden band of frequency. This effect is caused by different velocities of coupled modes.

2. If crystal cut is such, that in plane normal to the grooves Lamb and SH modes propagate independent each other then for $r=0$ there is no reflection associated with conversion of Lamb to SH modes. This effect is possible for slant incidence of wave onto the grooves.

3. For plate with both surfaces periodically corrugated, width of stopbands depends on phase shift between corrugation grooves ψ. Changing ψ we could obtain only reflection of certain kind. Those phenomena may be useful in elimination of parasitic effects of multimodal propagation in APM devices, especially in APM sensors [15] and resonators [13].

4. In the case of propagation along the grooves, propagation has a form of guiding wave by groove system. For plates corrugated on both sides, changes are not so large as for slant and normal incidence of wave onto the grooves.

Appendix A

Let us consider thin periodically corrugated layer made of piezoelectric material characterised by material tensors e_{qij}, ϵ_{ij}, c_{ijpq} and ρ — mass density. The layer is

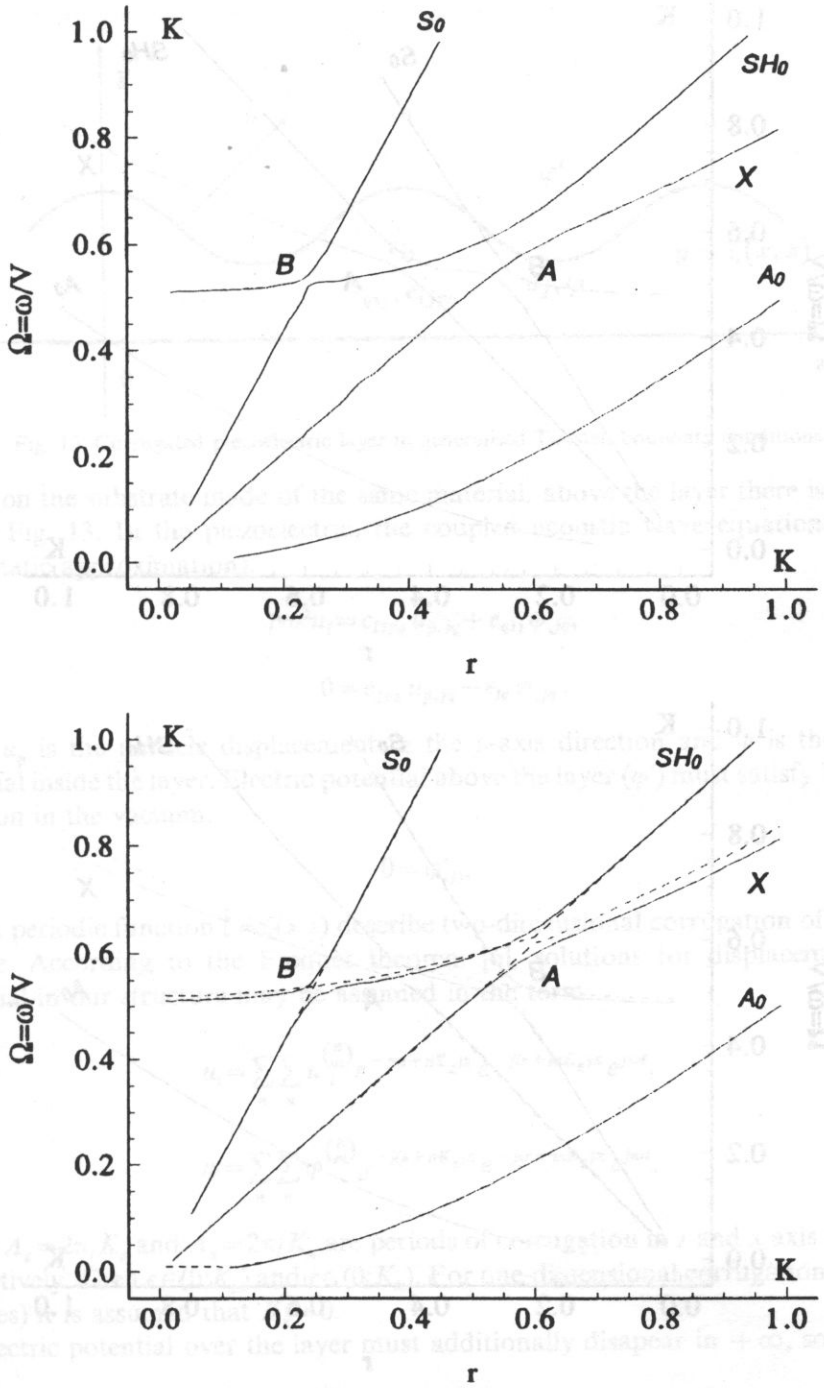

Fig. 11. Dispersion curves, propagation along the grooves ($s=0$)BGO YZ plate, $m=1$ thick. Above: plate corrugated on one side. Below: two-side corrugations phase-shifted by: a) $\psi=0$ — (solid line) and b) $\psi=\pi$ — (dashed line).

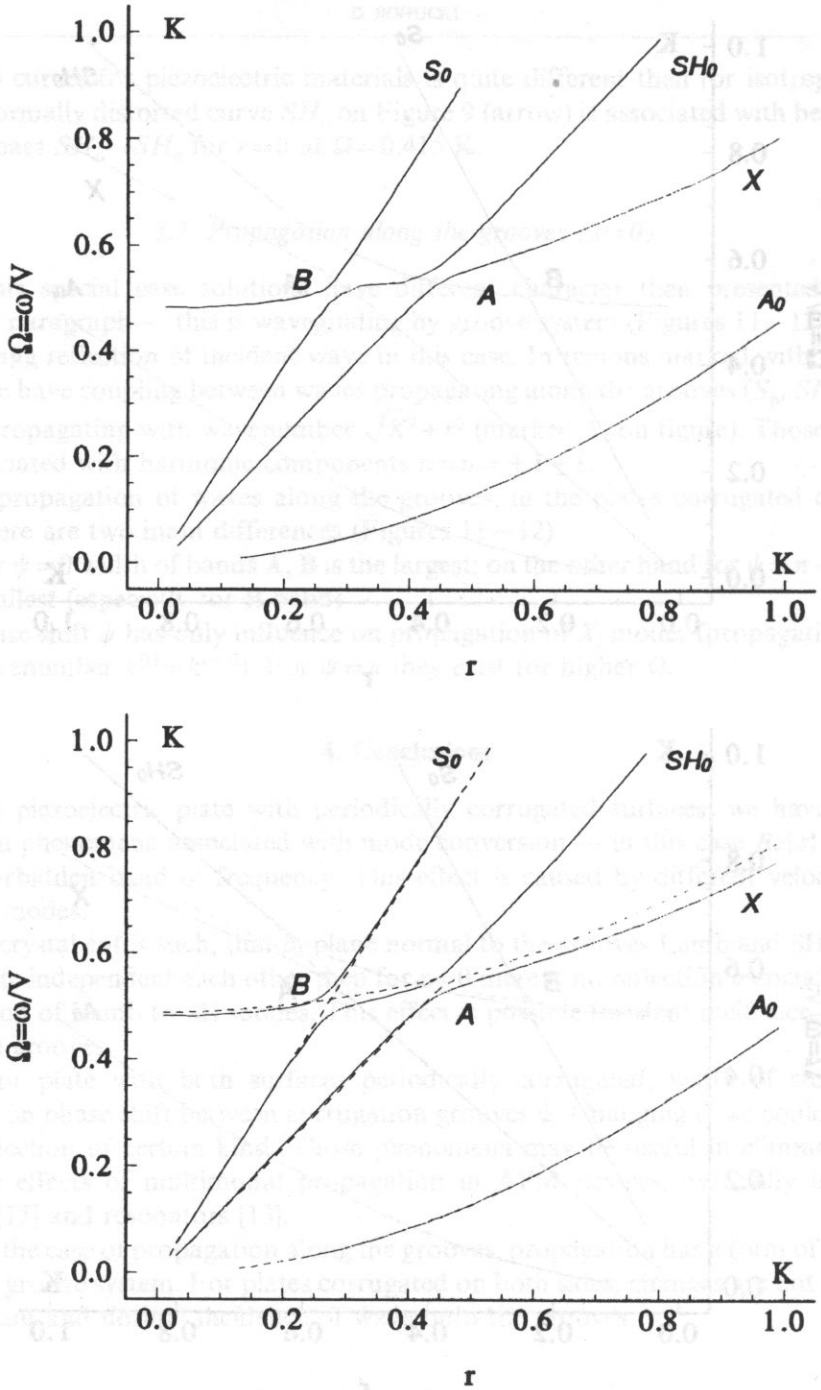

Fig. 12. Dispersion curves, propagation along the grooves $(s=0)LiNbO_3$ YZ plate, $m=1$ thick. Above: plate corrugated on one side. Below: two-side corrugations phase-shifted by: a) $\psi=0$ — (solid line) and b) $\psi=\pi$ — (dashed line).

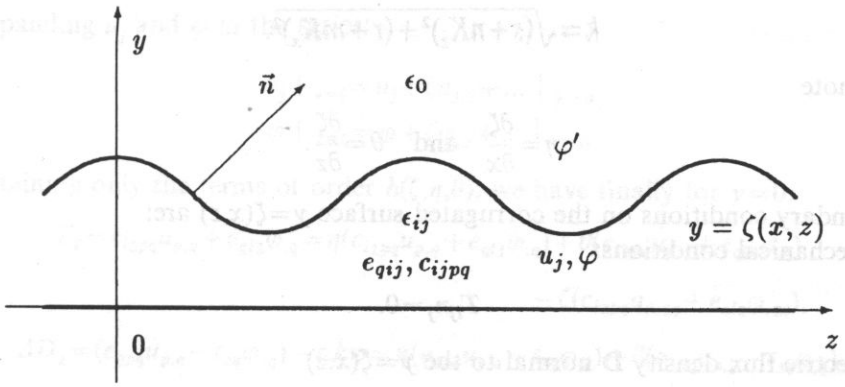

Fig. 13. Corrugated piezoelectric layer in generalised Tiersten boundary conditions.

placed on the substrate made of the same material, above the layer there is vacuum (ϵ_0) — Fig. 13. In the piezoelectric, the coupled acoustic wave equations are (in quasi-static approximation):

$$\rho\omega^2 u_i = c_{ijpq}\, u_{p,jq} + e_{qij}\, \varphi_{,jq},$$
$$0 = e_{jpq}\, u_{p,jq} - \epsilon_{jq}\, \varphi_{,jq}, \tag{A1}$$

where u_p is the particle displacement in the p-axis direction and φ is the electric potential inside the layer. Electric potential above the layer (φ') must satisfy Laplace's equation in the vacuum:

$$0 = \varphi'_{,jj}, \tag{A2}$$

Let periodic function $\zeta = \zeta(x,z)$ describe two-dimensional corrugation of the layer surface. According to the Floquet theorem [6], solutions for displacements and potential in our structure may be assumed in the form:

$$u_i = \sum_n \sum_n u_i^{(n)}_{(m)} e^{-j(s+nK_z)z}\, e^{-j(r+mK_z)x}\, e^{j\omega t},$$
$$\varphi = \sum_n \sum_n \varphi^{(n)}_{(m)} e^{-j(s+nK_z)z}\, e^{-j(r+mK_z)x}\, e^{j\omega t}, \tag{A3}$$

where $\Lambda_z = 2\pi/K_z$ and $\Lambda_x = 2\pi/K_x$ are periods of corrugation in z and x axis direction, respectively. Then $s \in (0; K_z)$ and $r \in (0; K_x)$. For one-dimensional corrugation (periodic grooves) it is assumed that $K_x = 0$.

Electric potential over the layer must additionally disapear in $+\infty$, so:

$$\varphi' = \sum_n \sum_n \varphi'^{(n)}_{(m)} e^{-j(s+nK_z)z}\, e^{-j(r+mK_z)x}\, e^{-ky} e^{j\omega t}, \tag{A4}$$

where:

$$k=\sqrt{(s+nK_z)^2+(r+mK_x)^2}. \tag{A5}$$

Let us note

$$\eta=\frac{\partial\zeta}{\partial x} \quad \text{and} \quad \theta=\frac{\partial\zeta}{\partial z}. \tag{A6}$$

Boundary conditions on the corrugated surface $y=\zeta(x,z)$ are:

• Mechanical conditions:

$$T_{ij}n_j=0. \tag{A7}$$

• Electric flux density **D** normal to the $y=\zeta(x,z)$

$$(D_j-D'_j)n_j=0. \tag{A8}$$

• Electric field **E** tangent to the $y=\zeta(x,z)$

$$\varepsilon_{ijk}(E_j-E'_j)n_i=0, \tag{A9}$$

where n_i are components of vector normal to the surface $y=\zeta(x,z)$

$$\mathbf{n}=[-\eta;\,1;\,-\theta], \tag{A10}$$

and ε_{ijk} is antisymmetric Levi–Civitta symbol.

It is easy to proove that (A9) is equivalent to the continuity of the electric ptoential on the corrugated surface:

$$\varphi'=\varphi \quad \text{at} \quad y=\zeta(x,z) \tag{A11}$$

Let us consider now condition (A8):

$$\text{inside the layer} \quad D_j=D_2-\eta D_1-\theta D_3, \tag{A12}$$

$$\text{in the vacuum} \quad D'_j=D'_2-\eta D'_1-\theta D'_3. \tag{A13}$$

Electric field in the vacuum must disapear in the $+\infty$, so according to the (A4) we have:

$$D'_2=-\epsilon_0\varphi'_{,2}=\epsilon_0 k\varphi' \quad \text{at} \quad y=\zeta(x,z)$$

and finally taking into account (A11) we have for $y=\zeta(x,z)$:

$$D'_jn_j=\epsilon_0\cdot(k\varphi+\eta\varphi_{,1}+\theta\varphi_{,3}), \tag{A14}$$

and, respectivelly:

$$D_jn_j=e_{2pq}u_{p,q}-\epsilon_{2q}\varphi_{,q}-\eta(e_{1pq}u_{p,q}-\epsilon_{1q}\varphi_{,q})-\theta(e_{3pq}u_{p,q}-\epsilon_{3q}\varphi_{,q}). \tag{A15}$$

Mechanical conditions (A7) may be written for $y=z(x,z)$ as follows:

$$T_{ij}n_j=c_{i2pq}u_{p,q}+e_{qi2}\varphi_{,q}-\eta(c_{i1pq}u_{p,q}+e_{qi1}\varphi_{,q})+\theta(c_{i3pq}u_{p,q}+e_{qi3}\varphi_{,q}). \tag{A16}$$

Expanding u_j and φ in the series:

$$u_j \mid_{y=\zeta} = u_j + \zeta u_{j,2} + \ldots \mid_{y=0}$$
$$\varphi \mid_{y=\zeta} = \varphi + \zeta \varphi_{,2} + \ldots \mid_{y=0}$$

and retaining only the terms of order $h(\zeta,\eta,\theta)$, we have finally for $y=0$:

$$T_I = c_{i2pq}u_{p,q} + e_{qi2}\varphi_{,q} = \eta(c_{i1pq}u_{p,q} + e_{qi1}\varphi_{,q}) + \theta(c_{i3pq}u_{p,q} + e_{qi3}\varphi_{,q}) - \zeta(c_{i2pq}u_{p,2q} + e_{qi2}\varphi_{,2q}), \tag{A17}$$

$$\Delta D_2 = (e_{2pq}u_{p,q} - \epsilon_{2q}\varphi_{,q}) - \epsilon_0 k\varphi = \eta(e_{1pq}u_{p,q} - \epsilon_{1q}\varphi_{,q}) + \theta(e_{3pq}u_{p,q} - \epsilon_{3q}\varphi_{,q}) - \zeta(e_{2pq}u_{p,2q} - \epsilon_{2q}\varphi_{,2q}) - \epsilon_0(\eta\varphi_{,1} + \theta\varphi_{,3} + \zeta k\varphi_{,2}) \tag{A18}$$

where $I=6, 2, 4$ for $i=1, 2, 3$ (in shorted notation).

Let us note that for $\zeta \equiv 0$ we have boundary conditions for free (uncorrugated) surface.

Note that derivatives with respect to x, z are known from (A3). Unknown derivatives $(u_{j,2}, \varphi_{,2})$ may be eliminated, taking into account that formulas (A17 – A18) are of first order in h and may be rewriten in the following form ($\delta,\gamma = 1, 3$):

$$c_{i2p2}u_{p,2} + e_{2i2}\varphi_{,2} = -(c_{i2p\delta}u_{p,\delta} + e_{2i\delta}\varphi_{,\delta} + O(h))$$
$$-(e_{2p2}u_{p,2} - \epsilon_{22}\varphi_{,2}) = -(e_{2p\delta}u_{p,\delta} - \epsilon_{2\delta}\varphi_{,\delta} - \epsilon_0 k\varphi + O(h))$$

Thus, if we introduce the symmetric matrix Γ_{ip} by:

$$\Gamma_{ip} \equiv c_{i2p2},$$
$$\Gamma_{i4} = \Gamma_{4p} \equiv e_{2p2} = e_{2i2}, \tag{A19}$$
$$\Gamma_{44} \equiv \epsilon_{22},$$

then we obtain derivatives $u_{j,2}$, $\varphi_{,2}$:

$$u_{\beta,2} = -\Gamma^{-1}_{\beta\alpha}(c_{\alpha 2q\gamma}u_{q,\gamma} + e_{\gamma\alpha 2}\varphi_{,\gamma}) - \Gamma^{-1}_{\beta 4}(e_{2q\gamma}u_{q,\gamma} - \epsilon_{2\gamma}\varphi_{,\gamma} - \epsilon_0 k\varphi), \tag{A20}$$
$$\varphi_{,2} = -\Gamma^{-1}_{4\alpha}(c_{\alpha 2q\gamma}u_{q,\gamma} + e_{\gamma\alpha 2}\varphi_{,\gamma}) - \Gamma^{-1}_{44}(e_{2q\gamma}u_{q,\gamma} - \epsilon_{2\gamma}\varphi_{,\gamma} - \epsilon_0 k\varphi).$$

Because this result holds for all x and z, differentiating with $\delta = 1, 3$ we have a second useful result:

$$u_{\beta,2\delta} = -\Gamma^{-1}_{\beta\alpha}(c_{\alpha 2q\gamma}u_{q,\delta\gamma} + e_{\gamma\alpha 2}\varphi_{,\delta\gamma}) - \Gamma^{-1}_{\beta 4}(e_{2q\gamma}u_{q,\delta\gamma} - \epsilon_{2\gamma}\varphi_{,\delta\gamma} - \epsilon_0 k\varphi_{,\delta}), \tag{A21}$$
$$\varphi_{,2\delta} = -\Gamma^{-1}_{4\alpha}(c_{\alpha 2q\gamma}u_{q,\delta\gamma} + e_{\gamma\alpha 2}\varphi_{,\delta\gamma}) - \Gamma^{-1}_{44}(e_{2q\gamma}u_{q,\delta\gamma} - \epsilon_{2\gamma}\varphi_{,\delta\gamma} - \epsilon_0 k\varphi_{,\delta}).$$

Writing equation of motion for piezoelectric (A1) as follows:

$$\begin{aligned} c_{i2pq}u_{p,2q}+e_{qi2}\varphi_{,2q} &= -(\rho\omega^2 u_i+c_{i\delta p\gamma}u_{p,\delta\gamma}+e_{\gamma i\delta}\varphi_{,\delta\gamma}+ \\ &+c_{i\delta p2}u_{p,\delta 2}+e_{\gamma i}\varphi_{,\delta 2}), \\ e_{2pq}u_{p,2q}-\epsilon_{2q}\varphi_{,2q} &= -(e_{\delta p\gamma}u_{p,\delta\gamma}-\epsilon_{\delta\gamma}\varphi_{\delta\gamma}+ \\ &+e_{\delta p2}u_{p,\delta 2}-\epsilon_{\delta 2}\varphi_{\delta 2}), \end{aligned} \tag{A22}$$

taking into account formula (A21 – A22) we obtain finally:

$$\begin{aligned} c_{i2pq}u_{p,2q}+e_{qi2}\varphi_{,2q} &= -(\rho\omega^2 u_i+c_{i\delta\tilde{p}\gamma}u_{p,\delta\gamma}+e_{\gamma i\delta}\tilde{\varphi}_{,\delta\gamma}+\kappa_{i\delta}\varphi_{,\delta}), \\ e_{2pq}u_{p,2q}-\epsilon_{2q}\varphi_{,2q} &= -(e_{\delta\tilde{p}\gamma}u_{p,\delta\gamma}-\epsilon_{\delta\gamma}\tilde{\varphi}_{\delta\gamma}+\kappa_{4\delta}\varphi_{,\delta}) \end{aligned} \tag{A23}$$

where are introduced the following symbols:

$$\begin{aligned} c_{i\delta\tilde{p}\gamma} &\equiv c_{i\delta p\gamma}-c_{i\delta\beta 2}(\Gamma^{-1}_{\beta\alpha}c_{\alpha 2p\gamma}+\Gamma^{-1}_{\beta 4}e_{2p\gamma})-e_{2i\delta}(\Gamma^{-1}_{4\alpha}c_{\alpha 2p\gamma}+\Gamma^{-1}_{44}e_{2p\gamma}), \\ e_{\delta i\gamma} &\equiv e_{\delta i\gamma}-c_{i\delta\beta 2}(\Gamma^{-1}_{\beta\alpha}e_{\gamma\alpha 2}-\Gamma^{-1}_{\beta 4}\epsilon_{2\gamma})-e_{2i\delta}(\Gamma^{-1}_{4\alpha}e_{\gamma\alpha 2}-\Gamma^{-1}_{44}\epsilon_{2\gamma}), \\ e_{\delta\gamma} &\equiv e_{\delta\gamma}+c_{\delta\beta 2}(\Gamma^{-1}_{\beta\alpha}e_{\gamma\alpha 2}-\Gamma^{-1}_{\beta 4}\epsilon_{2\gamma})-e_{2i\delta}(\Gamma^{-1}_{4\alpha}e_{\gamma\alpha 2}-\Gamma^{-1}_{44}\epsilon_{2\gamma}), \\ \kappa_{i\delta} &\equiv \epsilon_0 k(c_{i\delta\beta 2}\Gamma^{-1}_{\beta 4}+e_{2i\delta}\Gamma^{-1}_{44}), \\ \kappa_{4\delta} &\equiv \epsilon_0 k(c_{\delta\beta 2}\Gamma^{-1}_{\beta 4}+e_{\delta 2}\Gamma^{-1}_{44}). \end{aligned} \tag{A24}$$

Substituting (A21), (A22), (A23) and (A23) to the formulas (A17 – A18), we obtain finally **generalised Tiersten boundary conditions for piezoelectric** in the following compact form:

$$T_I=\zeta\rho\omega^2 u_i+c_{i\delta\tilde{p}\gamma}(\zeta u_{p,\gamma})_{,\delta}+\tilde{e}_{\gamma i\delta}(\zeta\varphi_{,\gamma})_{,\delta}+\kappa_{i\delta}(\zeta\varphi)_{,\delta}, \tag{A25}$$

$$\begin{aligned} \Delta D_2 &= e_{\delta\tilde{p}\gamma}(\zeta u_{p,\gamma})_{,\delta}-\epsilon_{\delta\gamma}(\zeta\varphi_{,\gamma})_{,\delta}+\kappa_{4\delta}(\zeta\varphi)_{,\delta}, \\ &+\epsilon_0(\eta\varphi_{,1}+\theta\varphi_{,3})-\zeta\epsilon_0 k(\kappa_{p\delta}u_{p,\delta}+\kappa_{4\delta}\varphi_{,\delta})+\zeta(\epsilon_0 k)^2\varphi. \end{aligned} \tag{A26}$$

Substituting u_j and φ from (A3) to above formulas, performing differentiation with δ, $\gamma=1, 3$ and collecting terms with the same m and n we obtain generalised Tiersten boundary conditions in matrix form, useful in numerical calculations. Generally they are complicated but for certain piezoelectric materials (i.e. BGO, α-quartz, $LiNbO_3$) they are much simpler due to limited number of non-zero elements of material tensors e_{qij}, ϵ_{ij}, c_{ijpq} [4].

For one-dimensional periodic grooves $K_x=0$, $\eta=0$, $m=0$ and presented above formulas may be written in the form (11).

Acknowledgment

This work is partially supported by KBN Grant 8 S501 001 07.

The author would like to thank prof. Eugene Danicki for his constructive suggestions and kindly remarks which were very helpful during preparation of this article.

References

[1] B.A. AULD, *Acoustic fields and waves in solids*, Wiley, 1973.

[2] E. DIEULESAINT and D. ROYER, *Ondes élastiques dans les solides*, Masson, 1974.

[3] I.A. VIKTOROV, *Rayleigh and Lamb waves*, Plenum Press, 1967.

[4] B.A. AULD, *Acoustic fields and waves in solids*, Wiley 1973.

[5] D.P. MORGAN, *Surface-wave devices for signal proceeding*, Elsevier 1985.

[6] A. PELCZAR, *Wstęp do teorii równań różniczkowych*, [in Polish], v. II, PWN, 1989.

[7] A.I. BELTZER, *Acoustic of solids*, Springer-Verlag, 1988.

[8] E. DANICKI, *Perturbation theory of surface acoustic wave reflection from a periodic structure with arbitrary angle of incidence*, Arch. Mech., **36** (1984).

[9] E. DANICKI, *Rezonator z AFP z konwersją modów* [in Polish], Biuletyn WAT, **37** (1988).

[10] E. DANICKI and D. BOGUCKI, *Wave propagation and scattering in elastic plate with periodically grooved surface*, Arch. of Acoustics, **18** (1993).

[11] A.P. MAYER, A.A. MARADUDIN and W. ZIERAU, *Surface acoustic waves propagation along the grooves of a periodic grating*, Journal of Appl. Phys., **69** (1990).

[12] A.A. MARADUDIN and X. HUANG, *Propagation of horizontal surface acoustic waves parallel to the groves of a random grating*, Journal of Appl. Phys., **70** (1991).

[13] S.G. JOSHI and Y. JIN, *Propagation of ultrasonic Lamb waves in piezoelectric plates*, J. Appl. Phys., **70** (1991).

[14] Y. JIN and S.G. JOSHI, *Electromechanical coupling coefficients of ultrasonics Lamb waves*, JASA, 93, 1993.

[15] F. JOSSE, J.C. ANDLE and J.F. VETELINO, *A theoretical study of acoustic plate modes as biosensing element*, Proc. of 1991 IEEE Ultrasonic Symposium, 1991.

Writing equation of motion for piezoelectric (A1) as follows:

$$[illegible] \qquad (A23)$$

where are introduced the following symbols:

$$[illegible] \qquad (A24)$$

Substituting (A21), (A22), (A23) and (A23) to the formulas (A17 - A18), we obtain finally generalised Tiersten boundary conditions for piezoelectric in the following compact form:

$$T_j = [illegible] \qquad (A25)$$

$$\Delta D_3 = [illegible] \qquad (A26)$$

$$[illegible]$$

Substituting u_j and φ from (A1) to above formulas, performing differentiation with δ, γ=1, 3 and collecting terms with the same m and n we obtain generalised Tiersten boundary conditions in matrix form, useful in numerical calculations. Generally they are complicated but for certain piezoelectric materials (i.e. PZT, x-quartz, $LiNbO_3$) they are much simpler due to limited number of non-zero elements of material tensors e_{ijk}, ϵ_{ij}, c_{ijkl} [4].

For one-dimensional periodic grooves $K_2 = 0$, $m = 0$, $n = 0$ and presented above formulas may be written in the form (11).

Acknowledgement

This work is partially supported by KBN Grant 8 S 501 001 07.

The author would like to thank prof. Eugeniusz Danicki for his constructive suggestions and kindly remarks which were very helpful during preparation of the article.

ARCHIVES OF ACOUSTICS
20, 3, 271–276 (1995)

ASYMPTOTIC SOLUTION OF ACOUSTIC NONLINEAR WAVE EQUATION WITH FRICTION

K. WERNEROWSKI

J. and A. Śniadecki Academy of Technology and Agriculture, Mechanical Department
Chair of Applied Mechanics
Dynamics and Vibroacoustic Establishment
(85-763 Bydgoszcz, S. Kaliski 7)

A contribution to the development of asymptotic method of small parameter was made and applied to the analysis of the propagation of nonlinear acoustic waves. The result is close to strict empiric function. Asymptotic solution of acoustic nonlinear wave equation with friction was found. The result enables the propagation velocity and the pressure of an acoustic wave to be evaluated.

1. Introduction

The computation problem of longitudinal acoustic wave with friction is very important for the duct model of porous material. Absorption of porous materials is mostly tested experimentally [1, 4]. Nonlinear approximate analysis is also performed to same extent [3 ÷ 5].

Next stage of the development of wave equation analysis is the asymptotic averaging [2].

Even today the strict solution of the non-linear propagation equation of acoustic waves with friction and partial derivatives is not known. The results approach strict formula.

2. Analysis

Theoretical analysis must be connected with reality. Taking into account the duct friction of prorous material we improve the compatibility of the theory with experiments.

Sound propagation is always partly nonlinear. For high intensity levels over 100 dB the nonlinearity cannot be neglected. An approximate theoretical analysis of acoustical waves with finite amplitude is to be performed.

The first method used in the nonlinear procedure of solving nonlinear equations was the method of small parameter H. Poincaré and others, the next one was the

method of Kryłowa – Bogoljubova [2] and now we present better results obained with asymptotic averaging of equations.

Nonlinear equation with friction of the propagation of longitudinal propagating in the direction of the Ox-axis can be written in the following form

$$\frac{\partial^2 u}{\partial t^2} - C_0^2 \frac{\partial^2 u}{\partial a^2} = \varepsilon f\left(\frac{\partial u}{\partial a}, \frac{\partial^2 u}{\partial a^2}, \frac{\partial u}{\partial t}\right), \tag{2.1}$$

$$a = x - u$$

where u — displacement, C_0 — sound velocity, a — Lagrange coordinate, ε — small parameter.

The main source of nonlinearity is the adiabatic process. Friction is a nonlinear function of velocity.

Nonlinear term f can be written in the following form

$$f = \left[\left(1+\frac{\partial u}{\partial a}\right)^{-(\varkappa+1)} - 1\right]\frac{\partial^2 u}{\partial a^2} - r_j \frac{\partial u}{\partial t}, \tag{2.1a}$$

where $\varkappa = 1, 4$ — adiabatic exponent, r_j — flow resistance.
For the value

$$\left|\frac{\partial u}{\partial a}\right| < 1, \tag{2.2}$$

we can epand the first part of nonlinear formula (2.1a) into convergent power series

$$\left(1+\frac{\partial u}{\partial a}\right)^{-(\varkappa+1)} = 1 - (\varkappa+1)\frac{\partial u}{\partial a} + \frac{1}{2}(\varkappa+1)(\varkappa+2)\left(\frac{\partial u}{\partial a}\right)^2 \tag{2.3}$$

$$-\frac{1}{3!}(\varkappa+1)(\varkappa+2)(\varkappa+3)\left(\frac{\partial u}{\partial a}\right)^3 + \ldots + (\pm 1)^k \frac{1}{k!}(\varkappa+1)(\varkappa+2)\ldots$$

$$\ldots(\varkappa+k)\left(\frac{\partial u}{\partial a}\right)^k \pm \ldots$$

Number k determines the numerical accuracy.
After inserting Eq. (2.3) into Eq. (2.1 a), we obtain

$$f\left(\frac{\partial u}{\partial a}, \frac{\partial^2 u}{\partial a^2}, \frac{\partial u}{\partial t}\right) = [-(\varkappa+1)k!\frac{\partial u}{\partial a} + (\varkappa+1)(\varkappa+2)(k-1)!\left(\frac{\partial u}{\partial a}\right)^2 \tag{2.4}$$

$$-\frac{1}{3!}(\varkappa+1)(\varkappa+2)(\varkappa+3)\left(\frac{\partial u}{\partial a}\right)^3 + \ldots + (\pm 1)^k \frac{1}{k!}(\varkappa+1)(\varkappa+2)\ldots$$

$$\ldots(\varkappa+k)\left(\frac{\partial u}{\partial a}\right)^k \pm \ldots - 1]\frac{\partial^2 u}{\partial a^2} - r_j \frac{\partial u}{\partial t},$$

$$\varepsilon=\frac{c_0^2}{k!}>0, \tag{2.5}$$

$$c_0=\left(\frac{P_0\varkappa}{\rho_0}\right)^{0.5}. \tag{2.6}$$

Equation (2.1) may now be rewritten as follows

$$\frac{\partial^2 u}{\partial t^2}-c_0^2\frac{\partial^2 u}{\partial a^2}=\varepsilon\left([-(\varkappa+1)k!\frac{\partial u}{\partial a}+(\varkappa+1)(\varkappa+2)(k-1)!\left(\frac{\partial u}{\partial a}\right)^2\right.$$

$$-\frac{1}{3!}(\varkappa+1)(\varkappa+2)(\varkappa+3)\left(\frac{\partial u}{\partial a}\right)^3+\ldots+(\pm 1)^k\frac{1}{k!}(\varkappa+1)(\varkappa+2)\ldots \tag{2.7}$$

$$\left.\ldots(\varkappa+k)\left(\frac{\partial u}{\partial a}\right)^k\pm\ldots-1\right]\frac{\partial^2 u}{\partial a^2}-r_j\frac{\partial u}{\partial t}.$$

The knowledge of the boundary conditions is necessary for solving Eq. (2.7). Displacement and velocity depend only on the Lagrange coordinate a

$$u(a,0)=\psi(a), \quad \frac{\partial u(a,0)}{\partial t}=\phi(a), \tag{2.8}$$

$$0<a<1. \tag{2.9}$$

The displacements at the ends of the duct vanishes

$$u(0,t)=0, \quad u(1,t)=0, \tag{2.10}$$

where: 1 — duct length of porous layer.
The overall solution has the form

$$u=\sum_{n=1}^{\infty}A_n(t,\varepsilon)\cos[\omega_n^{(0)}t+\delta_n(t,\varepsilon)]\sin\frac{n\Pi a}{l}, \tag{2.11}$$

$$\frac{\partial u}{\partial a}=\frac{\Pi}{1}\sum_{n=1}^{\infty}nA_n(t,\varepsilon)\cos[\omega_n^{(0)}t+\delta_n(t,\varepsilon)]\cos\frac{n\Pi a}{l}, \tag{2.12}$$

$$\frac{\partial^2 u}{\partial a^2}=-\frac{\Pi^2}{l^2}\sum_{n=1}n^2A_n(t,\varepsilon)\cos[\omega_n^{(0)}t+\delta_n(t,\varepsilon)]\sin\frac{n\Pi a}{l}, \tag{2.13}$$

$$\frac{\partial u}{\partial t}=\left(\sum_{n=1}^{\infty}\frac{\partial A_n(t,\varepsilon)}{\partial t}\cos[\omega_n^{(0)}t+\delta_n(t,\varepsilon)]\right.$$

$$\left.-\sum_{n=1}\left[\omega_n^{(0)}+\frac{\partial_n(t,\varepsilon)}{\partial t}\right]A_n(t,\varepsilon)\sin[\omega_n^{(0)}t+\delta_n(t,\varepsilon)]\right)\sin\frac{n\Pi a}{l}, \tag{2.14}$$

$$\frac{\partial^2 u}{\partial t^2}=\Bigg(\sum_{n=1}^{\infty}\frac{\partial^2 A_n(t,\varepsilon)}{\partial t^2}\cos[\omega_n^{(0)}t+\delta_n(t,\varepsilon)]\,(+)$$

$$-\sum_{n=1}^{\infty}\frac{\partial A_n(t,\varepsilon)}{\partial t}\left[\omega_n^{(0)}+\frac{\partial\delta_n(t,\varepsilon)}{\partial t}\right]\sin[\omega_n^{(0)}t+\delta_n(t,\varepsilon)]\,(+) \tag{2.15}$$

$$-\Bigg(\sum_{n=1}^{\infty}\frac{\partial^2\delta_n(t,\varepsilon)}{\partial t^2}A_n(t,\varepsilon)\sin[\omega_n^{(0)}t+\delta_n(t,\varepsilon)]+$$

$$+\sum_{n=1}^{\infty}\left[\omega_n^{(0)}+\frac{\partial\delta_n(t,\varepsilon)}{\partial t}\right]\frac{\partial A_n(t,\varepsilon)}{\partial t}\sin[\omega_n^{(0)}t+\delta_n(t,\varepsilon)]+$$

$$+\sum_{n=1}^{\infty}\left[\omega_n^{(0)}+\frac{\partial\delta_n(t,\varepsilon)}{\partial t}\right]^2 A_n(t,\varepsilon)\cos[\omega_n^{(0)}t+\delta_n(t,\varepsilon)]\Bigg)\cdot\sin\frac{n\Pi a}{l}$$

Taking into account

$$\omega_n^{(0)}t+\delta_n(t,\varepsilon)=\varphi_n(t,\varepsilon) \tag{1.15a}$$

we obtain the nonlinear part

$$\varepsilon f\equiv\varepsilon\Bigg(\Bigg[-(\varkappa+1)k!\frac{\Pi}{l}\sum_{n=1}^{\infty}n\,A_n(t,\varepsilon)\cos\varphi_n(t,\varepsilon)\cos\frac{n\Pi a}{l}+ \tag{2.16}$$

$$+\ldots-1\Bigg]\left(-\frac{\Pi^2}{l^2}\right)\sum_{n=1}^{\infty}(n^2A_n(t,\varepsilon)\cos\varphi_n(t,\varepsilon)\sin\frac{n\Pi a}{l}-r_j)\cdot$$

$$\cdot\Bigg(\sum_{n=1}^{\infty}\frac{\partial A_n(t,\varepsilon)}{\partial t}\cos\varphi_n(t,\varepsilon)-\sum_{n=1}^{\infty}\left[\omega_n^{(0)}+\frac{\partial\delta_n(t,\varepsilon)}{\partial t}\right]A_n(t,\varepsilon)\cdot\sin\varphi_n(t,\varepsilon)\Bigg)\sin\frac{n\Pi a}{l}\Bigg).$$

The utility of the asymptotic method can be seen after averaging and analysing the convergence of trigonometric terms

$$\lim_{T\to\infty}\frac{1}{T}\int_0^T(t,A_n,\varphi_n)\sin\varphi_n\,dt=X_{on}(A_n,\delta_n),$$

$$\lim_{T\to\infty}\frac{1}{T}\int_0^T f_{on}(t,A_n,\varphi_n)\sin\varphi_n\,dt=Y_{on}(A_n,\delta_n), \tag{2.17}$$

where: f_{on} — Fourier coefficients.

On the basis of Eqs. (2.15)–(2.17) we can write

$$f_{on}^{(1)}=(\varkappa+1)k!\frac{\Pi^3}{l^3}n^3A_n^2\cos^2\varphi_n^{(0)}-\left[\omega_n^{(0)}+\frac{\partial\delta_n(t,\varepsilon)}{\partial t}\right]A_n\sin\varphi_n^{(0)}. \tag{2.18}$$

Convergence of trigonometric terms leads to

$$\underset{t}{M}(\cos^2\varphi_n^{(0)}\sin\varphi_n^{(0)}) \equiv \lim \frac{1}{T}\int_0^T \cos^2\varphi_n^{(0)}\sin\varphi_n^{(0)}\,dt = 0. \tag{2.19}$$

$$\underset{t}{M}\{\cos\varphi_n^{(0)}\sin\varphi_n^{(0)}\} = 0. \tag{2.20}$$

$$\underset{t}{M}\{\sin^2\varphi_n^{(0)}\} = 0.5. \tag{2.21}$$

Often

$$\frac{\partial\delta_n(t,\varepsilon)}{\partial t} = \text{const} = C. \tag{2.22}$$

The amplitude A_n may be derived as A_n' from averaging

$$\frac{dA_n'}{dt} = -\frac{\varepsilon}{\omega_n^{(0)}} X_{on}. \tag{2.23}$$

$$\frac{dA_n'}{dt} = -0.5\,\varepsilon[\omega_n^{(0)}]^{-1}[\omega_n^{(0)} + C]A_n'. \tag{2.24}$$

After integration we obtain

$$A_n' = A_{no}\exp\{-0.5[\omega_n^{(0)}]^{-1}[\omega_n^{(0)} + C]\}. \tag{2.25}$$

Let us analyse the third part of expanding Eq. (2.17), (2.16)

$$f_{on}^{(0)} = \frac{1}{3!}(\varkappa+1)(\varkappa+2)(\varkappa+3)\frac{\Pi^5}{l^5}n^5 A_n^4\cos^4\varphi_n^{(0)}, \tag{2.26}$$

$$\underset{t}{M}\{\cos^4\varphi_n^{(0)}\} = \frac{3}{8}. \tag{2.27}$$

Mean value of δ_n is denoted by δ_n'. It is involved in the following equation:

$$\frac{d\delta_n'}{dt} = -\frac{\varepsilon}{\omega_n^{(0)}} Y_{on}, \tag{2.28}$$

After averaging A_{no} is replaced by $A_n^{(0)}$ and

$$\frac{d\delta_n'}{dt} = -\frac{\varepsilon}{\omega_n^{(0)}}\frac{1}{16}(\varkappa+1)(\varkappa+2)(\varkappa+3)\frac{\Pi^5}{l^5}n^5 A_n^{(0)4}. \tag{2.29}$$

$$\delta_n' = -685\frac{\varepsilon n^5}{\omega_n^{(0)} l^5}A_n^{(0)4}\,t. \tag{2.30}$$

Differentiating the formula (2.30) we obtain the mean value of constant (2.22)

$$c=c'=\frac{\partial\delta_n'}{\partial t}=-685\frac{\varepsilon n^2 A_n^{(0)4}}{\omega_n^{(0)} l^5} \tag{2.31}$$

The solution of equation (2.1) has the form

$$u=\sum_{n=1} A_{no}\exp\{-0.5[\omega_n^{(0)}]^{-1}\left[\omega_n^{(0)}-685\frac{\varepsilon n^5 A_n^{(0)4}}{\omega_n^{(0)} l^5}\right]\}\cdot \cdot\cos\left[\omega_n^{(0)}-685\frac{\varepsilon n^5 A_n^{(0)4}}{\omega_n^{(0)} l^5}\right]t\cdot\sin\frac{n\Pi a}{l} \tag{2.32}$$

3. Concluding remarks

After averaging and convergence analysis, the asymptotic solution is obtained to the nonlinear equation of longitudinal wave propagation. The obtained formula is a good approximation of the exact solution and is in good fitness with experimental result [1, 5]. The pressure level is very important parameter in this analysis since from formula (2.32).

References

[1] L.L. BERANEK [Ed.], *Handbook of Noise Control*, Mc Graw Hill Co., New York 1971.

[2] G.P. CHOMA, *Niekotorye woprosy obosnowanija asimptoticzeskogo metoda. N.M. Kryłowa–N.N. Bogoljubowa.*, Led U.AN, Kijew 1988.

[3] E. KARAŚKIEWICZ, *Teoria nieliniowa rezonatora dla niskich częstostliwości*, Proceedings of VIII Sem. Otw. z Akustyki, Szczecin 1961.

[4] I MAŁECKI, *Teoria fal i układów akustycznych*, Państwowe Wydawnictwo Naukowe, Warszawa 1964.

[5] Multi-author work, *Encyklopedia fizyki współczesnej, akustyka*, Państwowe Wydawnictwo Naukowe, Warszawa 1983.

ARCHIVES OF ACOUSTICS
20, 3, 277–286 (1995)

ACOUSTIC EMISSION IN MOISTENED BRICKS AND WOOD

W. KOŁTOŃSKI

Institute of Fundamental Technological Research
Polish Academy of Sciences
(00-049 Warszawa, Swiętokrzyska 21)

Initial investigations were carried out concerning an occurrence of acoustic emission in different kinds of bricks and woods under moistening. The results are presented and discussed of these investigations and possibilities of their practical applications for finding out water leakages in places difficult of access in buildings made of bricks and wood.

1. Introduction

Successful results of the experiments, which were carried out in the years from 1987 to 1990, indicated practical possibilities of applications of acoustic emission (AE) caused by water permeation into concrete. It has induced an interest in this kind of investigations for other materials used in building industry, such as bricks and wood.

2. Measurements of AE parameters for the samples of moistened bricks

2.1. Procedure of measurements

For experiments, 5 specimens (without cracks) of each kind of the following types of bricks were chosen:

common cavity brick
common solid brick
cement solid white brick
clinker solid brick

Each specimen was placed on the corrugated bottom of a laboratory dish in this manner that the largest surface of the brick was in contact with the bottom. This dish was supplied with water (0.25 l/h), which had been de-aerated. Owing to the corrugated bottom, water was able to contact with the almost whole lower surface of the brick and permeate from the brick bottom. The accelometer which was the receiver of AE signals was glued to the upper surface of the brick. Few minutes before

turning the water supply on, the measurement equipment was switched on and the natural level of AE was measured for the tested brick. According to that, the sensitivity level of the equipment was adjusted to eliminate unnecessary signals. Subsequently, after turning the water supply on, the densities of events N_e and energy E_s in 10-second intervals were measured during period of time longer than one hour and recorded by *Y-t* plotter. Every ten minutes, the fundamental frequency f_p of received signals of AE was also measured (at random).

To check whether the phenomenon of AE occurs in the moistened bricks some samples were immersed in 10 mm layer of water (the water supply was turned off) during 24 hours. After that, the measurements of $\dot{N}_e$, E_s and f_p were continued.

Repeatability of this phenomenon was also tested, by measurements of the same AE parameters as previously, for the bricks that were totally dried after first experiment and subsequently again exposed to the influence of water.

To carry out the above mentioned measurements, the setup, which is schematically presented in Fig. 1, was applied *1* denotes the accelometer KD32 made in GDR, *2*— the preamplifier of the AE signals type EA 233-5, Unipan, *3* — the band amplifier 232 B, Unipan, *4* — the apparatus (own construction) for measurements of $\dot{N}_e$ and E_s, *5* — the analog plotter *Y-t* B72BP, made in Japan, *6* — digital oscilloscope 2230, Tektronix, *7*— the sample of tested material.

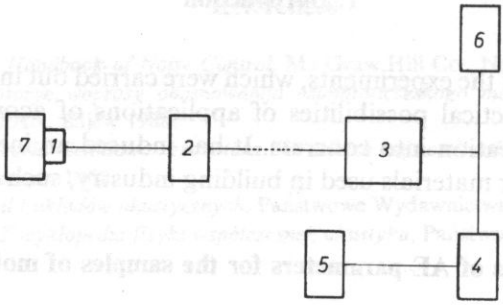

Fig. 1. Brock diagram of the measurement setup.

The signals of AE were received for 20 specimens of the bricks and the parameters of the signals were measured in the ranges of frequency 5 – 15 kHz and 15 – 50 khZ.

To avoid the most important results of testing are only presented.

2.2. Discussion of the measurement results

In Figure 2 examples of the records of changes $\dot{N}_e$ and E_s are presented for the common cavity brick. They began after compensation the natural level of AE and were continued during about one hour after turning water supply on. The zero level of the record corresponds to the time of water flowing up to the tested sample. After that flowing up, AE appeared immediately. The AE parameters, $\dot{N}_e$ and E_s, increase with the icreasing contact surface between the sample and water increases due to the

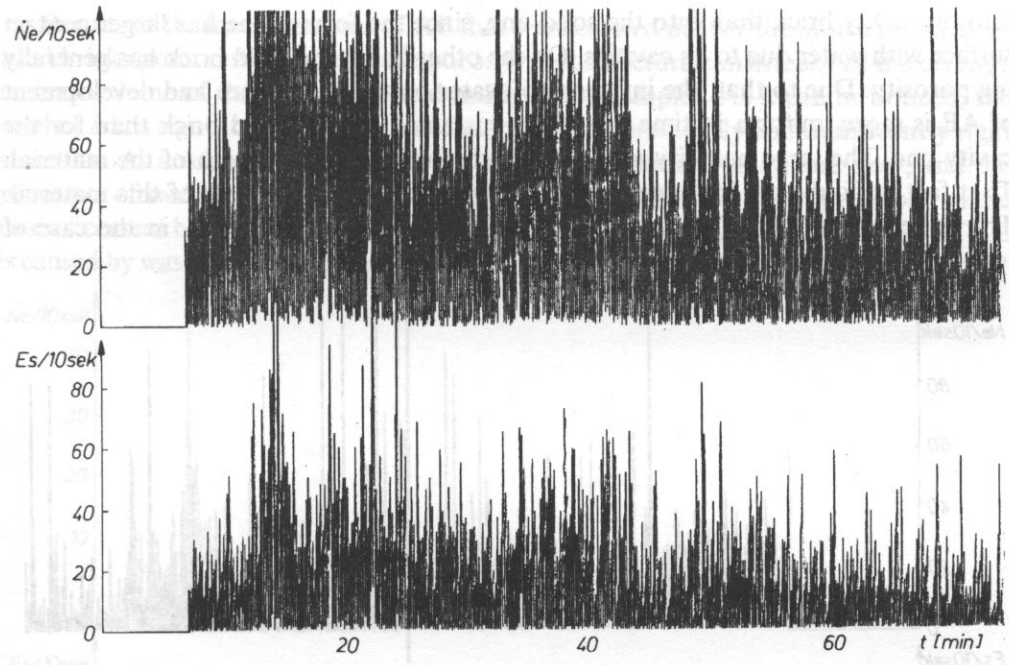

Fig. 2. Results of measurements of $\dot{N}_e$ and E_s in the moistened common cavity brick.

increase of water level. However, after about 60 minutes, the mean level of AE began to decrease slowly, but it remained large even after 24 hours, despite of turning water supply off. The randomly measured fundamental frequencies of AE signals were changed from about 5 kHz to about 75 kHz (see Fig. 3).

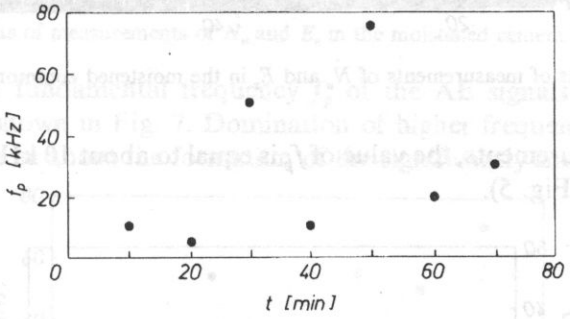

Fig. 3. Results of measurements of f_p in the moistened common cavity brick.

Exemplary results of measurements $\dot{N}_e$ and E_s are shown in Fig. 4 for the common solid bricks under moistening. In this case the mean level of AE is lower than that of the cavity brick but it decreases only slightly after 24 hours of the water influence. Most probably, the origin of this difference is the more intensive water permeation

into the cavity brick than into the solid one, since the former one has larger contact surface with water due to its cavities. On the other hand, the solid brick has generally big porosity. Due to that, the influence of water on the occurrence and development of AE is more uniform in time and more sustained for the solid brick than for the cavity one. The large porosity also reduces the rigidity and strength of the material. That fact undoubtedly influences on the course of sweeling process of this material. The large fluctuation of values of the AE parameters confirm that, in the case of longer moistening in particular.

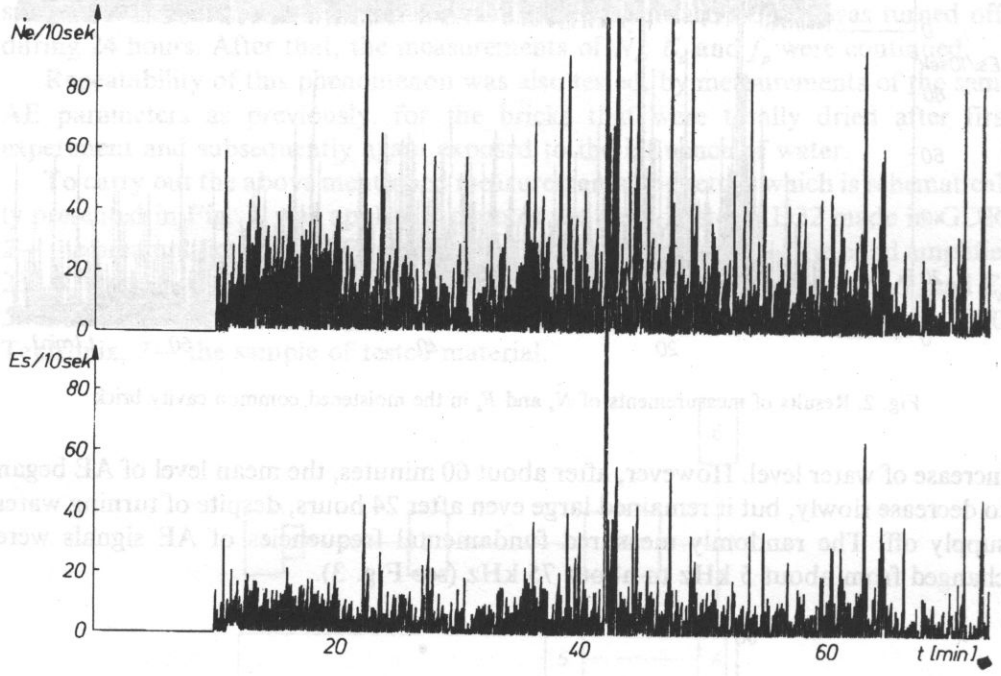

Fig. 4. Results of measurements of $\dot{N}_e$ and E_s in the moistened common solid brick.

From the measurements, the value of f_p is equal to about 10 kHz and rarely about 25 or 50 kHz (see Fig. 5).

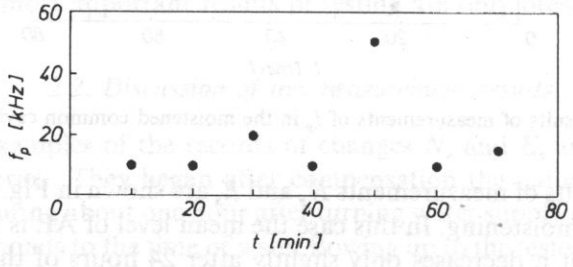

Fig. 5. Results of measurements of f_p in the moistened common solid brick.

Results of the measurements of AE that were carried out for the moistened cement solid bricks point out the role of the porosity and structure consistency of the ceramic material. Some of them are presented in Fig. 6 as examples. As it can be noticed, the level of AE is significantly lower than that measured previously and significantly rigid structure. As a consequence of that, the water permeation is small and slow, and the processes of swelling and cracking of the material are impeded. Most probably, in the case of cement bricks, the initial and momentary, but rapid increase of the level of AE is caused by washing out a cement dust from the pores near the surface of this brick [3].

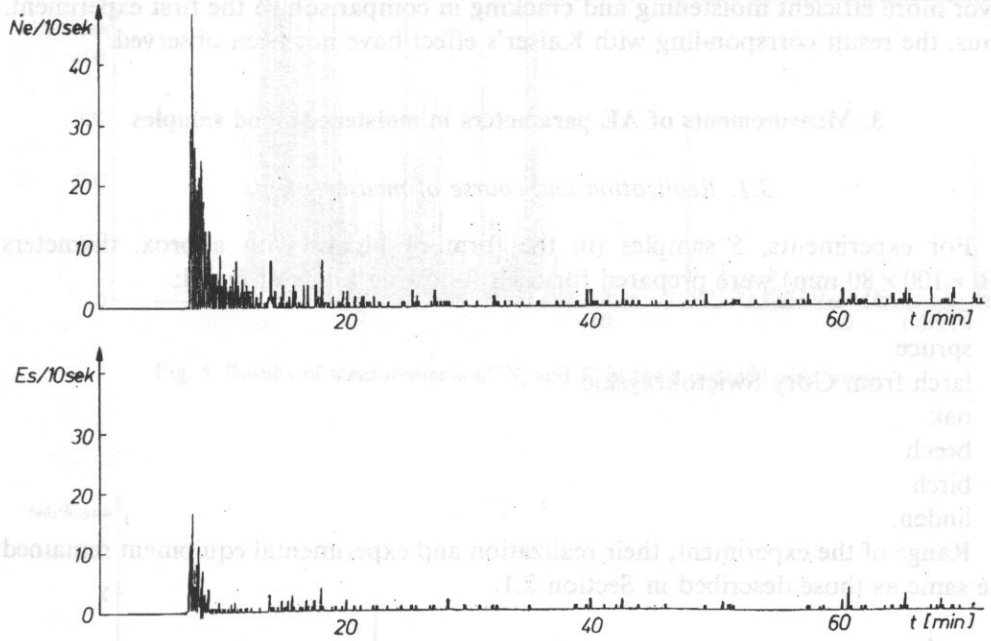

Fig. 6. Results of measurements of $\dot{N}_e$ and E_s in the moistened cement solid brick.

Changes of the fundamental frequency f_p of the AE signals, received for the cement brick, are shown in Fig. 7. Domination of higher frequencies in the end of experiment informs us about the formation of the significantly smaller cracks of the

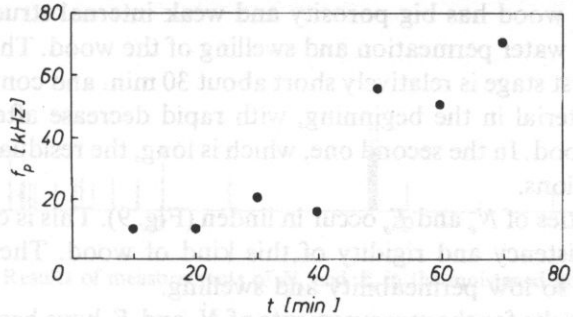

Fig. 5. Results of measurements of f_p in the moistened cement solid brick.

material in this period than the first stage of moistening. It is caused undoubtedly by the slow water permeation, and the large rigidity and structure consistency of this brick. All of them result in the microcracks appeared after 40 – 50 minutes from the start of sweeling.

After drying the bricks used in the first experiment, their repeated moistening produces higher level of AE than previously [3]. This increase of AE level, particularly large for the solid bricks, is caused by the changes destruction in the material structure, the destruction being caused by the first swell. These structure changes favor more efficient moistening and cracking in comparison to the first experiment. Thus, the result corrsponding with Kaiser's effect have not been observed.

3. Measurements of AE parameters in moistened wood samples

3.1. Realization and course of measurements

For experiments, 5 samples (in the form of blocks with approx. diameters $150 \times 100 \times 80$ mm) were prepared for each following kinds of wood:

pine
spruce
larch from Góry Świętokrzyskie
oak
beech
birch
linden.

Range of the experiment, their realization and experimental equipment remained the same as those described in Section 2.1.

3.2. Obtained results and discussion

In Figs. 8 and 9, the most interesting examples of the measurement results of $\dot{N}_e$ and E_s in the moistened samples of pine and linden woods, are presented. The highest level of AE, decreasing significantly after about half an hour, occurred for the pine wood, because this wood has big porosity and weak internal structure. This causes rapid and intensive water permeation and swelling of the wood. The swelling process is two stage. The first stage is relatively short about 30 min. and contains the intensive swelling of the material in the beginning, with rapid decrease after complete water saturation of the wood. In the second one, which is long, the residual swelling remains with small fluctuations.

The small densities of $\dot{N}_e$ and E_s occur in linden (Fig. 9). This is connected with the low porosity, consistency and rigidity of this kind of wood. These features of the linden wood cause so low permeability and swelling.

Intermediate results for the measurements of $\dot{N}_e$ and E_s have been obtained for the moistened spruce, beech and birch woods.

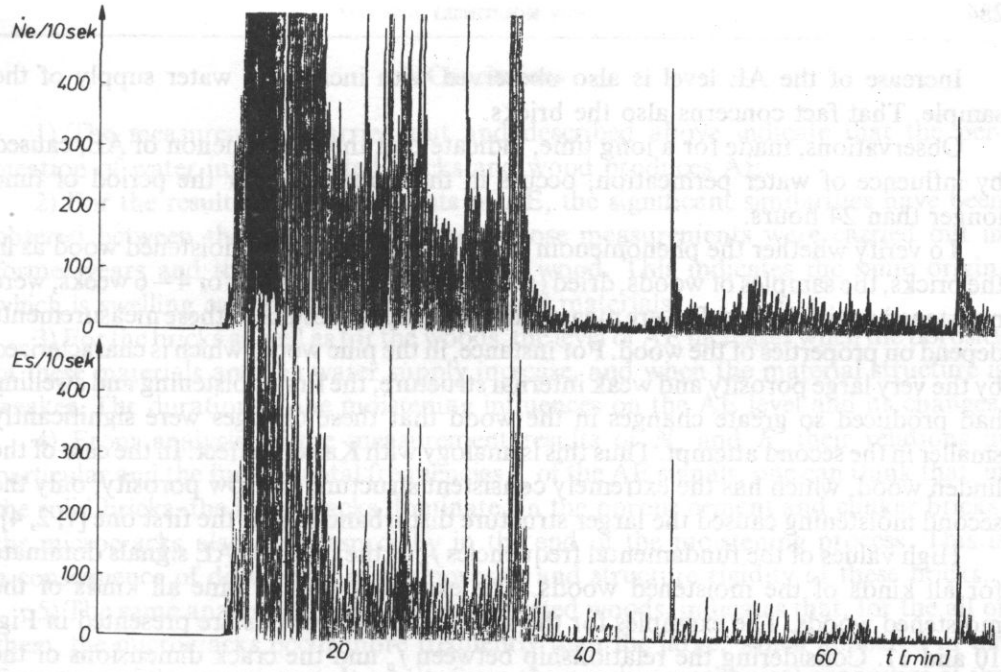

Fig. 8. Results of measurements of $\dot{N}_e$ and E_s in the moistened pine wood.

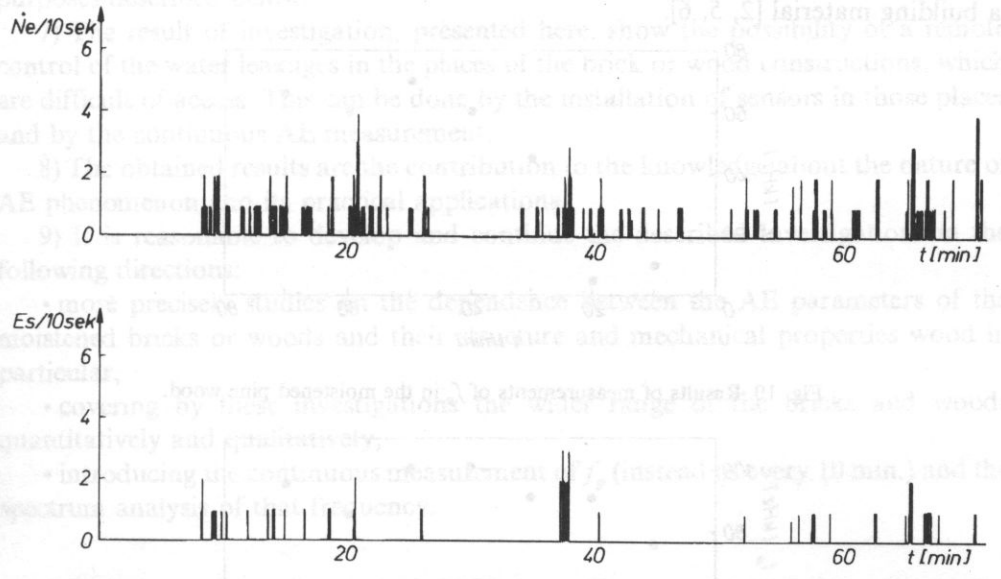

Fig. 8. Results of measurements of $\dot{N}_e$ and E_s in the moistened linden wood.

Increase of the AE level is also obeserved with increasing water supply of the sample. That fact concerns also the bricks.

Observations, made for a long time, indicate that the phenomenon of AE, caused by influence of water permeation, occurs in the wood even for the period of time longer than 24 hours.

To verify whether the phenomenoin of AE is reatable in the moistened wood as in the bricks, the samples of woods, dried (after the first experiment) for 4 – 6 weeks, were moistened again. $\dot{N}_e$ and E_s were measured. As fromerly, results of these measurements depend on properties of the wood. For instance, in the pine wood, which is characterized by the very large porosity and weak internal structure, the first moistening and swelling had produced so greate changes in the wood that these changes were significantly smaller in the second attempt. Thus this is analogy with Kaiser's effect. In the case of the linden wood, which has the extremely consistent structure and low porosity, only the second moistening caused the larger structure disturbances than the first one [1, 2, 4].

High values of the fundamental frequencies f_p of the received AE signals dominate for all kinds of the moistened woods. The examples for the pine all kinds of the moistened woods. The examples for the pine and linden woods are presented in Fig. 10 and 11. Considering the relationship between f_p and the crack dimensions of the material see the publication in Archives of Acoustics, **17**, 1 (1992), one can conclude that, in the not warped wood, the swelling process produces mainly the microcracks this makes distinction to the bricks. That fact is connected with the peculiar mechanical properties of the wood, owing to which the wood is so important as a building material [2, 5, 6].

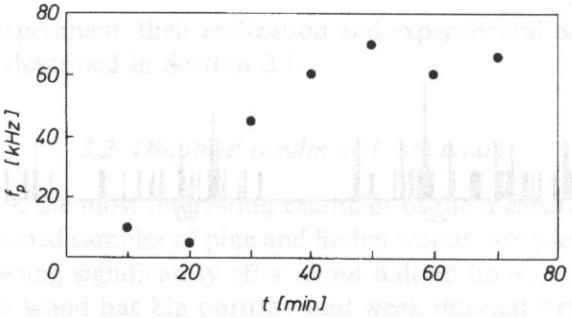

Fig. 10. Results of measurements of f_p in the moistened pine wood.

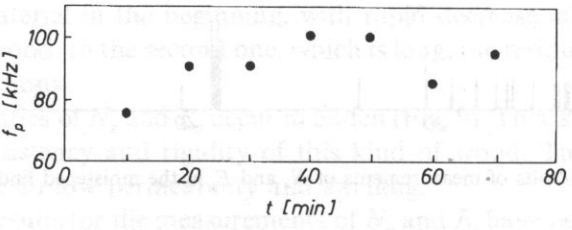

Fig. 11. Results of measurements of f_p in the moistened linden wood.

Conclusions

1) The measurements carried out and described above indicate that the permeation of water into the tested bricks and wood produces AE.

2) For the results of measurements of AE, the significant similarities have been observd between the moistened concrete those measurements were carried out in former years and the moistened bricks and wood. This indicates the same origin, which is swelling causing AE in all mentioned materials.

3) For the bricks as well as for the woods, the level of AE increases when the porosity of these materials and the water supply increase, and when the material structure is weaker. The duration of the moistening influences on the AE level and its changes.

4) From analysis of the measurement results of $\dot{N}_e$ and E_s their relations in particular and the fundamental frequencies f_p of the AE signals, one can think that, in the solid bricks, the large cracks dominate. In the porous cement and clinker bricks, the microcracks also exist, especially in the end of the moistening process. This is a consequence of differences of the porosity and structure rigidity of these bricks.

5) The same analysis performed for the tested woods, indicates that, for the all of them, the microcracks occur more frequently than the large, which appeared in the first stage of the experiment. It results from the peculiar mechanical properties of the wood low brittleness.

6) The established repeatibility and long duration of the AE phenomenon in the moistened bricks and woods are important from the practical point of view for purposes described below.

7) The result of investigation, presented here, show the possibility of a remote control of the water leakages in the places of the brick or wood constructions, which are difficult of access. This can be done by the installation of sensors in those places and by the continuous AE measurement.

8) The obtained results are the contribution to the knowledge about the nature of AE phenomenon and its practical applications.

9) It is reasonable to develop and continue the described investigations in the following directions:

- more precisely studies on the dependence between the AE parameters of the moistened bricks or woods and their structure and mechanical properties wood in particular,
- covering by these investigations the wider range of the bricks and woods quantitatively and qualitatively,
- introducing the continuous measurement of f_p (instead of every 10 min.) and the spectrum analysis of that frequency.

References

[1] F.G. BEALL, *Effect of moisture conditioning on acoustic emission from particleboard*, J. Acoustic Emiss., 5, 2, 71–76 (1986).

[2] A.F. BECKER, *Schallemissionen während der Holztrocknung*, Holz als Roh- und Werkst., **40**, 9, 345–350 (1982)

[3] W. KOŁTOŃSKI, *Acoustic emission in damp concrete and possibilities of its practical application* (in Polish) Arch. Akust.,

[4] A. MISHIRO, *Studies on the sweeling pressure of wood. II. The effect of initial moisture content of wood*, Mokuzai Gakk., **19**, 2, 63–68 (1973).

[5] W. MOLIŃSKI and J. RACZKOWSKI, *Mechanical stresses generated by water adsorption in wood and their determination by tension creep measurement*, Wood Sci. and Technol., **22**, 3, 193–198 (1988).

[6] P. SUCHORSKI and W. MOLIŃSKI, *Detection of structural changes in wood during moistening using acoustic emission method*, Proc. VIII Symp. „Fundamental Wood Research" Jadwisin 1990.

ARCHIVES OF ACOUSTICS
20, 3, 287–298 (1995)

THE DEVELOPMENT OF DEFORMATION PROCESS IN CARBON FIBER REINFORCED PLASTICS AND METALS ON ACOUSTIC EMISSION DATA

A.M. LEKSOVSKIJ*, S. PILECKI** AND G.N. GUBANOVA*

*Ioffe Physico-Technical Institute, Russian Acad. Sci., St. Petersburg
**Institute of Fundamental Technological Research, Polish Academy of Sciences
(00–049 Warszawa, Świętokrzyska 21)

There exists some correlation between deformation curve type and characteristics of acoustic emission flow. It is observed nonhomogeneous development of micro structure changes in the different parts of the specimens on diverse stages of deformation. The collective effects on various scale levels are observed in some local volumes at the concluding period of loading. It is shown that a process of the fracture occurring in some micro volumes of strained composite of the type of carbon fiber reinforced plastic (CFRP), takes place on a few levels of velocity and development times.

1. Introduction

A composite is subject to diverse micro mechanisms of damage, some of which contribute to its safe life time, ultimate strength or toughness. If one wishes fully to utilize the properties of these advanced materials, it is essential to understand the dynamic of each mechanism of damage and also the effect of constitutent scaling and interaction on the macro-response of the material. The fracture toughness of composites is a result of various mechanisms such as crack formation, fiber-matrix debounding and subsequent pullout. Under monotonic loading on a composite, small cracks form in the matrix normal to the direction of loading, what is specially seen in undirectional composites loaded in the direction of the fibrous reinforcement. This causes the transfer of load to the fibers with increasing shear stress, eventually producing the failure of the bound between the fiber and the surrounding matrix. The cylindrical crack at the interface propagates from the initial matrix crack, creating debounding along the fiber.

Each kind of cracking causes the creation of acoustic emission. Development of acoustic emission (AE) method of material and structure testing leads to more broad its using for studying fracture mechanisms of solids and especially of composites. The knowledge of the structure transformation in strained metals in real time gives a possibility to forecast the safe endurance and ultimate strength as well as makes

easier searching for the materials with better characteritics. From this point of view undirectional composites of the type of carbon fiber reinforced plastic (CFRP), are very convenient model objects for the investigation and on the other hand they create a new kind of structural materials with great application and development possibilities.

2. Specimens and measurements

The investigations were made using the specimens $160 \times 7 \times 1$ mm^3, cut off from the composite plates, undirectionally reinforced by carbon fibers. Two ceramic piezoelectric transducers were used with resonance frequency 400 ± 50 kHz. They were attached on the specimens on the distance $80-100$ mm apart. Signal recording and data converting systems were applied, based on the processors E-60 and HP-9835A. Discrimination level was 50 μV, and single carbon fiber fracture produced an AE signal of the amplitude $90-100$ μV.

The specimen straining under growing loading F was taken with a constant velocity 0.22 mm/min of testing machine holders. All experiments and measurements were performed at the Ioffe Physico-Technical Institute, St. Petersburg.

3. Study effects and discussion

Composite of the type undirectional CFRP makes possible to solve in the first approach an "old" problem of fiber breaking consequences and by this the role of appearing then microcracks which precede the formation of macrocracks, i.e. in shaping of macro-fracture. According to [1], a final destroying of fiber composite, the main component of which is reinforcing carbon fiber surrounded by plastic matrix, occurs due to such a big concentration of fiber cracks that external stress in working section of the specimen achieves a critical value. According to the second extreme point of view [2, 8], catastrophic destroying can take place as a result of cracking of a poor few neighbouring fibers, if this event leads to a great concentration of local stress. However, the direct observation of the development of microcracks done *in situ* in a chamber of scanning electron microscope [3], has shown a lack of active mutual interactions of microcracks in almost the whole time when the material is under an external loading. In real solids appearing the micro-plasticity, mutual interaction of microcracks takes place only at the first moments ($10^{-2}-10^{-1}$ s) after the creation of new microcracks, as later they deteriorate due to stress relaxation. Acoustic emission method gives the opportunity for solving this serious topic of fracture physics and mechanics in real composites and/or structures, and not only in model situations [3]. It seems that such an information can be delivered by statistical analysis of measurement of AE event rate in particular local microvolumes of greater objects.

A graph of changes in event rate $\dot{N}(t)$ as a function of time t of tensile loading action on the whole of specimen is shown in Fig. 1a. This traditional way of result presentation shows a spontaneous increment of event rate in the final stage of loading

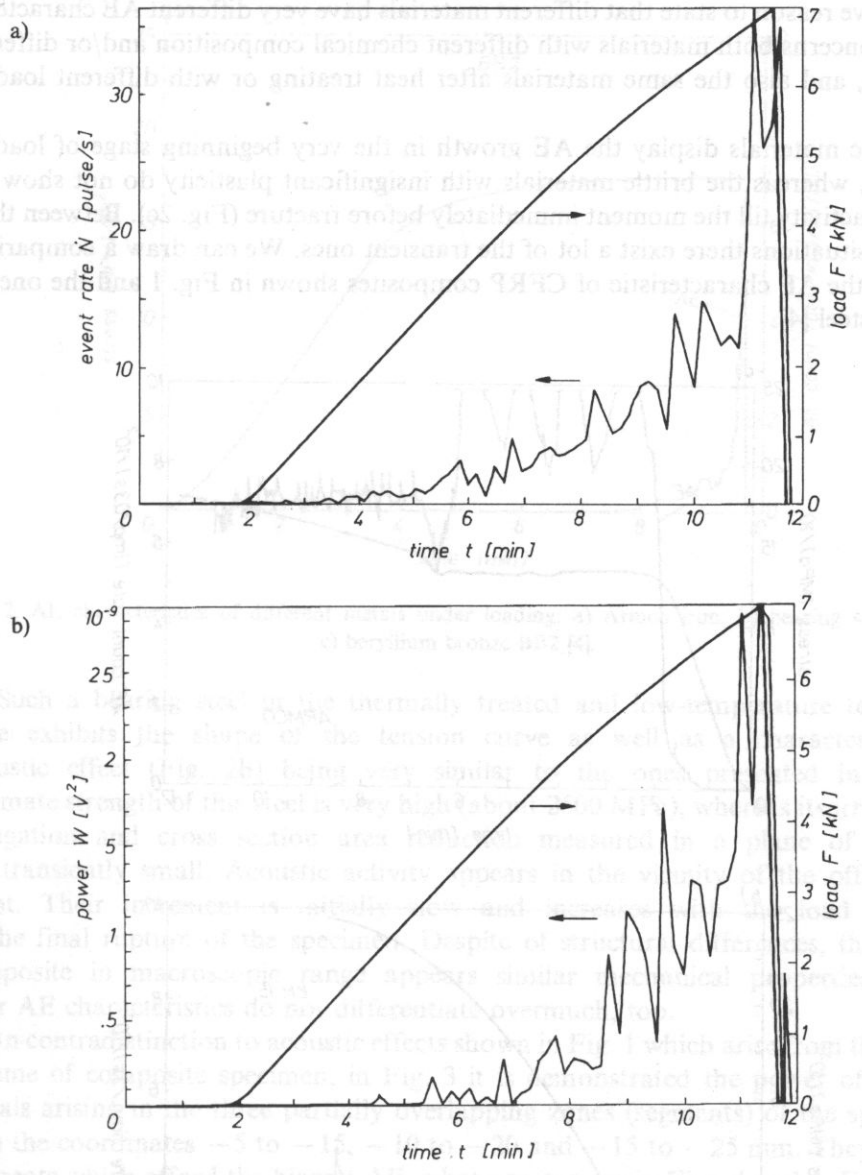

Fig. 1. AE event rate and signal power in the whole of specimen.

increase and this was distinguished from the monotonic loading growth. Character of changes in AE power, $W(t)$, i.e. AE signal energy in time unit, presented in Fig. 1b, is very similar to count rate $\dot{N}(t)$ graph in Fig. 1a.

From the similar investigations of AE effects accompanying metal straining it is well-known [4] that AE characteristics are very different, depending on the kind of crystal space lattice and the structure of the particular materials. The experiment

results give reason to state that different materials have very different AE characteristics. It concerns both materials with different chemical composition and/or different structure, and also the same materials after heat treating or with different loading history.

Plastic materials display the AE growth in the very beginning stage of loading (Fig. 2a), whereas the brittle materials with insignificant plasticity do not show the acoustic activity till the moment immediately before fracture (Fig. 2c). Between these extreme situations there exist a lot of the transient ones. We can draw a comparison between the AE characteristic of CFRP composites shown in Fig. 1 and the one for bearing steel [4].

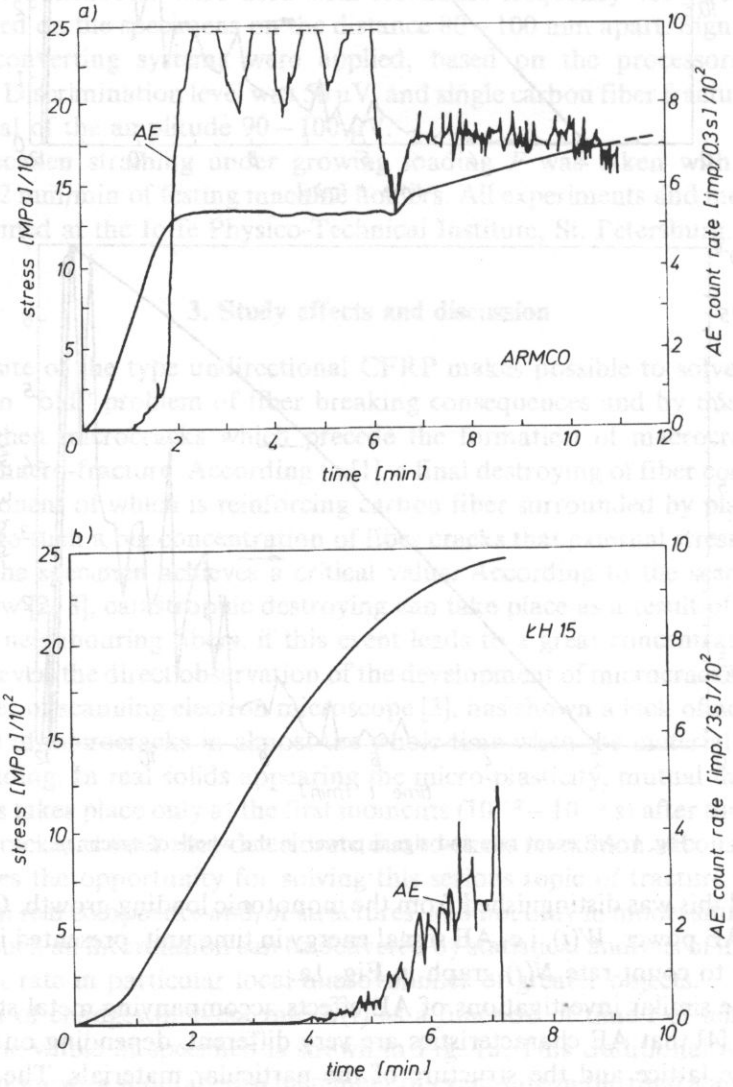

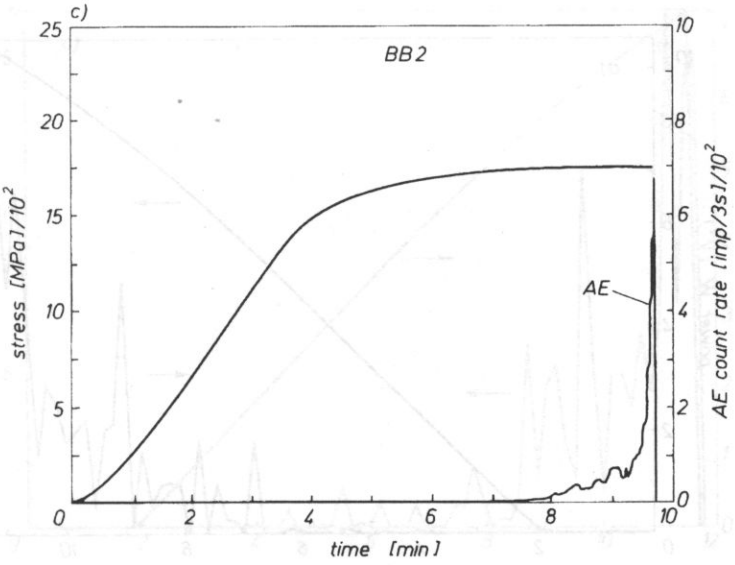

Fig. 2. AE characteristics of different metals under loading: a) Armco iron, b) bearing steel ŁH15, c) beryllium bronze BB2 [4].

Such a bearing steel in the thermally treated and low-temperature tempering state exhibits the shape of the tension curve as well as a character of the acoustic effect (Fig. 2b) being very similar to the ones presented in Fig. 1. Ultimate strength of this steel is very high (about 2500 MPa), whereas its irreversible elongation and cross section area reduction measured in a plane of fracture are transiently small. Acoustic activity appears in the vicinity of the offset yield point. Their increment is initially slow and increases with the load increase to the final rupture of the specimen. Despite of structural differences, the CFRP composite in macroscopic range appears similar mechanical properties. Thus, their AE characteristics do not differentiate overmuch, too.

In contradistinction to acoustic effects shown in Fig. 1 which arise from the whole volume of composite specimen, in Fig. 3 it is demonstrated the power of the AE signals arising in the three partially overlapping zones (segments) of the specimen, with the coordinates -5 to -15, -10 to -20 and -15 to -25 mm. They are the segments which afford the biggest AE, what one can see in Figs. 4 and 5. From Fig. 3 it is obvious that by common similarity of the process course, there exist also the significant quantitative differences between them and neighbouring segments (with the same longitude) of the same specimen whose deliver the AE signals of different power.

The comprehensive graph of signal power $W(L,t)$ from the particular specimen segments is shown in Fig. 4; they are gotten in the function of length coordinate L and loading time t. Non-regularity in AE distribution as the process bonded with fiber fracture can be clearly seen, both in the function of time (loading) and of specimen

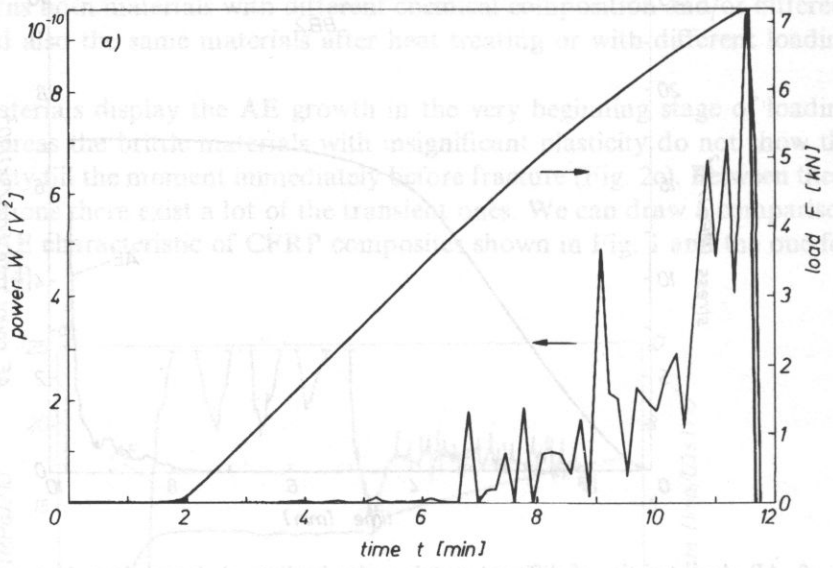
a)
power W [V²]
load F [kN]
time t [min]

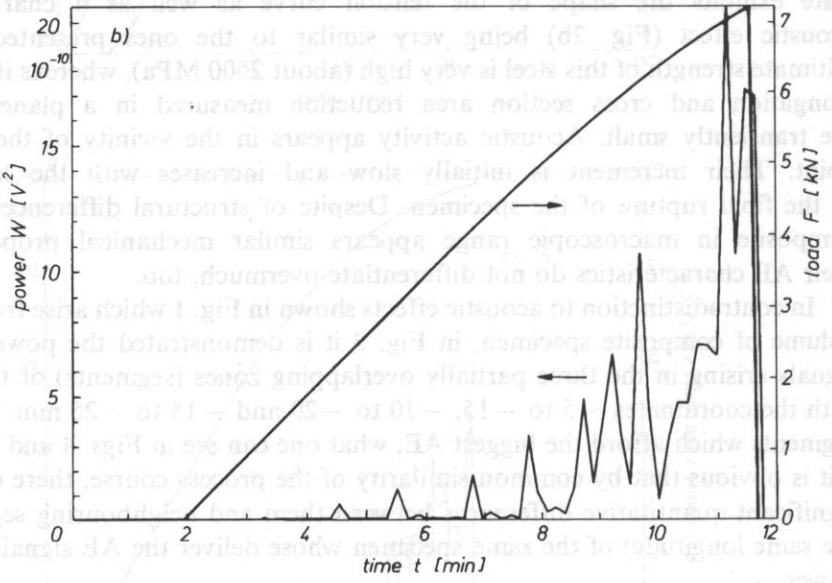
b)
power W [V²]
load F [kN]
time t [min]

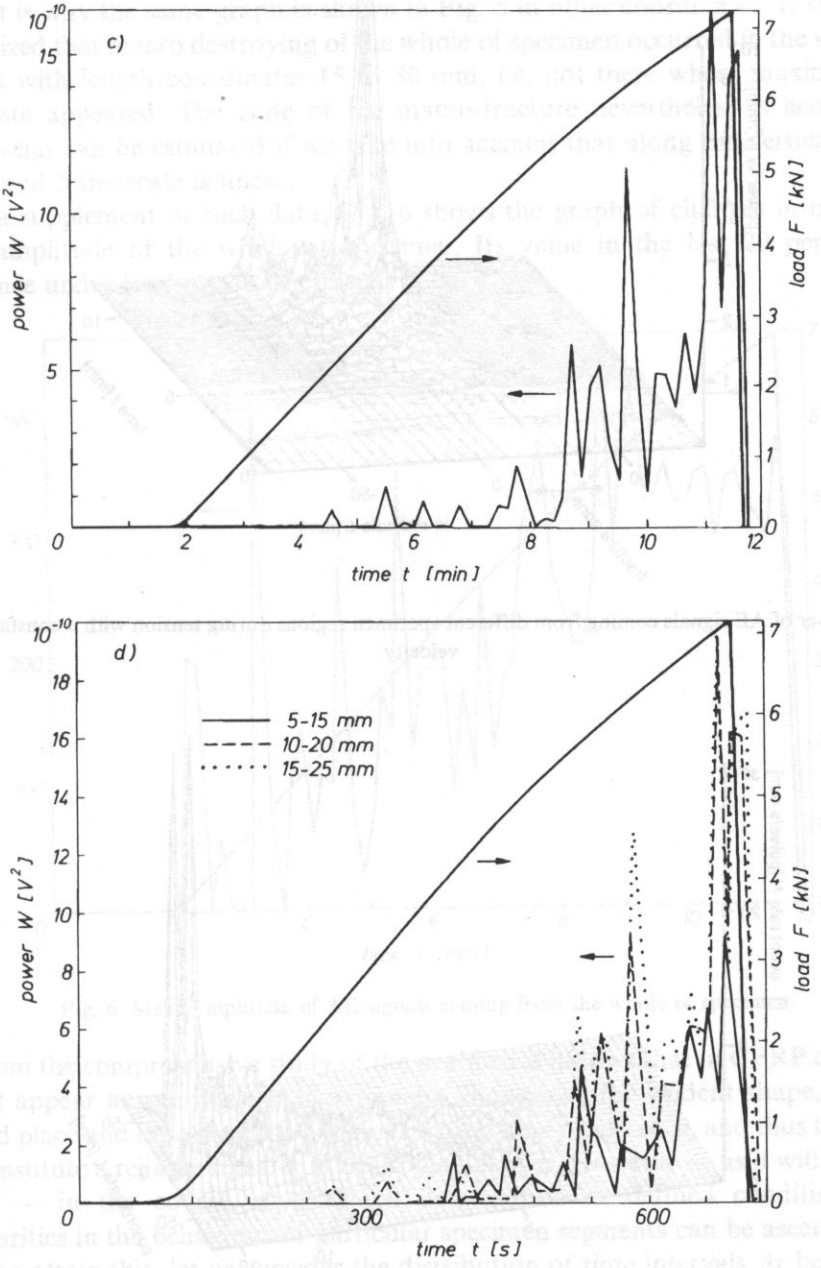

Fig. 3. AE signal power in the particular specimen segments: a) −5 to −15 mm; b) −10 to −20 mm; c) −15 to −25 mm; d) −5 to −25 mm — summary graph.

length co-ordinate. In the last stage of the process, the AE increment is very fast, what is expressed by local inclination of the AE graph, and it is rather difficult to estimate quantitative the process development in the final its moments.

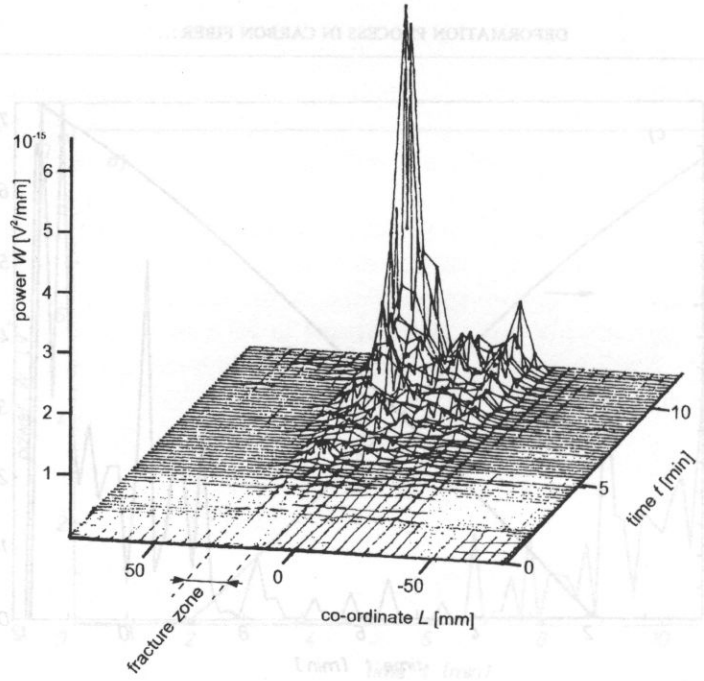

Fig. 4. Power of AE signals coming from different specimen regions during tension with a constant holder velocity.

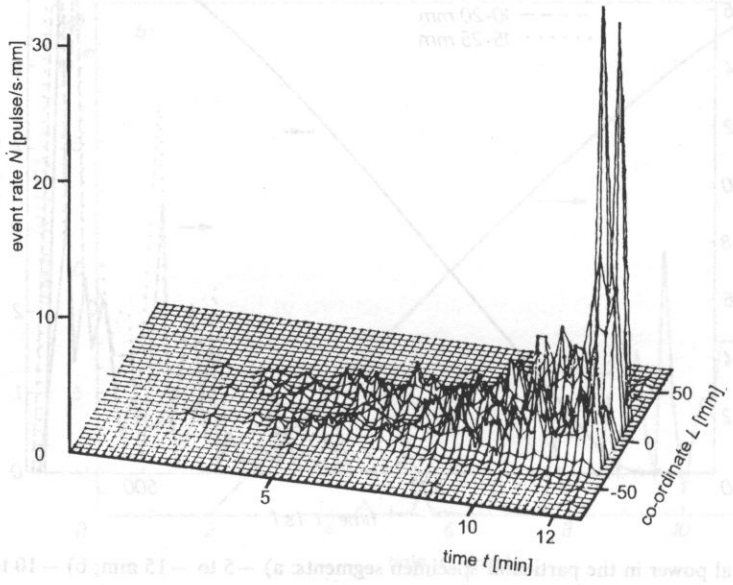

Fig. 5. AE event rate from different specimen regions during tension with a constant holder velocity.

That is why the same graph is shown in Fig. 5 in other coordinates. It should be emphasized that macro destroying of the whole of specimen occurred in the specimen segment with length coordinates 15 to 30 mm, i.e. not there where maximum AE event rate appeared. The zone of the macro-fracture nevertheless is acoustically active, what can be estimated if we take into account that along the vertical axis in Figs. 4 and 5 the scale is linear.

As a supplement of such data, Fig. 6 shows the graph of changes in mean AE signal amplitude of the whole of specimen. Its value in the last 20 per cent of endurance under loading is rather steady.

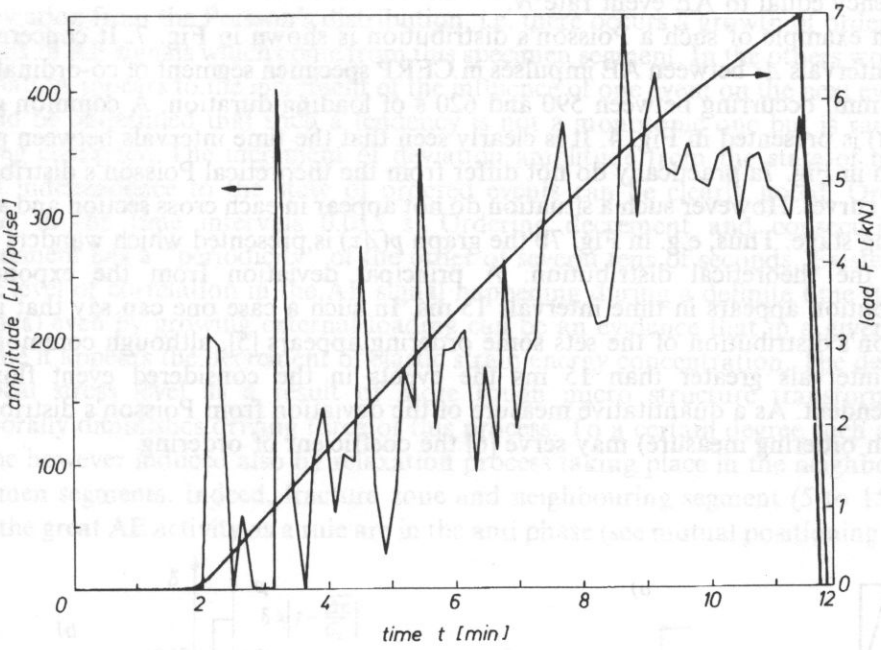

Fig. 6. Mean amplitude of AE signals coming from the whole of specimen.

From the comprehensive study of the problem it follows that in CFRP composite do not appear any univocal AE parameter changes of the evident shape, which in defined place and time could be a prelude to cracking occurrence, and thus they could not constitute a reliable signaler of destroying danger. However — as it will be shown below — in the course of specimen deformation in defined conditions some peculiarities in the behaviour of particular specimen segments can be ascertained. In order to attain this, let us consider the distribution of time intervals $\Delta\tau$ between the AE pulses in the particular specimen segments at different moments of loading process (i.e. by different loading values).

For correct statistical analysis the appropriate sets should be sufficiently representative (70 to 100 events), and the process itself ought to be stationary, i.e. the changes in AE signal flux as a rule ought to be not greater than 20 per cent of stationary level.

In the case of full independence of signal appearance it can be an exponential or a Poisson's distribution. The Poisson's distribution is a frequency distribution which often applies when the probability of an event happening is extremely small. Suppose that in a large number of trials the probability of an event happening is p, where p is small, but the average number of events in any given set of trials is a finite number. If Poisson's distribution applies, the probability of event occurrence is

$$p(\Delta\tau)=me^{-m\Delta\tau}, \tag{3.1}$$

where p is the probability density, $\Delta\tau$ is time interval between the events and m is event frequency equal to AE event rate $\dot{N}$.

An example of such a Poisson's distribution is shown in Fig. 7. It concerns the time intervals $\Delta\tau$ between AE impulses in CFRP specimen segment of co-ordinates 10 to 20 mm, occurring between 590 and 620 s of loading duration. A common graph $W(L,t)$ is presented in Fig. 4. It is clearly seen that the time intervals between pulses shown in Fig. 7a practically do not differ from the theoretical Poisson's distribution (solid curve). However such a situation do not appear in each cross section and at any loading stage. Thus, e.g. in Fig. 7b the graph $p(\Delta\tau)$ is presented which wanders away from the theoretical distribution. A principal deviation from the exponential distribution appears in time intervals 15 ms. In such a case one can say that in the Poisson's distribution of the sets some ordering appears [5], although commonly in time intervals greater than 15 ms the events in the considered event flux are independent. As a quantitative measure of the deviation from Poisson's distribution (i.e. an ordering measure) may serve [6] the coefficient of ordering

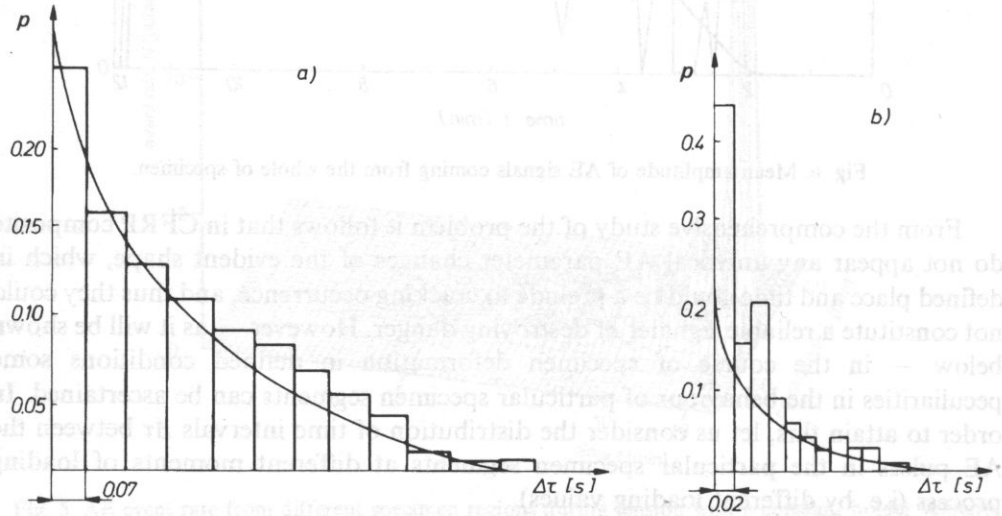

Fig. 7. Probability distribution $p(\Delta\tau)$ of time intervales $\Delta\tau$ of AE signal happening in the segment (-10 to -20 mm) loaded during: a) 590–620 s; b) 670–690 s.

$$\delta = \left| 1 + \frac{\overline{\Delta\tau}}{\sigma_\tau} \right|, \tag{3.2}$$

where $\overline{\Delta\tau}$ is the mean time interval between the events in a given event set and σ_τ is the medium square deviation. It became evident that such an ordering leads to the interesting and more conclusive information about the destroying process development than the one illustrated by three-dimensional graphs $W(L,t)$ in Figs. 4 and 5.

Figure 8 presents the deviation degree of the considered distribution from the Poisson's distribution. It seems that during the final 25 per cent of loading time in the fracture zone of the CFRP composite it appears a peculiar tendency for the increment of deviation from the Poisson's distribution, i.e. there occurs a growth of ordering in the flux of AE signals which come from this specimen segment. In the others words an inclination appears to the increment of the influence of one event on the next event. It should be underlined that such a tendency is not a monotonic one but is rather of pulsing character. The increment of deviation amplitude from the state of mutual event independence to the state of ordered events can be clearly noted. Ordering occurs in the time intervals 0.015 s. Ordering decrement and consecutive its reincrement has a "periodicity" of the order of several tens of seconds. Existence of some level of correlation in the AE signal happening during a definite time (tens of seconds) even by growing external loading can be an evidence that in a given local volume it appears the decrement of elastic strain energy concentration. The decrease of local stress level as a result of more rough micro structure transformation temporally diminishes driving force of this process. To a certain degree such a state can be however induced also by relaxation process taking place in the neighbouring specimen segments. Indeed, fracture zone and neighbouring segment (5 to 15 mm) with the great AE activity as a rule are in the anti phase (see mutual positioning of the

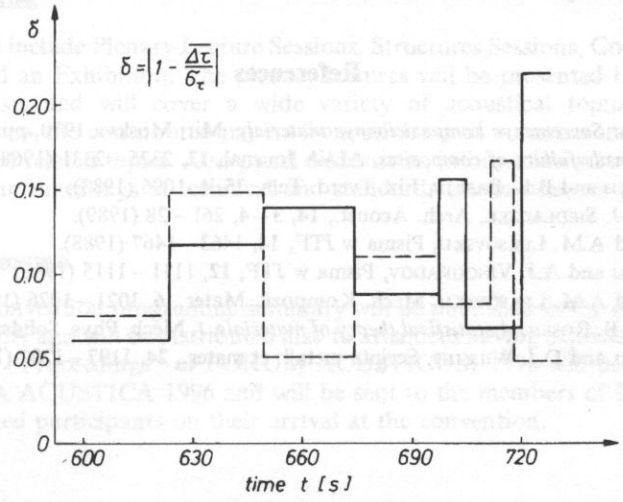

Fig. 8. Changes in coefficient δ in fracture zone (15 to 30 mm) and in neighbouring zone (5 to 15 mm) in final ca. 120 s loading stage (——— fracture zone, ----- active zone).

solid and dotted lines in Fig. 8 and the differences between them). It can be signified that in the final moment of a mutual interaction this anti phase frequently is the most visible and quantitatively the most significant.

Statistical analysis of time intervals between the successive pulse happening shows the existence of specific ordering, i.e. the mutual connection between the events in millisecond intervals — in the range from 0 to 100 ms. Besides the collective effects in such a short time intervals, an analysis of the parameter $\delta(t)$ justifies the existence of collective effects in much greater time intervals — of several tens of seconds, i.e. there appear also the relaxation process in time interval 10^3 – fold longer than in the former case.

On the ground of the general circumstances one can suppose that in heterogeneous solids there ought to appear at the lowest estimate one more time scale of mutual effects, i.e. on the load of sound velocity. Such different time scales of the plastic deformation process in different degree influence the formation of the state which precedes the fracture in this strongly isotropic composite of high strength. One can suppose that knowledge of the sequence of microstructural transformation process and transition mechanism from one scale of group effects to another one could be helpful in searching for a manner of process shaping and safe endurance forecasting of this kind of materials.

It is worth to underline that similar phenomena can occur not only in composites but also in metals with similar AE characteristics. Thus, e.g. in bearing steel ŁK15, graph of which during the monotonic tension is presented in Fig. 2b, is like in CFRP composite, i.e. the strong AE signals appear only in the loading stage immediately before the destroying. The discussed problems and graphs such as presented in Figs. 7 and 8 are analogous for both these materials. An analysis of the topic will be presented separately.

References

[1] B.W. ROSEN, in: *Sovremenye kompozicionnye materialy*, Mir, Moskva 1970, pp. 141–158.
[2] C. ZWEBEN, *Tensile failure of composites*, AIAA Journal, **12**, 2325–2331 (1968).
[3] A.M. LEKSOVSKIJ and B.L. BASKIN, Fiz. Tverd. Tela, **25**, 4, 1096 (1983).
[4] S. PILECKI and J. SIEDLACZEK, Arch. Acoust., **14**, 3–4, 261–28 (1989).
[5] A.P. TISKIN and A.M. LEKSOVSKIJ, Pisma w JTF, **14**, 1463–1467 (1988).
[6] A.P. BRAGINSKIJ and A.J. VINOGRADOV, Pisma w JTF, **12**, 1111–1115 (1986).
[7] W.E. JUDIN and A.M. LEKSOVSKIJ, Mech. Kompozit. Mater., **6**, 1021–1026 (1986).
[8] C. ZWEBEN and B. ROSEN, *A statistical theory of materials*, J. Mech. Phys. Solids, **18**, 189–206 (1970).
[9] V.M. KARBHARI and D.J. WILKINS, Scripta metall. et mater., **24**, 1197–1202 (1990).

ARCHIVES OF ACOUSTICS
20, 3, 299–300 (1995)

C H R O N I C L E

FORUM ACUSTCUM 1996

THE 1ST CONVENTION OF THE EUROPEAN ACOUSTICS ASSOCIATION EAA ANTWERPEN, BELGIUM 1–4 APRIL 1996

FORUM ACUSTICUM 1996, the first Convention of the European Acoustics Association EAA-EEIG, is to be held on the campus of the University of Antwerpia, U.I.A. Belgium. from 1 to 4 April, 1996. In order to ensure a high quality convention and a large number of participants, a number of EAA Societies merge their national meetings into the European Convention. One of the main goals of this convention will be to foster scientific and cultural exchanges, especially among the young acousticians. EAA is in charge of the overhead organization. The convention is organized by the Belgian Acoustical Association ABAV and the Technological Institute of the Royal Flemish Society of Engineers TI-K VIV.

Local organizing committee:

Chairman: André Cops

Pierre Chapelle, Christine Mortelmans. Stefaan Peeters, Hans Roamaen, Paul Sas, Jan Thoen, Gerrit Vermeir, Diane Voet.

Convention activities

The convention include Plenary Lecture Sessions, Structures Sessions, Contributed Papers, Poster Sessions and an Exhibition. The plenary lectures will be presented by internationally well-known scientists and will cover a wide variety of acoustical topics. The Scientific Committee will review the contributed papers from all areas of acoustics in order to arrange them into sessions of related topics. Also panel discussions, information sessions on European issues, workshops and meetings of technical and standards committees are planned.

Convention programme

An advanced convention programme summary will be published in the December issue of ACTA ACOUSTICA and will be distributed also to attendees having expressed their intention to participate. The "Proceedings" of FORUM ACUSTICUM 1996 will be published as the first issue of ACTA ACUSTICA 1996 and will be sent to the members of EAA and handed over to the registered participants on their arrival at the convention.

Call for papers

Proposals for papers in **all areas of acoustics** are welcome. THE DEADLINE FOR RECEIPT OF PAPERS IS FRIDAY, 1 SEPTEMBER 1995. THIS DEADLINE WILL BE

STRICTTLY ENFORCED. The papers must be prepared in accordance with the enclosed **Instructions for the Preparation of Papers** and with the additional guidelines as indicated in this call under the section **Papers** and **Special Instructions**. Please note the maximum permitted length of the paper is 3500 characters including formulae, figures, tables and references but not title and author's names, which together with spaces between paragraphs amount to about 400 characters.

Technical programme

Contributed papers in all branches of acoustics are welcome will be considered for presentation at the convention. The following areas are of particular interst for planning special sessions invited and contributed papers:

1. Acoustic Materials
2. Audio-systems
3. Auditory Systems — Physiology
4. Building and Room Acoustics
5. Computational Methods for Acoustics
6. Environmental Acoustics
7. Flow Acoustics
8. Measurment and Instrumentation
9. Musical Acoustics
10. Nonlinear Acoustics
11. Photo-acoustics and Acousto-optics
12. Psychoacoustics
13. Signal Processing
14. Speech
15. Structural Acoustics
16. Ultrasonics
17. Underwater Acoustics

A paper is allowed one column in ACTA ACUSTICA. Each full column has 60 lines hence 3900 characters. **The maximum permitted lenght of the paper is 3500 characters** including formulae, figures, tables, and references but not title and author's names, which together with spaces between paragraphs amount to about 400 equivalent characters. ABSTRACTS LONGER THAN 3500 CHARACTERS MAY NOT BE EDITED OR TRUNCATED. Papers should be prepared in accordance with the enclosed **Instructions for the Preparation of Papers**.

Mail the **orginal and three copies** of the paper to the Convention Secretariat:

FORUM ACUSTICUM 1996
Convention Secretariat
Technological Institute — K VIV
Desguinlei 214
B — 2018 ANTWERPEN, Belgium

Authors invited for special sessions should send an additional copy of their paper to their session organizer for receipt one week prior to the deadline, and should indicate at the bottom of each copy: "INVITED FOR SPECIAL SESSION ON

_____ (title of session)"

The 1 September 1995 deadline for receipt of papers at the above address will be strictly anforced. Allow at least 5 days for delivery of ordinary European mail, 2 days for express mail, and 10 days for international air mail. FACSIMILE TRANSMITTED ABSTRACTS CANNOT BE ACCEPTED. Authors will be informed in due time by mail of the time their paper(s) are scheduled.